Doctor Thesis

Observation of Free Surface Flow Behavior Using Laser Tagging Method by Photochromic Dye Tracer

NURRINA BINTI ROSLI

Department of Mechanical Science and Technology
Gunma University
Japan

Under the guidance of
PROFESSOR DR. KENJI AMAGAI, Ph. D. Eng.

Table of Contents

Nomenclature

A	area framed by 4-points of dye traces	[mm^2]
b	width of inclined wall in liquid film flow experiment	[m]
B	measured absorbance in Beer-Lambert law	[-]
c	molar concentration of sample liquid in Beer-Lambert law	[mol]
C	closed line connecting dye traces to form plane region S	[-]
d_1	diameter of dye trace parallel to liquid film flow direction	[mm]
d_2	diameter of dye trace perpendicular to liquid film flow direction	[mm]
d_c	diameter or cylinder	[mm]
dl	small linear element on closed line C	[-]
e	molar extinction coefficient in Beer-Lambert law	[mol^{-1}cm^{-1}]
f	arbitrary function in calculation formula of flow deformation	[-]
k	range of diode laser irradiation to the test piece in calibration procedure of light absorption method	[mm]
h	diameter of optical flat used in calibration procedure of light absorption method	[mm]
H	known-spacing between optical fiber A and B in liquid film flow experiment	[mm]
I	intensity of light passes through sample liquid in calibration procedure of light absorption method	[a.u.]
I_0	intensity of incident light irradiated to sample liquid in calibration procedure of light absorption method	[a.u.]
l_{ij}	length between dye trace point i and j (i, j=1, 2, 3,)	[mm]
L_c	distance between origin points to the center position in between 4-points of dye traces in liquid sheet spray experiment	[mm]
L_i	distance between origin point to the center point of each dye trace in liquid sheet spray experiment	[mm]
L_m	distance travelled by liquid film flow from liquid inlet in inclined wall	[mm]
L_p	distance between center point of dye trace and wave peak	[mm]
L_w	length of wake vortex in creeping flow experiment	[mm]
$\boldsymbol{n}$	outward-pointing normal vector from small line dl	[mm]
n_x	outward-pointing normal vector from small line dl in x direction	[mm]

n_{xij}	x component of normal vector on line between dye trace point i and j $\quad$ $(i, j=1, 2, 3, 4)$	[mm]
n_y	outward-pointing normal vector from small line dl in y direction	[mm]
n_{yij}	y component of normal vector on line between dye trace point i and j $\quad$ $(i, j=1, 2, 3, 4)$	[mm]
Q	flow rate of liquid sheet spray and liquid film flow experiments	[m^3/s]
Re	Reynolds number in creeping flow and liquid film flow experiments	[-]
S	plane region bounded by the closed line C formed by the 4-points of dye traces	[-]
t	unit tangent vector from small line dl	[mm]
t_x	unit tangent vector from small line dl in x direction	[mm]
t_y	unit tangent vector from small line dl in y direction	[mm]
T	transmittance of light in Beer-Lambert law	[-]
T_e	room temperature during experiments	[°C]
u	velocity component of dye trace bounding plane region S in x direction	[mm/s]
u_i	velocity component of dye trace point i bounding plane region S in x direction $\quad$ $(i =1, 2, 3, 4)$	[mm/s]
u_j	velocity component of dye trace point j bounding plane region S in x direction $\quad$ $(j=1, 2, 3, 4)$	[mm/s]
$\overline{U_w}$	average velocity of wave calculated by FFT analyzer	[mm/s]
v	velocity component of dye trace bounding plane region S in x direction	[mm/s]
v_i	velocity component of dye trace point i bounding plane region S in y direction $\quad$ $(i =1, 2, 3, 4)$	[mm/s]
v_j	velocity component of dye trace point j bounding plane region S in y direction $\quad$ $(i =1, 2, 3, 4)$	[mm/s]
v_n	normal direction component of velocity vector V	[mm/s]
v_t	tangent direction component of velocity vector V	[mm/s]
V	interpolated velocity vector by velocity of dye trace point i bounding plane region S $\quad$ $(i=1, 2, 3, 4)$	[mm/s]
V_a	velocity of dye trace in creeping flow experiment	[mm/s]
V_c	velocity of moving cylinder in creeping flow experiment	[mm/s]
V_i	velocity of dye trace point i in liquid sheet spray experiment $(i=1, 2, 3, 4)$	[m/s]
$\overline{V_l}$	average velocity of dye trace in liquid film flow experiment	[mm/s]

V_l	velocity of dye trace in liquid film flow experiment	[mm/s]
V_w	velocity of wave in liquid film flow experiment	[mm/s]
$\overline{V_w}$	average velocity of wave passing dye trace calculated by image analysis method	[mm/s]
X	distance vector of dye trace bounding plane region S	[mm]
X_l	distance travelled by dye trace in liquid film flow experiment	[mm]
X_w	distance travelled by wave in liquid film flow experiment	[mm]
Θ	divergence of creeping flow	[s^{-1}]
$\overline{\gamma}$	total average shear strain of liquid sheet spray	[-]
γ	shear strain rate of liquid sheet spray	[s^{-1}]
$\overline{\delta}$	average thickness of liquid in liquid film flow experiments	[mm]
δ	thickness of liquid in liquid sheet spray and liquid film flow experiments	[mm]
δ_p	known-thickness of plate used in calibration procedure of light absorption method	[mm]
$\overline{\varepsilon_x}$	total average normal strain of liquid sheet spray in x direction	[-]
ε_x	normal strain rate of liquid sheet spray in x direction	[s^{-1}]
$\overline{\varepsilon_y}$	total average normal strain of liquid sheet spray in y direction	[-]
ε_y	normal strain rate of liquid sheet spray in y direction	[s^{-1}]
$\overline{\varepsilon_z}$	total average normal strain of liquid sheet spray in z direction	[-]
ε_z	normal strain rate of liquid sheet spray in z direction	[s^{-1}]
η	dynamic viscosity of working fluid	[Pa·s]
θ	wall inclination angle in liquid film flow experiment	[deg.]
λ	wavelength of laser light	[nm]
ρ	density of working fluid in liquid film flow experiment	[kg/m^3]
τ	time delay between the two signals cross-correlated by FFT analyzer	[s]
ω	vorticity of creeping flow and liquid sheet spray	[s^{-1}]

Chapter 1

Introduction

1.1   Background and literature review

1.1.1   Free surface flow and the measurement technique

Free surface flows are ubiquitous in our daily life. For instances, the river flow, sea wave, rain droplet, water column flow out from a water tap and water flow in a drain are among the examples of free surface flow that commonly found in our everyday life. Moreover, the free surface flow is also observed in many branches of the industrial fields including the atomization process in automotive engine, wall surface flow related to heat and mass transfer facilities as well as the wave surface flow related two phase flow in thermal exchanger.

In response to the increasing demands to enhance the performance of those industries, study on the liquid flow behavior is fundamentally important. Consequently, the liquid flow visualization has become a significant interest among engineers and researchers to better understand the flow behaviors of free surface flow. Generally, various kinds of measurement were used to estimate the liquid flow behavior such as the hot wire anemometry [1], [2], particle image velocimetry [3], [4], [5], laser Doppler anemometry [6], [7], [8] and many more. From our survey, the well-known particle image velocimetry (PIV) has taken very large portion among the techniques applied in the past to measure the flow field structure.

However, the main capital in handling the technique of PIV, i.e. the seeding particles presents limitation and weakness in estimating the liquid flow behavior. For examples, Luo and Wang [9] used the 3D-PIV measurement system to investigate bubble flow in between two plates of microchannel. Through their experimental test, the measurement accuracy was slightly affected since the seeding particles stuck around the wall surface. Another limitation was also found by Bress and Dowling [10] in their investigation of resins flow. Certain part in the cavity was unable to be visualized due to the uneven brightness of the laser sheet in the flow field. The rapid change of the resins flow also cause the laser sheet to be reflected back the flow behind it and this cause the over-brightness to the region.

Particularly in the free surface flow which presents very large deformation on the liquid surface, the PIV may not become the best choice of method to deal with such flow behavior because it is difficult to detect the flow signal of liquid surface. Therefore,

the PIV method is certainly unreliable to be used as the measurement technique for the free surface flow.

Here, a laser tagging method is developed as a new approach to measure the free surface flow behavior. The technique is implemented based on a temporary color change of liquid containing the photochromic dye. Briefly explained, this non-intrusive measurement technique utilizes the color change of the liquid containing the photochromic dye when a laser light source such as ultraviolet (UV) light was irradiated to the liquid. The crucial advantage of this method is that it enables the visualization of flow structure directly without using the seeding particles, and the liquid surface area can be easily traced by the irradiation of UV laser light. An extensive introduction about the laser tagging method using the photochromic dye will be done hereafter.

1.1.2   Laser tagging method using photochromic dye tracer

The laser tagging method was first developed by Popovich and Hummel **[11]** in 1967 to study the viscous sublayer occurred in a turbulent flow in a pipe. **Fig. 1-1** shows the photochromic dye traces images formed in the pipe. Along with the time elapsed, the traces line seen as perpendicular to the pipe and formed the angle from the pipe wall. Thus, the existence of laminar sublayer was successfully proved from their experimental works. The results were also found to meet agreement with Spalding's equation and several results in the past, as shown in **Fig. 1-2**.
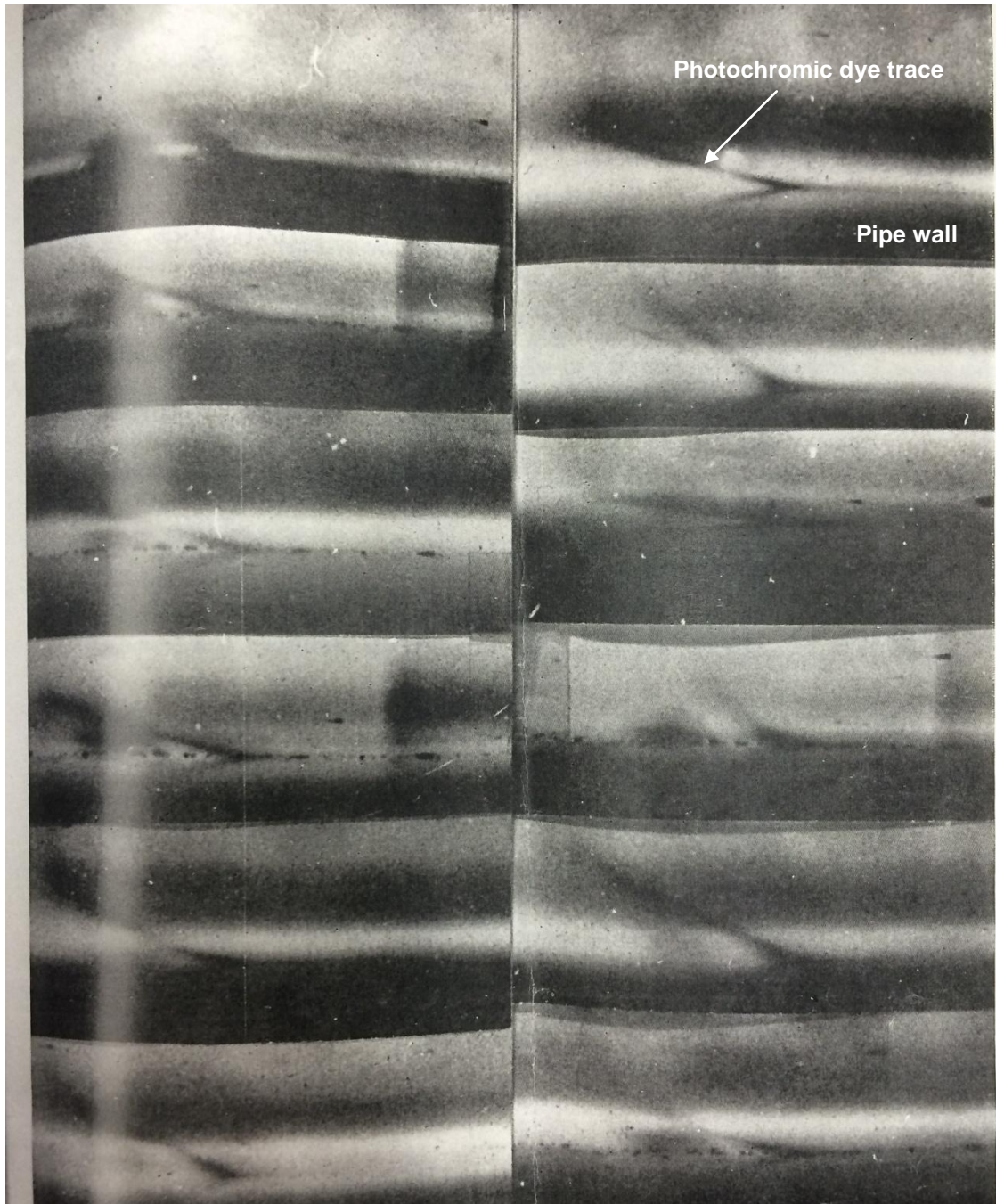
Fig. 1-1   Laminar sublayer in pipe flow observed by photochromic dye tracer reported by Popovich and Hummel **[11]**
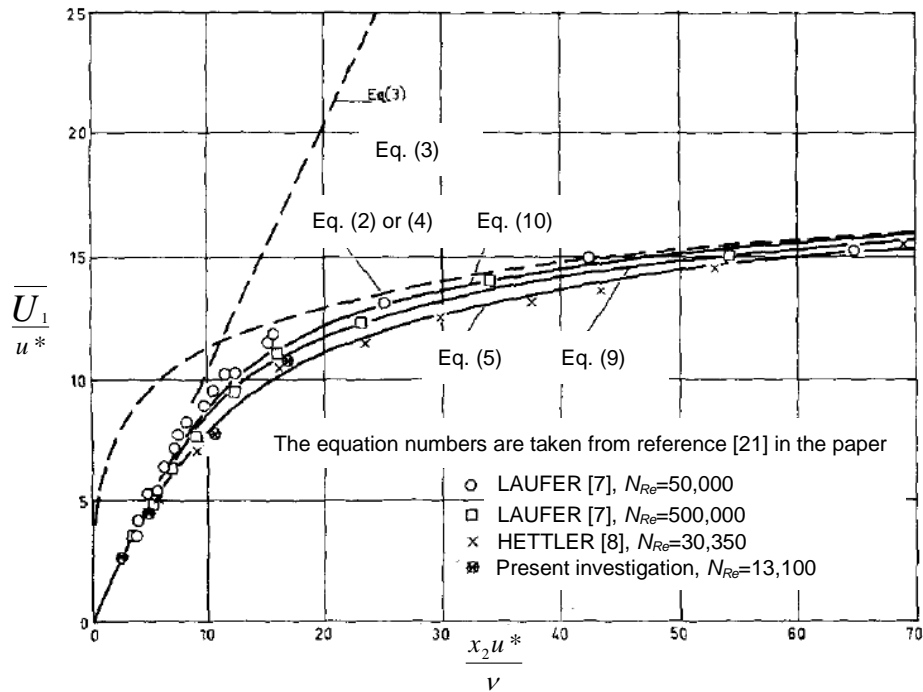
Fig. 1-2 Average velocity distribution near pipe wall compared with several results in the previous literature **[12]**

Since then, its usage has been extensively applied to develop various research fields, especially in the flow field measurements. For instance, Johnson and Marschall **[13]** used the technique to investigate droplet formation from various kinds of nozzle. The photochromic dye tracer in their experiment was seen clearly as the flow patterns in the droplets as shown in **Fig. 1-3**. The mechanism for the liquid to disperse once discharged from nozzle was clarified by the technique.

(a)

Photochromic dye trace

(b)

Photochromic dye trace

Fig. 1-3 Internal flow visualization of **(a)** slow and **(b)** droplet formation **[13]**
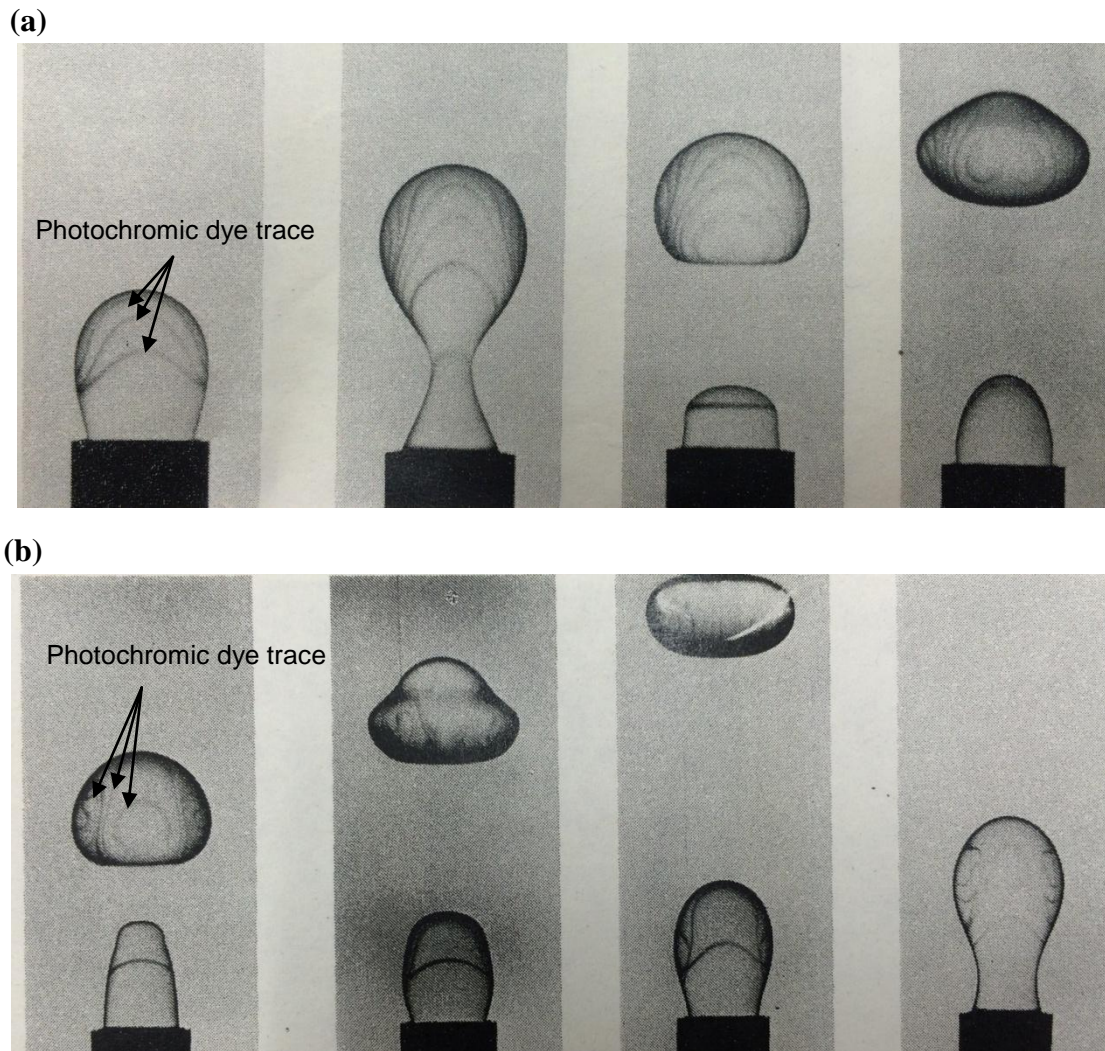
Kawaji **[14]** described several sample experiments conducted by his research team in order to prove the benefit of this technique in visualizing two-phase flow in a pipe. Sample experiments carried out include the wavy-stratified, free falling film, annular and slug flows. Their studies made greater understanding to the flow structures. This time, previous reports in the studies were also confirmed by well-agreements and denials. They successfully observed the vortex motion under large amplitude of disturbance waves in a pipe flow as shown in **Fig. 1-4**.

In the measurement of countercurrent annular flow of falling film, some retardation of velocity was found near the interface as shown in **Fig. 1-5**. This retardation was induced by the countercurrent interfacial shear caused by the gas flow.
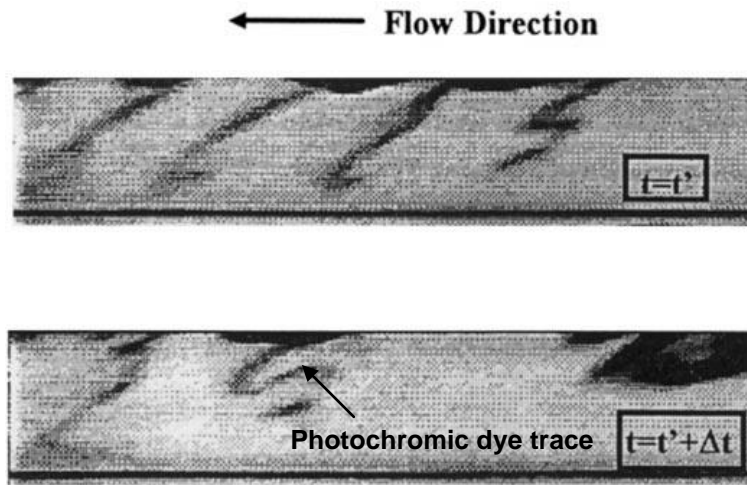
Fig. 1-4 Vortex motion of photochromic dye traces under a disturbance wave in a pipe **[14]**
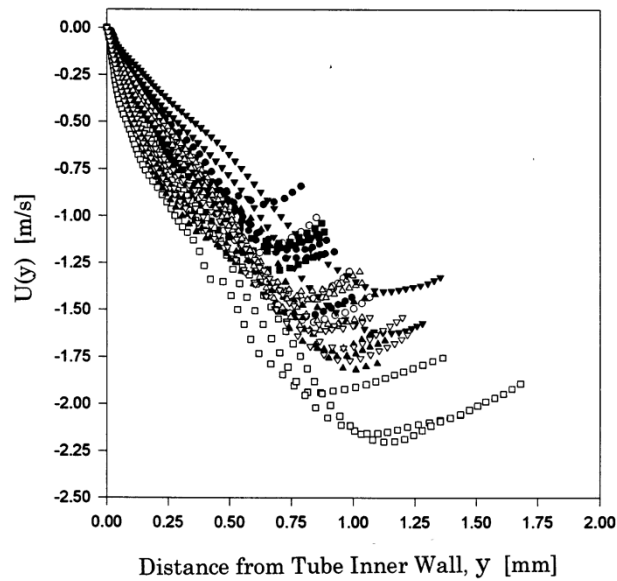

Fig. 1-5 Instantaneous velocity profiles in a falling film at the onset of flooding for countercurrent annular flow **[14]**

Homescu and Desevaux **[15]** applied this technique to investigate liquid velocity of curved-surface between groove structures. The dye traces was formed with two consecutive pulsed UV laser as presented in **Fig. 1-6**.

(a)

(b)
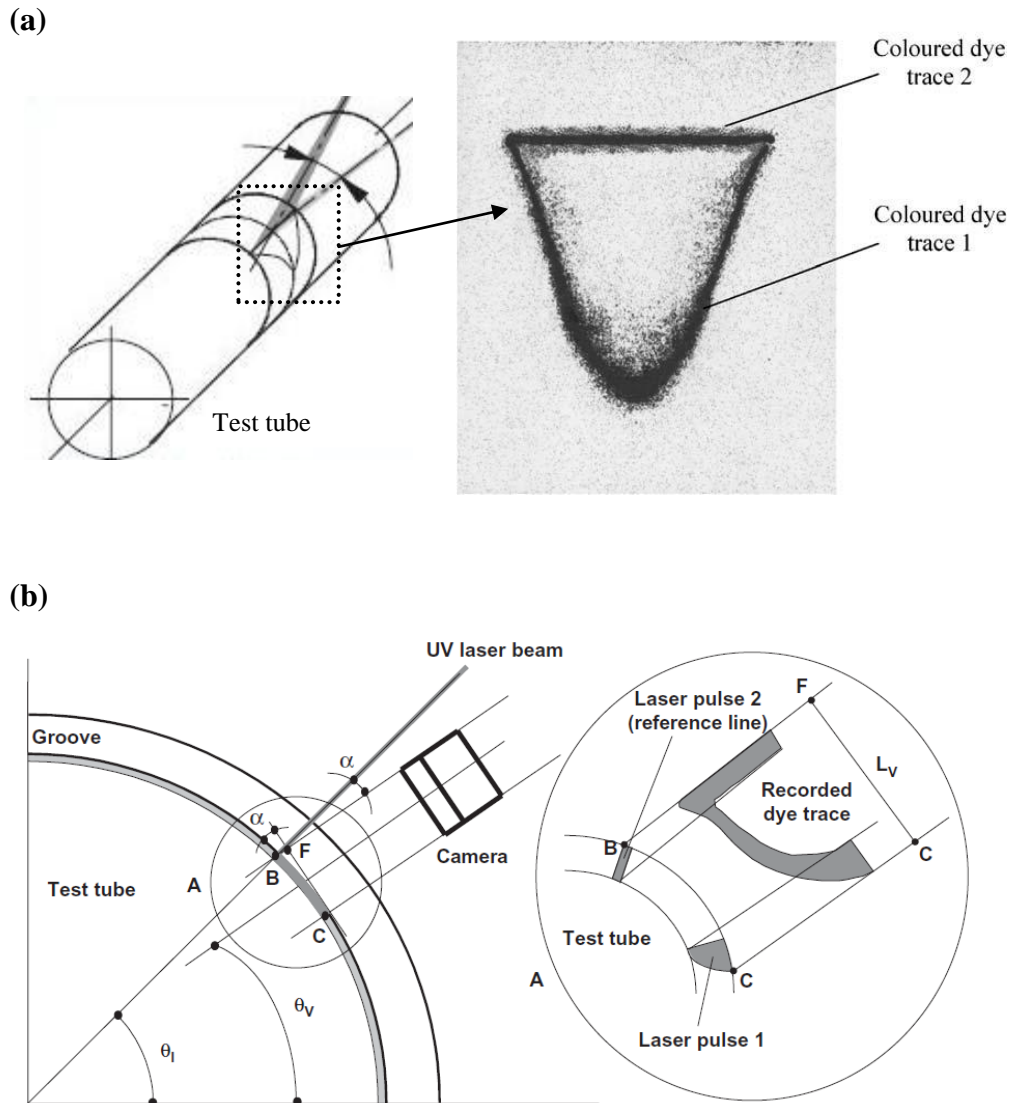
Fig. 1-6 Image of **(a)** photochromic dye traces in the test tube with **(b)** observation method in curved surfaces **[15]**

The advantages as well as limitations of using the photochromic dye marking method were also described. According to them, this technique must be done with suitable optical devices. However, with very little quantity of dye contained in the liquid test, the physical properties are not affected. This is an important point to prove that the technique is trustful and reliable for liquid velocity measurement in various kinds of flow fields which cannot be well-observed by other methods.

Park et al. **[16]** used this technique to measure the flow vorticity occurred in a curved vessel. The photochromic grids as shown in **Fig. 1-7** were formed by using two UV beams sourced from a multi-stage nitrogen laser which were consecutively

separated and focused by a pair of lens arrays. In order to ensure the measurements accuracy of the method, the numerical flow field calculations were also performed. The comparison between both results was done and the validity of the laser tagging method was then strengthened from the good agreement of it, as can be seen in **Fig. 1-8**.

(a)   **(b)**

| a   t = 0 ms | b   t = 18 ms |
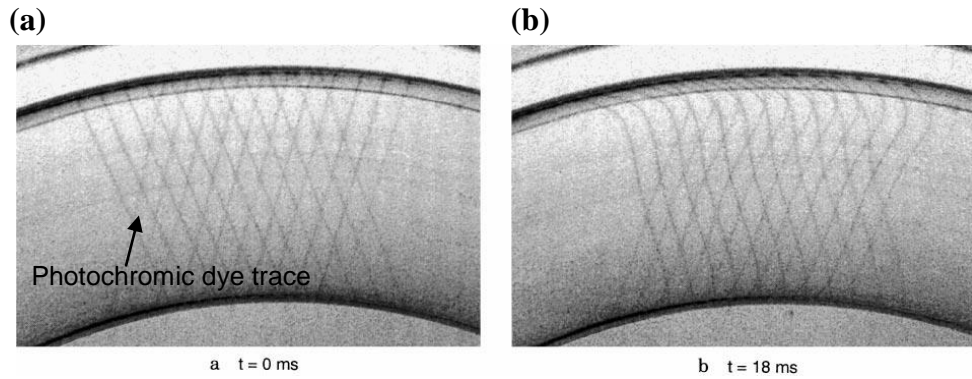
Fig. 1-7   Photochromic grids in curved vessels **(a)** without flash time delay and **(b)** with flash time delay **[16]**
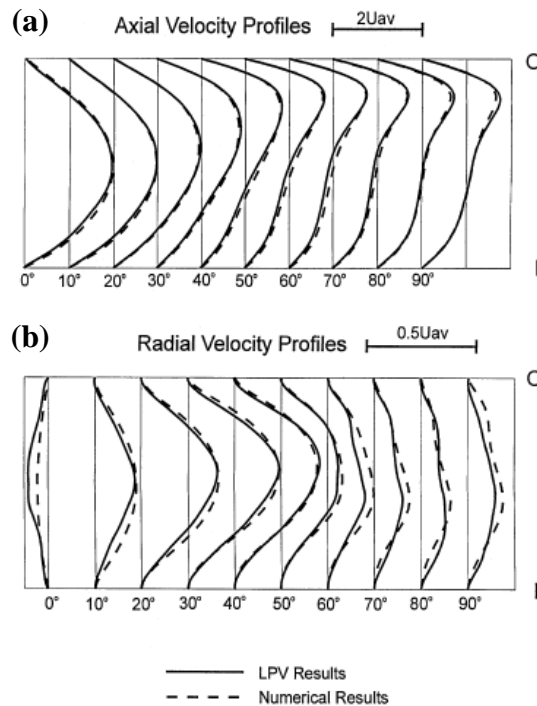
Fig. 1-8   Velocity profiles in **(a)** axial and **(b)** radial components **[16]**

Kai et al. **[17]** proved the successful of using this technique to observe the particle motions in a two-dimensional fluidized catalyst bed. **Fig. 1-9** shows the images of photochromic dye trace motion beside bubble in time interval. The dark areas represent

8

the bubble cavities or activated particles. They enabled to measure the local velocity of emulsion particles around the bubble. As shown in **Fig. 1-10**, the velocity of particles was found to decrease with increasing distance from the bottom of the bubble. The particle velocity at just below the bubble was also found to meet a good agreement with the mean ascending velocity of bubble.
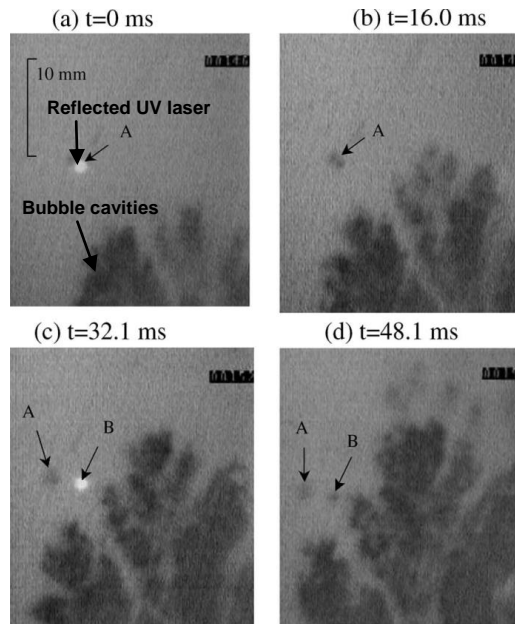
Fig. 1-9 Photochromic dye traces formed beside bubble in fluidized bed **[17]**
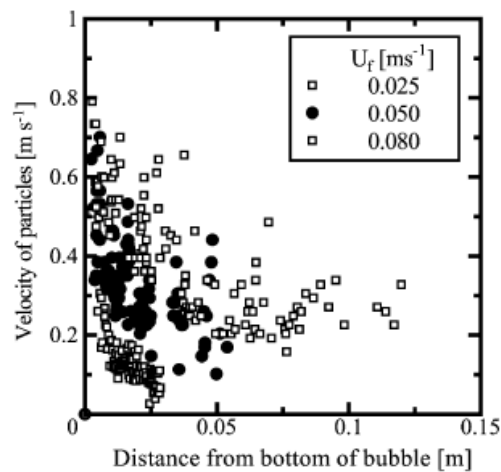
Fig. 1-10 Relationship between distance from bubble and particle ascending velocity **[17]**

Another experiment of the laser tagging method by photochromic dye associated with bubble flow visualization was done by Sanada et al. **[18]**. They successfully visualized the wake flow structure of bubble moving to higher position from the trajectory of colored liquid in the bubble wake, as shown in **Fig. 1-11**. A single bubble was formed, immediately after UV sheet light illuminated the part of the liquid just above the bubble generation nozzle in order to activate photochromic dye trace.

Once the bubble passed across the colored area of the liquid, the bubble was accompanied by some portion of activated dye tracers and thus the flow structure in the rear of the single rising bubble can be observed. The bubble shape, trajectory, and aspect ratio as bubble rose for 0.1s is shown in **Fig. 1-12**. As can be confirmed, the bubble wake was found to fluctuate several times and moved one periodical zigzag motion.

Fig. 1-11 Photochromic dye trace of single rising bubble wake with zigzag motion **[18]**

Fig. 1-12   Single rising bubble in **(a)** shape, **(b)** trajectory and **(c)** aspect ratio **[18]**

In regards to the properties of photochromic dye, Fogwell and Hope **[19]** described this matter through their works including the mecha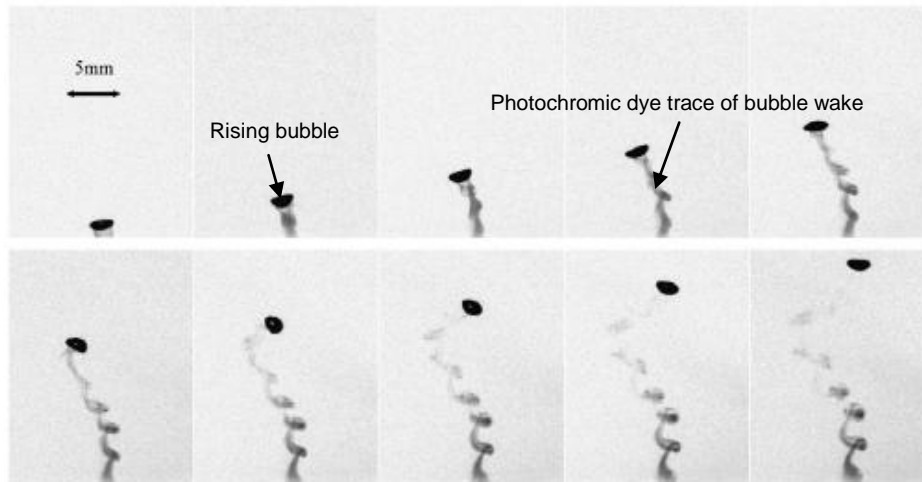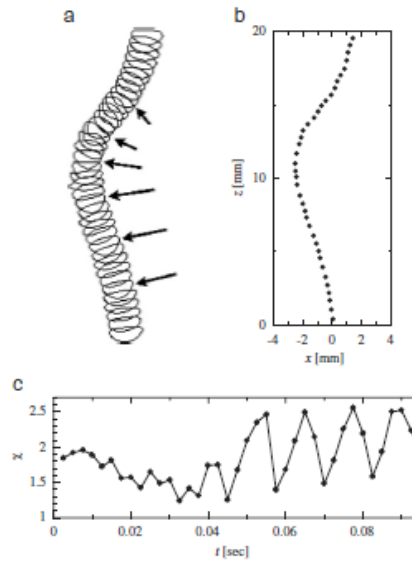nisms and theory of chemical changes presented by many types of photochromic dye. Their investigation especially in describing the dye concentration is greatly beneficial in properly using the photochromic dye for the flow visualization.

From these experimental works reported in the past, the laser tagging method using the photochromic dye tracer is reliable to be used as measurement technique of fluid flow. Especially, since the photochromic dye traces are able to be formed easily with various desired trace patterns in the liquid flow field, the deformation occurred in the flow field thus can be easily observed by using the photochromic dye tracer. Therefore, the technique is applied to our research in order to further study the free surface flow behavior. Here, the research work is conducted to two kinds of free surface flow, i.e. the liquid sheet spray and liquid film flow on inclined wall. Findings and discussion made throughout this research study are described in the respective chapters.

1.2   Objective of this research

The purpose of this research is to investigate the free surface flow behavior using the laser tagging method by photochromic dye tracer. In order to check the applicability of this technique for the free surface flow measurement, this research study was carried out in three different flow fields, i.e. creeping flow of moving cylinder in a channel, liquid

sheet spray injected from a nozzle and liquid film flow on inclined wall.

The experiment of creeping flow is carried out as the preliminary experiment to confirm the ability of using the proposed technique for measurement of flow field. Then, the liquid sheet and liquid film flow experiments are conducted to clarify the flow behavior of free surface flow by using the proposed technique.

1.2.1 Measurement of creeping flow around moving cylinder

In the measurement of creeping flow, the laser tagging method by using photochromic dye tracer is applied to assess the ability of the technique to the measurement of flow field. The experiment is carried out to visualize the creeping flow around a moving cylinder in a rectangular cavity. From the movement of the dye traces, the velocity, vorticity and divergence profiles of the creeping flow are estimated. Detailed explanation regarding the experiment of creeping flow is described in chapter 3.

1.2.2 Measurement of liquid sheet spray injected from nozzle

In the measurement of liquid sheet, we focus on the liquid sheet spray as a fundamental study of the atomization phenomena. The laser tagging method using photochromic dye is developed to study the breakup process of liquid sheet in detail, covering from the behavior in the liquid film until disintegrated into ligament and droplets. The motions of the dye traces are analyzed as the liquid surface velocity. By forming a set of 4-points of dye traces on the liquid sheet, the changes of relative position of the set allow the measurement of deformation and rotational motion of liquid film. Moreover, the measurement of average thickness of the liquid sheet is also carried out by using light absorption method. Detailed explanation regarding the experiment of liquid sheet spray is described in chapter 4.

1.2.3 Measurement of liquid film flow on inclined wall

In the measurement of liquid flow on inclined wall, the laser tagging method using photochromic dye tracer is developed to clarify the flow structure of liquid film on inclined wall. Here, the movement of wave is analyzed together with the movement of dye traces. Then, comparison between the wave and liquid velocities is done. The wave velocity is also measured by cross correlating two signals of light intensity from two laser beams spaced in a known distance. The thickness measurement is also conducted

to clarify the internal structure of liquid film flow. Furthermore, the diameter change of dye traces is also measured to estimate the internal flow state of the liquid film. Detailed explanation regarding the experiment of liquid film flow is described in chapter 5.

References

[1] Ueda, T. and Tanaka, H.: Measurements of Velocity, Temperature and Velocity Fluctuation Distributions in Falling Liquid Films, *International Journal of Multiphase Flow*, **2**-3 (1975), 261-272.

[2] Zhang, Y.: Experimental Studies of the Turbulence Structures of Impinging Reacting Jets Using Time-Resolved Particle Image Velocimetry Visualisation, Hot Wire Anemometry and Acoustic Signal Processing, *Experiments in Fluids*, **29**-1 Supplement (2000), 282-290.

[3] Jong, A.D. and Spruijt, M.: Particle Image Velocimetry for Quantification of High Pressure CO_2 Release, *Energy Procedia*, **37** (2013), 4682-4691.

[4] Dobrev, I. and Massouh, F.: CFD and PIV Investigation of Unsteady Flow through Savonius Wind Turbine, *Energy Procedia*, **6** (2011), 711-720.

[5] Saleh, S., Thovert, J.F. and Adler, P.M.: Measurement of Two-Dimensional Velocity Fields in Porous Media by Particle Image Displacement Velocimetry, *Experiments in Fluids*, **12**-3 (1992), 210-212.

[6] Yu, L.M., Zeng, A.W. and Yu, K.T.: Effect of Interfacial Velocity Fluctuations on The Enhancement of the Mass-Transfer Process in Falling Film Flow, *Industrial & Engineering Chemistry Research*, **45**-3 (2006), 1201-1210.

[7] Ju, J., Yamagata, Y., Inoue, K. and Higuchi, T.: A Study on Atomization Characteristics of Surface Acoustic Wave Atomizer using Laser Doppler Anemometry, *Service Robotics and Mechatronics*, (2010), 309-312.

[8] Albrecht, H.E., Borys, M. and Fuchs, W.: The Cross Sectional Area Difference Method-A New Technique for Determination of Particle Concentration by Laser Doppler Anemometry, *Experiments in Fluids*, **16**-1 (1993), 61-69.

[9] Luo, R. and Wang, L.: Liquid Flow Pattern around Taylor Bubbles in an Etched Rectangular Microchannel, *Chemical Engineering and Research Design*, **90**-8 (2012), 998-1010.

[10] Bress, T.J. and Dowling, D.R.: Particle Image Velocimetry in Molten Plastics, *Polymer Engineering and Science*, **51**-4 (2011), 730-745.

[11] Popovich, A.T. and Hummel, R.L.: A New Method for Non-Disturbing Turbulent Flow Measurements Very Close to a Wall, *Chemical Engineering Science*, **22**-1 (1967), 21-25.

[12] Popovich, A.T. and Hummel, R.L.: Experimental Study of the Viscous Sublayer in Turbulent Pipe Flow, *AlChE Journal*, **13**-5 (1967), 854-860.

[13] Johnson, G. and Marschall, E.: On the Temperature Jump in Liquid-Liquid Direct-Contact Heat Exchangers, *International Journal of Multiphase Flow*, **12**-1 (1986), 127-133.

[14] Kawaji, M.: Two-Phase Flow Measurements Using a Photochromic Dye Activation Technique, *Nuclear Engineering Design*, **184** (1998), 379-392.

[15] Homescu, D. and Desevaux, P.: Laser Photochromic Dye Activation Technique for the Measurement of Liquid Free Surface Velocity on the Curved Surfaces, *Optics and Lasers in Engineering*, **41** (2004), 879-888.

[16] Park, H., Moore, J.A. Trass, O. and Ojha M.: Laser Photochromic Velocimetry Estimation of the Vorticity and Pressure Field Two-Dimensional Flow in a Curved Vessel, *Experiments in Fluids*, **26** (1999), 55-62.

[17] Kai, T., Kanda, T., Takahashi, T. and Kawaji, M.: Application of Photochromic Dye to the Measurement of Particle Movement in a Fluidized Bed, *Powder Technology*, **129** (2003), 22-29.

[18] Sanada, T., Shirota, M. and Watanabe, M.: Bubble Wake Visualization by Using Photochromic Dye, *Chemical Engineering Science*, **62** (2007), 7264-7273.

[19] Fogwell, T.W. and Hope, C.B.: Photochrome Dye Tracing in Water Flows, *Experimental Heat Transfer*, **1**-2 (1987), 141-154.

Chapter 2

Laser tagging method by photochromic dye

2.1 Principle of the laser tagging method

The main role in implementing the laser tagging method in this study comes from the reversible transformation called as photochromism. Briefly said, photochromism refers to a reverseble color change of transparent liquid containing photochromic dye when exposed to light resource such as UV light.

The photochromism can be described as a reversible transformation of a chemical species between two forms triggered by electromagnetic radiation in the wavelengths area of light resource such as UV light. The color change is resulted from the breakup C-O bonding of the dye molecules once irradiated to the UV light. There are two kinds of photochromic dye widely applied in the research fields, i.e. spirooxazine (SO) and spiropyran (SP) types. As shown in **Fig. 2-1**, the broke up C-O bonding in the chemical structure represents the merocyanine form of the dye in the colored state [1]. The color change is induced by the change of light absorption spectrum in the photochromic dye upon UV light irradiation. As can be seen in **Fig. 2-2**, the absorption band of photochromic dye from invisible ray area (solid curve) was found to appear in the visible ray area (broken curve) under UV exposure [2]. Thus, the dye solution will be seen in a colored state.
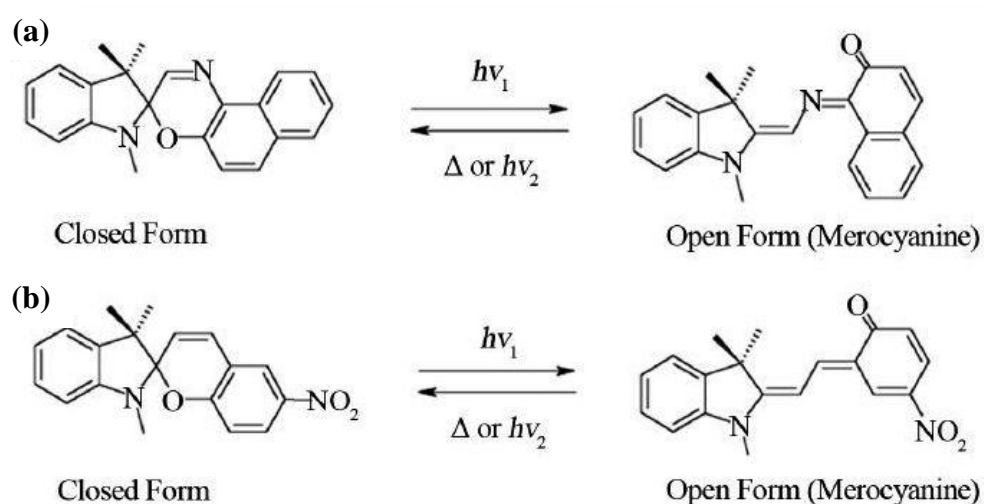

(a)

Closed Form   Open Form (Merocyanine)

(b)

Closed Form   Open Form (Merocyanine)

Fig. 2-1 Chemical structure of **(a)** SO type and **(b)** SP type photochromic dye under UV light irradiation [1]
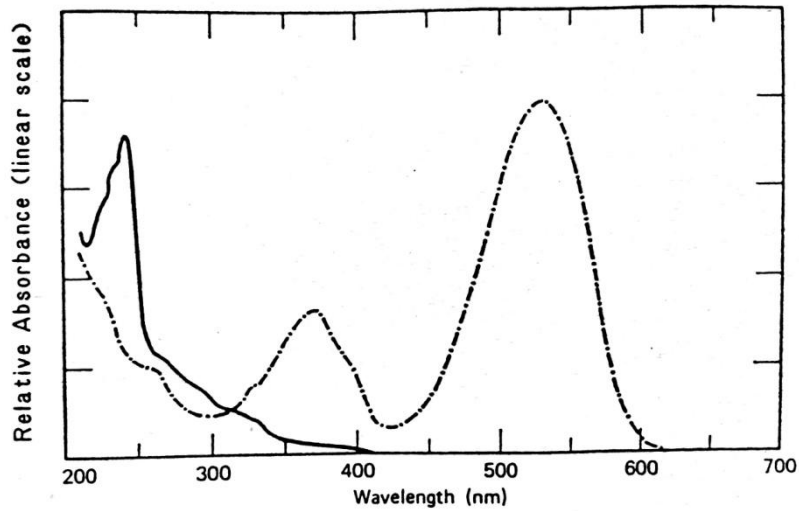
Fig. 2-2   Absorption spectrum of photochromic dye without UV light exposure (solid
curve) and with UV light exposure (broken curve) **[2]**

The SP type of photochromic dye was the most preferred by many researchers **[3]**,
[4], **[5]**, **[6]**, **[7]**, **[8]**, **[9]**, **[10]**, **[11]**, **[12]**. The superiority of SP dye lies in their high
sensitivity to UV light as well as capability of presenting sharp color change.
Photochromic dye solution usually takes within less than 3μs **[2]**, **[5]**, **[8]** to change into
colored state under UV light exposure and the color will remain in several seconds after
the UV light is removed.

2.2   Application in this research

2.2.1   Preparation of working fluid

We used the photochromic dye from SP type of
1'3'3-trimethylindolino-6'-nitrobenzopyryospiran (TNSB) in all experiments of
creeping flow, liquid sheet spray and falling liquid film. This type of dye has been
selected by several researchers **[4]**, **[6]**, **[9]**, **[10]**, **[11]**, **[12]** due to its wide applicable to
various kinds of liquid such as kerosene, toluene, xylene, benzene, acetone and many
more. The only demerit of using TNSB dye lies in its inability to be dissolved in the
water **[2]**.

In the experiment of creeping flow, the TNSB dye was dissolved in kerosene with
concentration of about 0.02wt%. In the experiments of liquid sheet spray and falling
liquid film, the TNSB dye was dissolved in kerosene with concentration of about

0.12wt%. This concentration of the dye is sufficient to yield a vivid colored state of working fluid when irradiated by UV light. **Fig. 2-3** shows the photographs of the color change occurred in kerosene when exposed to the UV light. As can be seen, the kerosene obviously turns into dark blue-purple color state from its initial colorless state under the UV light exposure. **Table 2-1** shows the physicochemical property of kerosene oil **[13]**.

(a)   **(b)**
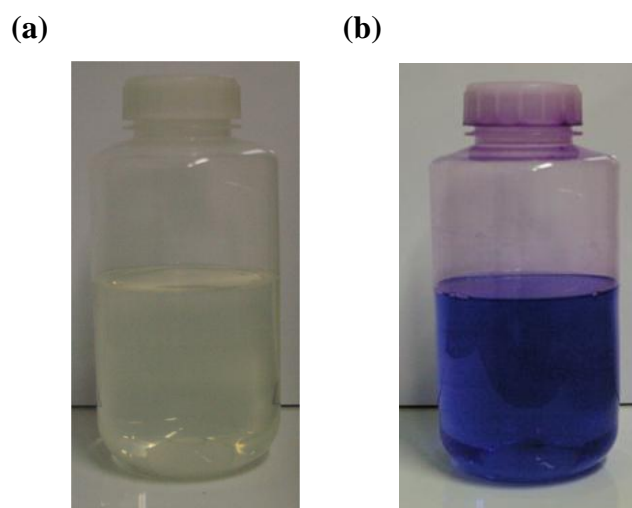
Fig. 2-3   Photochromic dye solution **(a)** before UV light exposure and **(b)** after UV light exposure

Table 2-1   Physicochemical property of kerosene oil **[13]**

Characteristics	Value
Specific gravity	0.7879
API gravity	48.091
Kinematic viscosity cSt @ 100 F	2.1808
Aniline point (°C)	58
Flash point (°C)	42
Ash contents (wt%)	0.002
Conradson carbon residue (wt%)	0.13
Total sulfur (wt%)	0.0542

2.2.2　Ultraviolet light source

In this study, another important role in achieving photochromic dye formation on the liquid film is the UV light irradiation. In the experiments of creeping flow, the UV light was sourced from a KrF excimer laser with wavelength, $\lambda=248$nm. It was a vacuum UV range that able to form the photochromic dye traces on the liquid surface.

In the experiments of liquid sheet spray and falling liquid film, the UV light was sourced from a Nd: YAG laser. Nonlinear crystals of beta barium borate (BBO) crystals were placed on the laser beam in order to derive the third harmonic light with wavelength, $\lambda=355$nm. The illustration of optical arrangement to produce the light is shown in **Fig. 2-4**.

Specifically, the first BBO crystal was used to extract the second harmonic light with wavelength, $\lambda=532$nm from the fundamental light with wavelength, $\lambda=1064$nm. The second BBO crystal then extracted the first and second harmonic lights into the desired third harmonic light with wavelength, $\lambda=355$nm. Furthermore, a harmonic separator was also used to reflect the unwanted first and second harmonic lights.

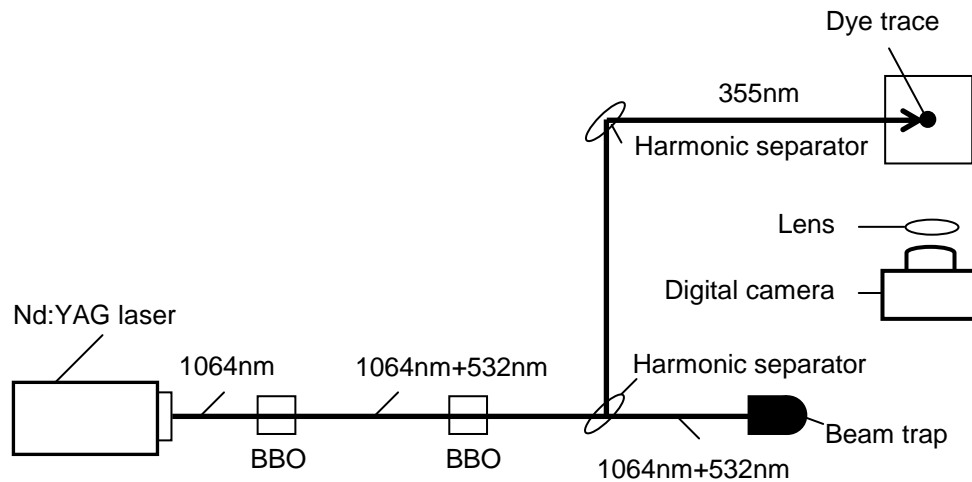**Fig. 2-4**　Illustration of optical arrangement for UV light production from Nd: YAG laser

2.2.3　Estimation of flow velocity and deformation

Each trace point in the 4-points of dye traces was assumed to move along with the liquid flow. From the digitized data of the dye trace images, the displacement over consecutive frames can be divided by the time elapsed to calculate the velocity of the dye trace. In

specifically, the local velocity V of each traces moving through a displacement ΔX during a time interval Δt is described by the below equation:

$$V = \frac{\Delta X}{\Delta t} \qquad (2\text{-}1)$$

The u and v are the velocity components of x direction and y direction of velocity vector, V. Thus, the normal strain rate, ε_x and ε_y are given as:

$$\varepsilon_x = \frac{\partial u}{\partial x} \qquad (2\text{-}2)$$

$$\varepsilon_y = \frac{\partial v}{\partial y} \qquad (2\text{-}3)$$

In the case of incompressible two-dimensional flow, the equation of continuity is described as:

$$\frac{\partial u}{\partial x} + \frac{\partial v}{\partial y} = \varepsilon_x + \varepsilon_y = 0 \qquad \text{or} \qquad \nabla \cdot V = \operatorname{div} V = 0 \qquad (2\text{-}4)$$

where, ∇ represents the two-dimensional nabla operator. Therefore, in the use of two-dimensional flow, $\varepsilon_x + \varepsilon_y = 0$.

The liquid sheet can be assumed as approximately two-dimensional flow. In the case of liquid sheet thickness change with the deformation in two-dimensional direction, the normal strain rate in the thickness direction, ε_z can be defined as below equation using the equation of continuity:

$$\varepsilon_z = \frac{\partial w}{\partial z} = -\left(\frac{\partial u}{\partial x} + \frac{\partial v}{\partial y} \right) = -\left(\varepsilon_x + \varepsilon_y \right) \qquad (2\text{-}5)$$

The shear strain rate, γ can be defined as:

$$\gamma = \frac{\partial v}{\partial x} + \frac{\partial u}{\partial y} \qquad (2\text{-}6)$$

and the vorticity, ω can be defined as:

$$\omega = \frac{\partial v}{\partial x} - \frac{\partial u}{\partial y}$$

(2-7)

As described here, the strain rate and vorticity are usually defined by using the partial differential. However, in the case of the velocity measurement, the differentiation causes the large errors because the large value is divided by very small value. Therefore, we used the integral method for the estimation of strain rate and vorticity [see Appendix].

There are the integral theorems of vector fields known as Green's theorem, Gauss' theorem, and Stokes' theorem. Although these theorems are commonly manifested as transformation formula of volume integral and surface integral in tree-dimensional space, they are also applicable as transformation formula between the surface integral and line integral over two-dimensional space.

Figure 2-5 shows a plane region S bounded by the closed line C formed by the 4-points of dye traces. If we consider small linear element dl on the line C, the outward-pointing normal vector is expressed as $\boldsymbol{n}$, its x and y direction component is expressed as n_x and n_y.
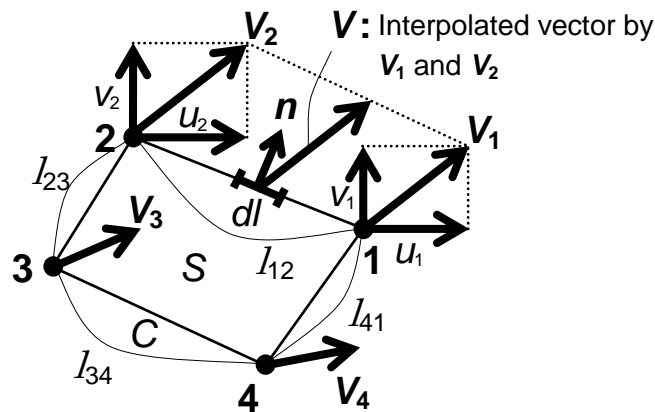

Fig. 2-5 Plane region S bounded by the closed line C formed by the 4-points of dye traces

Here, the Green's theorem over the arbitrary function $f(x,y)$ is given as:

$$\iint_S \frac{\partial f}{\partial x} dS = \oint_c f n_x dl$$

(2-8)

20

$$\iint_S \frac{\partial f}{\partial y} dS = \oint_c f n_y \, dl$$

(2-9)

Here, by setting $f=u$ in **Eq. (2-8)** and $f=v$ in **Eq. (2-9)**, i.e. the u and v direction component of the velocity V for the dye traces as shown in **Fig. 2-5**,

$$\iint_S \frac{\partial u}{\partial x} dS = \oint_c u n_x \, dl$$

(2-10)

$$\iint_S \frac{\partial v}{\partial y} dS = \oint_c v n_y \, dl$$

(2-11)

are derived. Although these equations represent the integration by area S of normal strain rate, ε_x and ε_y of **Eq. (2-2)** and **Eq. (2-3)**, they actually shows the line integral by closed line C surrounding it. Here, the average normal strain rate, $\bar{\varepsilon}_x$ and $\bar{\varepsilon}_y$ can be obtained as:

$$\bar{\varepsilon}_x = \frac{1}{S} \iint_S \frac{\partial u}{\partial x} dS = \frac{1}{S} \oint_c u n_x \, dl$$

(2-12)

$$\bar{\varepsilon}_y = \frac{1}{S} \iint_S \frac{\partial v}{\partial y} dS = \frac{1}{S} \oint_c v n_y \, dl$$

(2-13)

Line integral of **Eq. (2-12)** and **Eq. (2-13)** may be replaced as the following simple formula as below:

$$\bar{\varepsilon}_x \cong \frac{1}{S} \oint_c u n_x \, dl = \frac{1}{S} \sum_{(ij)=(12,23,34,41)} \frac{u_i + u_j}{2} n_{xij} l_{ij}$$

(2-14)

$$\bar{\varepsilon}_y \cong \frac{1}{S} \oint_c v n_y \, dl = \frac{1}{S} \sum_{(ij)=(12,23,34,41)} \frac{v_i + v_j}{2} n_{yij} l_{ij}$$

(2-15)

where, we assumed that the closed line C was formed by 4-points of dye traces. Moreover, u_i, u_j and v_i, v_j are, respectively the x and y direction velocity measurements of point i and j. n_{xij} and n_{yij} are, respectively the x and y components of normal vector on line between i and j. l_{ij} is a length between point i and j.

By summing **Eq. (2-10)** and **Eq. (2-11)**, the following equation is derived.

$$\iint_S \left(\frac{\partial u}{\partial x} + \frac{\partial v}{\partial y} \right) dS = \oint_c \left(un_x + vn_y \right) dl \tag{2-16}$$

Here, the integrand of right-hand side is given as:

$$un_x + vn_y = v_n \tag{2-17}$$

where, v_n is the magnitude of the normal vector, $\boldsymbol{n}$ on the small line segment dl. Thus, the **Eq. (2-16)** can be written as:

$$\iint_S \left(\frac{\partial u}{\partial x} + \frac{\partial v}{\partial y} \right) dS = \oint_c v_n dl \tag{2-18}$$

This equation is also known as divergence theorem of Gauss. Similarly, the average normal strain rate in the thickness direction, $\bar{\varepsilon}_z$ of **Eq. (2-5)** can be obtained as:

$$\overline{\varepsilon}_z = -\frac{1}{S} \iint_S \left(\frac{\partial u}{\partial x} + \frac{\partial v}{\partial y} \right) dS = -\frac{1}{S} \oint_c v_n dl$$

$$= -\frac{1}{S} \sum_{(ij)=(12,23,34,41)} \frac{v_{ni} + v_{nj}}{2} l_{ij} \tag{2-19}$$

Next, by setting $f = v$ in **Eq. (2-8)** and $f = u$ in **Eq. (2-9)**, the following equations are derived:

$$\iint_S \frac{\partial v}{\partial x} dS = \oint_c vn_x dl \tag{2-20}$$

$$\iint_S \frac{\partial u}{\partial y} dS = \oint_c un_y dl \tag{2-21}$$

By summing the **Eq. (2-20)** and **Eq. (2-21)**, the following equation is derived.

$$\iint_S \left(\frac{\partial v}{\partial x} + \frac{\partial u}{\partial y} \right) dS = \oint_c \left(vn_x + un_y \right) dl \tag{2-22}$$

The left-hand side represents the surface integral of shear strain rate, γ. Thus, the average shear strain rate $\bar{\gamma}$ can be obtained as:

$$\bar{\gamma} = \frac{1}{S}\iint_S \left(\frac{\partial v}{\partial x} + \frac{\partial u}{\partial y}\right) dS = \frac{1}{S}\oint_c \left(vn_x + un_y\right) dl$$

$$= \frac{1}{S}\sum_{(ij)=(12,23,34,41)} \left(\frac{v_i+v_j}{2}n_{xij} + \frac{u_i+u_j}{2}n_{yij}\right)l_{ij}$$

(2-23)

By subtracting **Eq. (2-21)** from **Eq. (2-20)**, the below equation is given.

$$\iint_S \left(\frac{\partial v}{\partial x} - \frac{\partial u}{\partial y}\right) dS = \oint_c \left(vn_x - un_y\right) dl$$

(2-24)

Here, the normal vector, $\boldsymbol{n}$ is given as:

$$n = \left(n_x, n_y\right) = \left(\frac{dy}{dS}, -\frac{dx}{dS}\right)$$

(2-25)

Thus, the integrand of right-hand side is given as:

$$vn_x - un_y = v\frac{dy}{dS} + u\frac{dx}{dS}$$

(2-26)

Unit tangent vector, $\boldsymbol{t}$ is given as:

$$t = \left(t_x, t_y\right) = \left(\frac{dx}{dS}, -\frac{dy}{dS}\right)$$

(2-27)

By using unit tangent vector, $\boldsymbol{t}$ into **Eq. (2-26)**, below equations is derived.

$$vn_x - un_y = vt_y + ut_x = v_t = \boldsymbol{v}\cdot\boldsymbol{t}$$

(2-28)

Here, v_t represents the tangent direction component of velocity vector, $\boldsymbol{V}$. Thus, the **Eq. (2-24)** can be written as:

$$\iint_s \left(\frac{\partial v}{\partial x} - \frac{\partial u}{\partial y} \right) dS = \oint_c v_t \, dl \tag{2-29}$$

This equation is called as two-dimensional Stokes' theorem. The left-hand side represents the surface integral of vorticity, ω. Thus, the average vorticity $\bar{\omega}$ can be obtained as:

$$\bar{\omega} = \frac{1}{S} \iint_s \left(\frac{\partial v}{\partial x} - \frac{\partial u}{\partial y} \right) dS = \frac{1}{S} \oint_c v_t \, dl$$

$$= \frac{1}{S} \sum_{(ij)=(12,23,34,41)} \frac{v_{ti} + v_{tj}}{2} l_{ij} \tag{2-30}$$

Thus, the average area of normal strain rate, shear strain rate and vorticity can be obtained from the linear integral of closed line C. The calculation accuracy by using the integral method was confirmed (see Appendix).

References

[1] Bonefacino, J., Tse, M.L.V., Pun, C.F.J., Cheng, X., Chan, W.K.E., Boersma, A. and Tam, H.Y.: Characterization of Spirooxazine and Spiropyran Hosted in Poly(Methyl Methacrylate) for Germicidal UV Source Indicator Application, *Optics and Photonics Journal*, **12**-1 (2013), 11-16.

[2] Fogwell, T.W. and Hope, C.B.: Photochrome Dye Tracing in Water Flows, *Experimental Heat Transfer*, **1**-2 (1987), 141-154.

[3] Wagner, N. and Theato, P.: Light-Induced Wettability Changes on Polymer Surfaces, *Optics and Lasers in Engineering*, **55** (2014), 3436-3453.

[4] Sanada, T., Shirota, M. and Watanabe, M.: Bubble Wake Visualization by Using Photochromic Dye, *Chemical Engineering Science*, **62** (2007), 7264-7273.

[5] Homescu, D. and Desevaux, P.: Laser Photochromic Dye Activation Technique for the Measurement of Liquid Free Surface Velocity on the Curved Surfaces, *Optics and Lasers in Engineering*, **41** (2004), 879-888.

[6] Ishiwatari, T., Kondo, T. and Mitsuishi, M.: Photochromism of Spirobenzopyran in the Membrane of Surfactant Vesicle and in the Cavity of Cyclodextrins, *Colloid and Polymer Science*, **274** (1996), 1000-1005.

[7] Zolotorofe, D.L. and Scheele, G.F.: Photochromic Dye Tracer Measurements of Small Liquid Velocities, *Industrial & Engineering Chemistry Fundamentals*, **9**-2 (1970), 291-293.

[8] Popovich, A.T. and Hummel, R.L.: A New Method for Non-Disturbing Turbulent Flow Measurements Very Close to a Wall, *Chemical Engineering Science*, **22**-1 (1967), 21-25.

[9] Lin, J.S.: Interaction between Dispersed Photochromic Compound and Polymer Matrix, *European* Polymer Journal, **39** (2003), 1693-1700.

[10] Park, H., Moore, J.A. Trass, O. and Ojha M.: Laser Photochromic Velocimetry Estimation of the Vorticity and Pressure Field Two-Dimensional Flow in a Curved Vessel, *Experiments in Fluids*, **26** (1999), 55-62.

[11] Kai, T., Kanda, T., Takahashi, T. and Kawaji, M.: Application of Photochromic Dye to the Measurement of Particle Movement in a Fluidized Bed, *Powder Technology*, **129** (2003), 22-29.

[12] Kawaji, M.: Two-Phase Flow Measurements Using a Photochromic Dye Activation Technique, *Nuclear Engineering Design*, **184** (1998), 379-392.

[13] Ahmad, W., Ahmad, I., Ishaq, M. and Ihsan, K.: Adsorptive Desulfurization of Kerosene and Diesel Oil by Zn Impregnated Montmorollonite Clay, *Arabian Journal of Chemistry*, In press (2014).

Chapter 3

Application to creeping flow around moving cylinder

3.1   Introductory remarks

A lot of research related to the study of liquid flow behavior has been conducted in the past. In order to enhance the operating performance of machine such as the heat exchanger in largest equipment of energy facilities to the smallest device of micro-reactor, the study of liquid flow behavior has been extensively applied in various industrial fields. Until now, numerous measurement techniques have been developed in order to investigate the flow characteristics in those equipments.

Through our survey, quite quantitative works [1], [2], [3], [4], [5], [6] have been dedicated to clarify the liquid flow behavior in micro-channel. For example, Ngoma and Erchiqui [7] through their mathematical calculation investigated the effects of slip coefficient and heat flux on the liquid flow in between two plates of micro-channel. They confirmed that the liquid flow behavior in the micro-channel significantly affected by the slip coefficient, pressure difference, heat flux, electro-kinetic separation imposed to the liquid but in various ways of affection.

On the other hand, Kawahara et al. [8] conducted their experimental work to investigate the effects of various liquid properties on adiabatic two-phase flows in a micro-channel. Among their findings, bubble in the micro-channel with contraction flow was found to elongate and rapidly flow and thus causing the reduction in the void fraction. Another experiment of bubble in micro-channel was done by Luo and Wang [9] through their 3D-PIV system. Through their experimental test, the measurement accuracy was slightly affected since the seeding particles stuck around the walls of the micro-channel.

The measurement method of PIV has been developed time to time to enhance its application in various liquid flow fields not only in relatively large scale of flow, but also in the thin micro-channel and thin liquid film flow. However, the limitations that usually caused by the seeding particles is inevitable. As an alternative technique to clarify the flow behavior of liquid film in various flow fields, laser tagging method using photochromic dye tracer is developed.

In this study, we applied the laser tagging method to study the creeping flow of moving cylinder in a rectangular channel with the aim to evaluate its applicability in the flow field measurement.

3.2 Objective of this experiment

The purpose of this experiment is to assess the applicability of laser tagging method by photochromic dye tracer to the measurement of fluid flow. The experiment is carried out to visualize the creeping flow around a moving cylinder. From the movement of the dye traces, the velocity profiles of the creeping flow in the rectangular cavity are measured. The dye traces are formed in a dot matrix shape to allow vorticity and divergence characteristics of flow field.

3.3 Methodology

3.3.1 Experimental setup and procedure

Figure 3-1 shows the schematic view of the experimental setup for the creeping flow experiment. We generated the flow test by using a circular cylinder with diameter, d_c=10mm placed in a channel (length=190mm, width=50mm, depth=20mm) and connected to a movable stand. The circular cylinder was moved by the movable stand with a constant velocity, V_c=18.8mm/s. The depth of the liquid was approximately 15mm.

Above the channel, UV laser light (λ=248nm) sourced from a KrF Excimer laser was irradiated to the liquid film surface to activate the photochromic dye traces. The laser light was possible to be irradiated around the moving cylinder by using the laser tagging method. However, the irradiation timing must be controlled accurately. In order to achieve the closest visualization of wake flow around the cylinder, we irradiated the laser light around 4mm from the cylinder edge. The laser pulse was 17ns in duration and 450mJ/pulse in energy.

Furthermore, a 20mm×20mm screen plate composed of arrayed holes (diameter= 0.5mm, pitch= 2mm) was placed on the laser light path to form a set of dot matrix dye traces. A cylindrical lens was placed before the screen on the light path to expand the irradiation range of the UV light. Moreover, a halogen lamp was used as the lighting source to assist the visualization of the dye traces movement.

The traces images were then captured by CCD camera and recorded by a video camera recorder (SONY's DCR-TRV20) with 30fps at 3008×2000 pixel resolution. Thus, the spatial resolution of actual space and temporal resolution were respectively, 17μm and 0.03s. The motion pictures were then transferred to a still image data for analysis. The images were changed to the binary images in order to enhance the contrast between liquid and dye traces. The position of the each dye trace was determined by digitizing their coordinates.
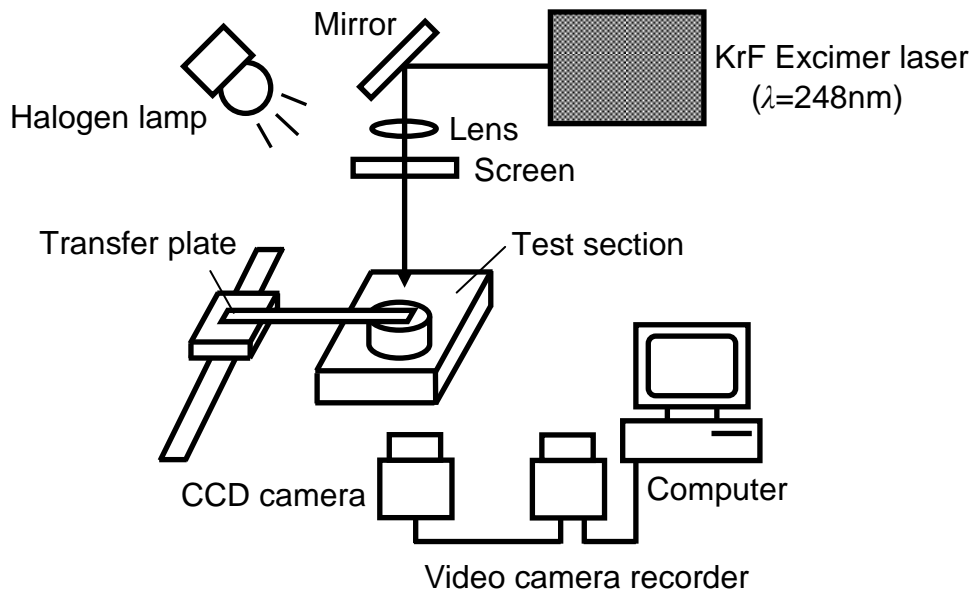

Fig. 3-1   Schematic view of experimental setup for creeping flow experiment

3.3.2   **Experimental condition**

The Reynolds number, *Re* is defined by the following equation:

$$Re = \frac{\rho V_c d_c}{\eta} \tag{3-1}$$

where, ρ is the density, V_c is the cylinder velocity, η is the dynamic viscosity of the working fluid and d_c is the cylinder diameter. The experiment was conducted at three positions in *x*-axis around the cylinder, i.e. -15mm<*x*<10mm, 10mm<*x*<15mm and 25mm<*x*<30mm. The cylinder was moved in negative direction of *x*-axis. The Reynolds number, *Re* was fixed at 61 (cylinder velocity, V_c=18.8mm/s). The experiment was done at room temperature, T_e= 20~22 °C.

3.4 Results and discussion

3.4.1 Velocity and vorticity distributions

The data recorded by the video camera was changed to a binary image in order to get a high contrast between the liquid and the dye traces. **Fig. 3-2** shows the sample image of dye traces formed in the creeping flow. The dark points in the image represent the dye traces formed by the UV light from the KrF excimer laser irradiation.
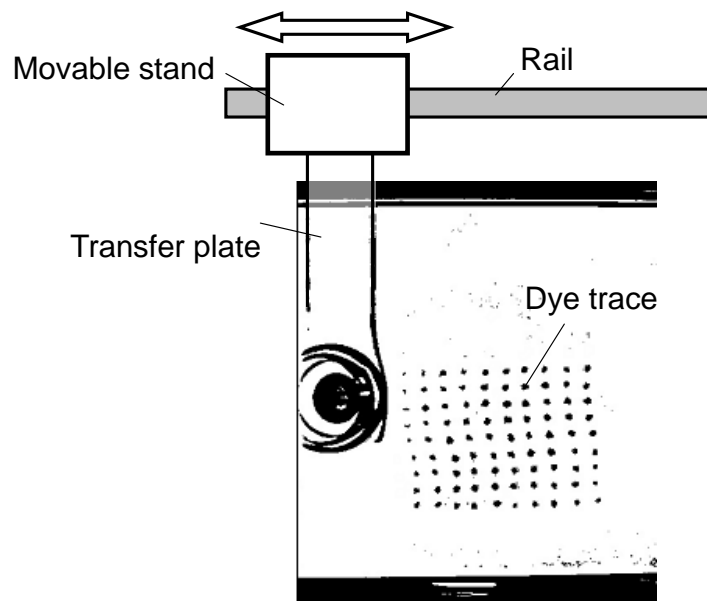

Fig. 3-2   Sample image of dye traces formed in the creeping flow

Figure **3-3(a)** shows the visualization image of the cylinder wake. In order to visualize the flow pattern, white paint was painted around the cylinder wake. As can be seen, a pair of eddy formation obviously appeared only in the rear part of the moving cylinder. Furthermore, since the depth of dye traces formed by the excimer laser irradiation was approximately 2mm, the measurement in this experiment was limited only to the surface area. However, the flow pattern of cylinder wake still can be visualized because the cylinder wake was a two-dimensional flow field.

Figure **3-3(b)** and **Fig. 3-3(c)** respectively show the results of velocity and vorticity distributions. As can be seen, the eddy structure as shown in **Fig. 3-3(b)** appeared around the same region in **Fig. 3-3(a)**. On the other hand, the vorticity as shown in **Fig. 3-3(c)** appeared around the center of the eddy structure.
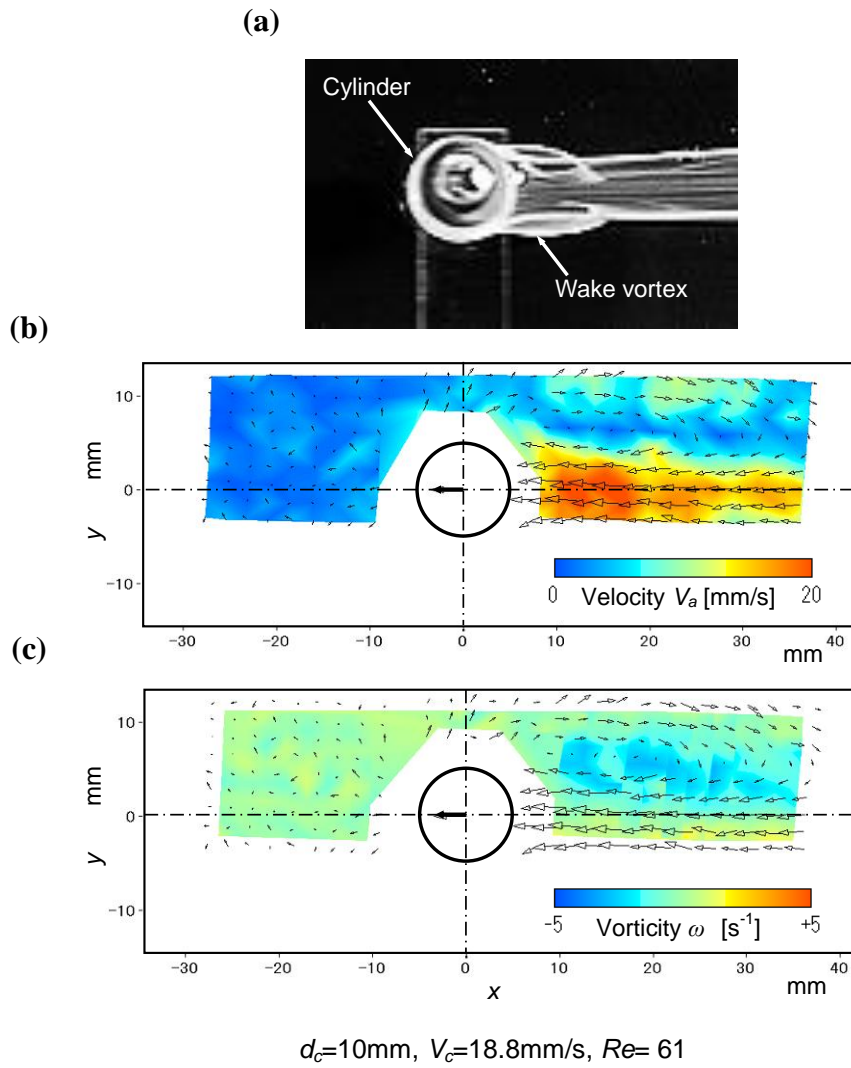
(a)

(b)

(c)

d_c=10mm, V_c=18.8mm/s, Re= 61

Fig. 3-3   Visualization result of **(a)** cylinder wake flow pattern with **(b)** velocity and **(c)** vorticity distributions
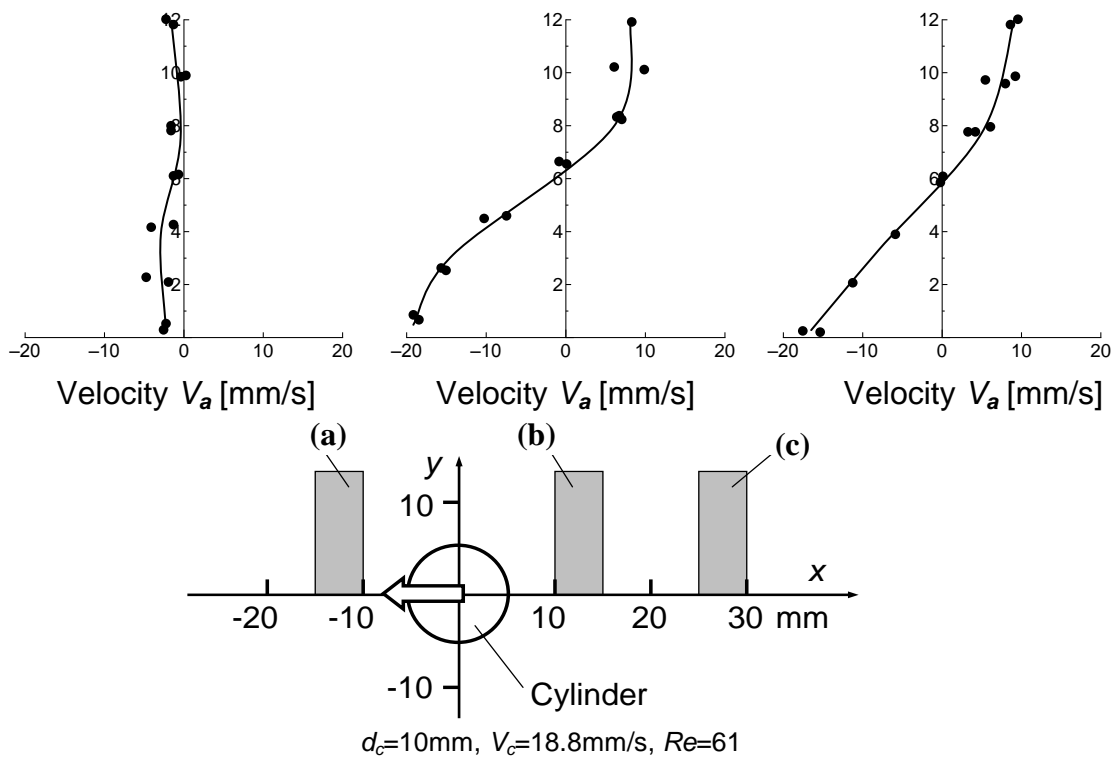
Fig. 3-4 Distributions of *x*-component velocity at **(a)** -15mm<*x*<-10mm, **(b)** 10mm<*x*<15mm and **(c)** 25mm<*x*<30mm
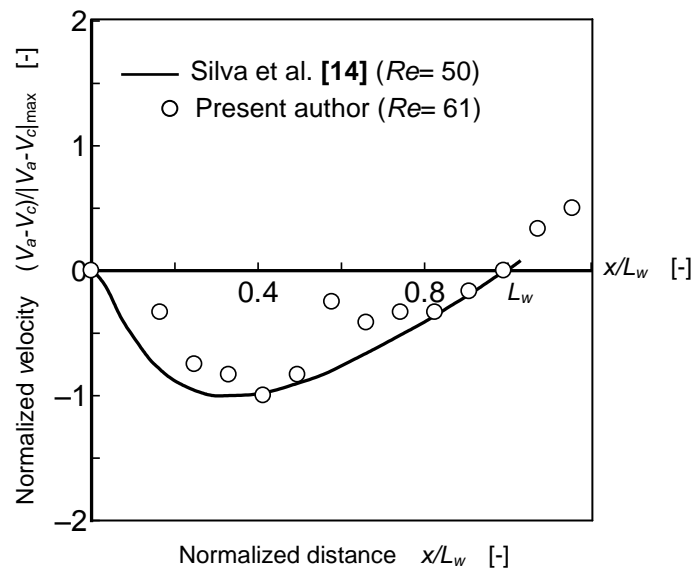

Fig. 3-5 Comparison of normalized velocity profiles between data of author and previous literature **[14]**

Figure 3-4 shows the distributions of *x*-component velocity in the cross-section of *y*-direction at three positions on *x*-axis, i.e. -15mm<*x*<-10mm, 10mm<*x*<15mm and 25mm<*x*<30mm. As can be seen, a very weak flow appeared in the negative area of *x*-axis in the liquid film. This indicates that not only in the rear part, the cylinder that moved in the negative direction in the channel still can induce the liquid flow at the cylinder front.

In the case of 10mm<*x*<15mm, the negative velocity appeared to decrease and settle down at approximately *y*=6.5mm from the center line of *x*-axis. This value indicates that it was the center point of the eddy occurred in the cylinder wake, where the velocity is normally zero. Moreover, flow velocity around the centerline of *x*-axis was found approximately 19mm/s, which is almost near to the cylinder velocity. A similar trend also appeared in the case of 25mm<*x*<30mm, but the absolute values of velocity were slightly lower.

In order to confirm the validity of data of present experiment, it is needed to compare the cylinder wake velocity with previous literature. Many research works of flow around cylinder have been done in numerical simulations **[10]**, **[11]**, **[12]**, **[13]**, **[14]**, **[15]**, **[16]**, **[17]**. According to our survey, there was no previous works that conducting the same value of Reynolds number as applied in our study. However, most of the studies in the past **[11]**, **[12]**, **[13]**, **[14]**, **[15]** were found to be done by calculating the length of wake vortex in the cylinder wake, L_w.

Here, the data of present study was compared to the data of Silva et al. **[14]** based on the length of wake vortex calculation done by Taneda's experiment **[11]**. In the study of Silva et al. **[14]**, they simulated an internal channel flow and the creeping flow around of a stationary cylinder. In order to confirm their numerical simulation, they used the Physical Virtual Model (PVM) method which was based on the force field calculation applied into two-dimensional Navier-Stokes Equations. The equations were then discretized by using the finite differences method.

Since the value of Reynolds number applied by the study of Silva et al. **[14]** and our study were different, the data of the closest Reynolds number, i.e. *Re*=50 owned by Silva et al. **[14]** was normalized and compared with the data of present study as shown in **Fig. 3-5**. This figure shows the velocity profiles on the centerline of *x*-axis normalized by the length of wake vortex. As a result, quite a good agreement between both studies was found. The mismatch of few data shown in the results comparison can be attributed to several reasons. Firstly, it may be caused by the fact that experiment conducted in the present study was done in a cavity. Furthermore, the experiments of present study were done in quite a short timing for the data to be taken. Therefore, the

wake vortex resulted in the experiments were actually just started and still not completely formed.

3.4.2 Vorticity and divergence profiles

The vorticity profiles were derived by using the **Eq. (2-7)** in chapter 2. **Fig. 3-6** shows the vorticity profiles against the distance from centerline y. As shown in the figure, the vorticity found in the case of -15mm$<x<$-10mm was distributed around zero. This suggests that the rotational motion in that region was very weak. In the case of 10mm$<x<$15mm, the negative value of vorticity appeared around 0mm$<y<$10mm. This indicates the scale of eddy formation in the cylinder wake. The maximum absolute value of vorticity appeared around $y=6.0$mm, which is close to the position of velocity settled down in **Fig. 3-4**.
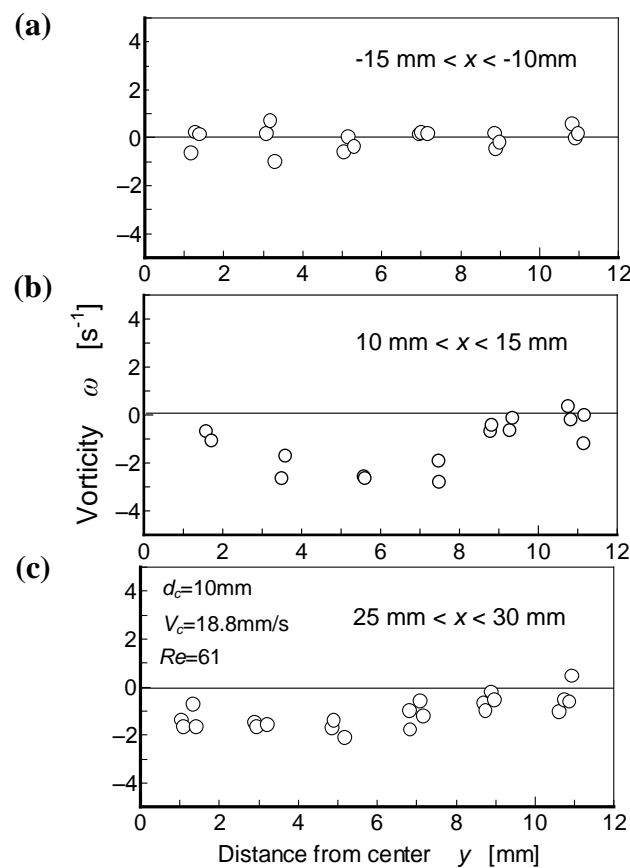

Fig. 3-6 Vorticity profiles at **(a)** -15mm$<x<$-10mm, **(b)** 10mm$<x<$15mm and **(c)** 25mm$<x<$30mm

In the case of 25mm<x<30mm, the vorticity was found to gradually decrease than that in the previous region. The maximum absolute value was found approximately 3s^{-1} and the variability of the result was about 1.5s^{-1}. Therefore, the accuracy of the vorticity result can be estimated as 50%. The divergence profiles were derived by using the **Eq. (2-4)** in chapter 2 in order to evaluate the accuracy of integral method introduced in this study. **Fig. 3-7** shows the divergence profiles against the distance from centerline. In all cases, the divergences were found to distribute around zero. Since the creeping flow of moving cylinder was a two-dimensional incompressible fluid flow, the divergence of velocity field is indeed always zero.
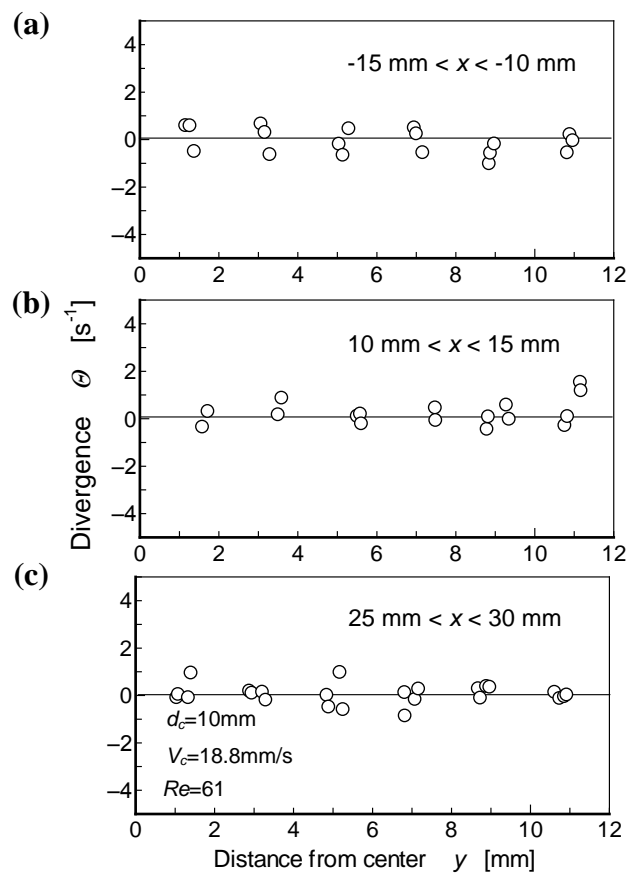

Fig. 3-7 Divergence profiles at **(a)** -15mm<x<-10mm, **(b)** 10mm<x<15mm and **(c)** 25mm<x<30mm

3.5 Summaries

The experiment was conducted in order to ensure the applicability of laser tagging method using photochromic dye tracer on the measurement of liquid film flow. The experiment was carried out to visualize the creeping flow around a moving cylinder. From the movement of the dye traces, the velocity profiles of the creeping flow were successfully measured. The reliability of laser tagging method by photochromic dye tracer was also successfully confirmed from the good agreement with the data of previous literature. The conclusions of the present experiment can be drawn as below:

1. From the dot matrix shape of dye traces formation, the vorticity and divergence characteristics were successfully derived by the laser tagging method using photochromic dye tracer.
2. The eddy formation was found merely in the cylinder wake and its velocity was close to the velocity of the cylinder.
3. The divergence profiles at various positions were found to distribute around zero.

References

[1] Sharma, D., Singh, P.P. and Harry, G.: Comparative Study of Rectangular and Trapezoidal Microchannels Using Water and Liquid Metal, *Procedia Engineering*, **51** (2013), 791-796.

[2] Patsis, G.P., Ninos, K., Mathioulakis, D. and Kaltsas, G.: Simulation and Experimental Evaluation of Gas Mass Flow Transfer Rate in Microchannels, *Procedia Engineering*, **25** (2011), 447-450.

[3] Qian, D. and Lawal, A.: Numerical Study on Gas and Liquid Slugs for Taylor Flow in a T-Junction Microchannel, *Chemical Engineering Science*, **61**-23 (2006), 7609–7625.

[4] Roy, P., Anand, N.K. and Banerjee, D.: A Review of Heat Transfer in Rotating Microchannels, *Procedia Engineering*, **56** (2013), 7-17.

[5] Raimondi, N.D.M., Prat, L., Gourdon, C. and Tasselli, J.: Experiments of Mass Transfer with Liquid–Liquid Slug Flow in Square Microchannels, *Chemical Engineering Science*, **105** (2014), 169–178.

[6] Han, Y., Liu, Y., Lia, M. and Huang, J.: A Review of Development of Micro-Channel Heat Exchanger Applied in Air-Conditioning System, *Energy Procedia*, **14** (2012), 148-153.

[7] Ngoma, G.D. and Erchiqui, F.: Heat Flux and Slip Effects on Liquid Flow in a Microchannel, *International Journal of Thermal Sciences*, **46**-11 (2007), 1076-1083.

[8] Kawahara, A., Sadatomi, M., Nei, K., and Matsuo, H.: Experimental Study on Bubble Velocity, Void Fraction and Pressure Drop for Gas–Liquid Two-Phase Flow in a Circular Microchannel, *International Journal of Heat and Fluid Flow*, **30**-5 (2009), 831-841.

[9] Luo, R. and Wang, L.: Liquid Flow Pattern around Taylor Bubbles in an Etched Rectangular Microchannel, *Chemical Engineering and Research Design*, **90**-8 (2012), 998-1010.

[10] Sato, M. and Kobayashi, T.: A Fundamental Study of the Flow Past A Circular Cylinder using Abasqus/CFD, Proceeding of *2012 SIMULIA Community Conference*, 1-15.

[11] Taneda, S.: Experimental Investigation of the Wakes behind Cylinders and Plates at Low Reynolds Numbers, *Journal of the Physical Society of Japan*, **11**-3 (1956), 302-307.

[12] Hu, H.H.: Motion of a Circular Cylinder in a Viscous Liquid between Parallel Plates, *Theoretical and Computational*, **7** (1995), 441-455.

[13] Rao, A., Thompson, M.C., Leweke, T. and Hourigan, K.: The Flow Past a Circular Cylinder Translating at Different Heights above a Wall, *Journal of Fluids and Structures*, **41** (2013), 9-21.

[14] Silva, A.L.F.L.E., Silveira-Neto, A. and Damasceno, J.J.R.: Numerical Simulation of Two-dimensional Flows Over a Circular Cylinder Using the Immersed Boundary Method, *Journal of Computational Physics*, **189** (2003), 351-370.

[15] Rajani, B.N., Kandasamy, A. and Majumdar, S.: Numerical Simulation of a Laminar Flow Past a Circular Cylinder, *Applied Mathematical Modeling*, **33** (2009), 1228-1247.

[16] Zovatto, L. and Pedrizzetti, G.: Flow about a Circular Cylinder between Parallel Walls, *Journal of Fluid Mechanics*, **440** (2001), 1-25.

[17] Chatterjee, D., Chatterjee, K. and Mondal, B.: Control of Flow Separation around Bluff Obstacles by Transverse Magnetic Field, *Journal of Fluids Engineering*, **134** (2012), 1-11.

Chapter 4

Measurement of liquid sheet spray

4.1   Introductory remarks

Liquid atomization presents in many industrial fields. From pesticides spray in agricultural to internal combustion engine in transportation and power generation industry, liquid atomization system has been extensively applied as the most significant process to ensure their continuous operations.

In the internal combustion engine, for example, the fuel combustion of diesel engine plays an important role in the engine performance. However, the combustion phenomenon is strongly influenced by the spray characteristics of the fuel given by the atomization process. This has attracted attention from researchers to clarify the spray flow behavior. However, most of the studies carried out by the researchers merely described the spray characteristics caused by the atomization process. For instance, Turner et al. [1] developed a breakup model based on the injection process of liquid spray to study the transient fuel sprays evolution. Specifically through the model, the breakup time and length were clarified.

On the other hand, Rashid et al. [2] focused on the observation to the spray cone angle and the spray width generated from the inlet slots number in the spray. They found that widest liquid spray comes from the most number of inlet slots. Furthermore, Shinjo et al. [3] through their mathematical simulation investigated the disintegrated phase of liquid spray such as droplet size and vortex shedding to the turbulence and mixing behavior of solid spray area.

To our best knowledge, in order to completely understand the whole process of atomization, a detail investigation of relations between the liquid jet characteristics and breakup phenomenon is required. Although there was various measurement techniques developed by researchers [4], [5], [6], [7], [8] in the past, the methods being used sometimes present limitation that merely allow investigation for certain flow mechanism in the liquid spray. The PIV method especially is not able to precisely evaluate the spray flows which presents liquid sheet, since the irregular refraction of laser light will appear when it enter the liquid.

In order to achieve better understand the overall process of liquid spray until disintegrated to the ligament and droplet phase, an appropriate measurement technique

is critically needed. Here, we applied the laser tagging method using photochromic dye tracer to clarify the flow behavior of liquid film sheet spray as a fundamental study of the atomization phenomena. Furthermore, it is needed to acknowledge that the present experiment was conducted with lower flow rates as it is a fundamental study to know the liquid behavior prior to breakup process of liquid jet. Such exploratory from the basic element of atomization is undeniably important as it helps to validate modeling equation of numerical simulation for liquid jet in the future.

4.2   Objective of this experiment

In this experiment, the laser tagging method using photochromic dye tracer is applied for measuring velocity distribution in liquid sheet by focusing on the liquid sheet atomization as a fundamental study of the atomization phenomena. The method is developed with aim to study the breakup process of liquid sheet in detail, covering from the behavior in liquid film until disintegrated into ligament and droplets. The motions of the dye traces tagged by UV laser are analyzed as the liquid surface velocity. By forming a set of 4-points of dye traces on the liquid sheet, the change of relative position of the set enables the measurement of deformation and rotational motion. Moreover, the measurement of average thickness of the liquid sheet is also done using light absorption method. Several interesting results are obtained and discussed in detail.

4.3   Methodology

4.3.1   Experimental apparatus and procedure

Figure 4-1 shows the schematic view of experimental setup for liquid sheet spray experiment. As shown in **Fig. 4-2**, two types of liquid sheet spray were formed in this study, i.e. impingement spray and flat spray.
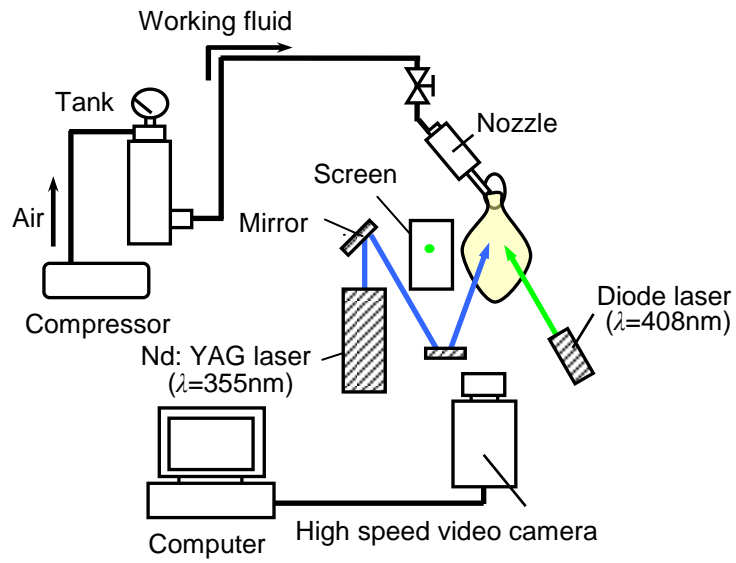
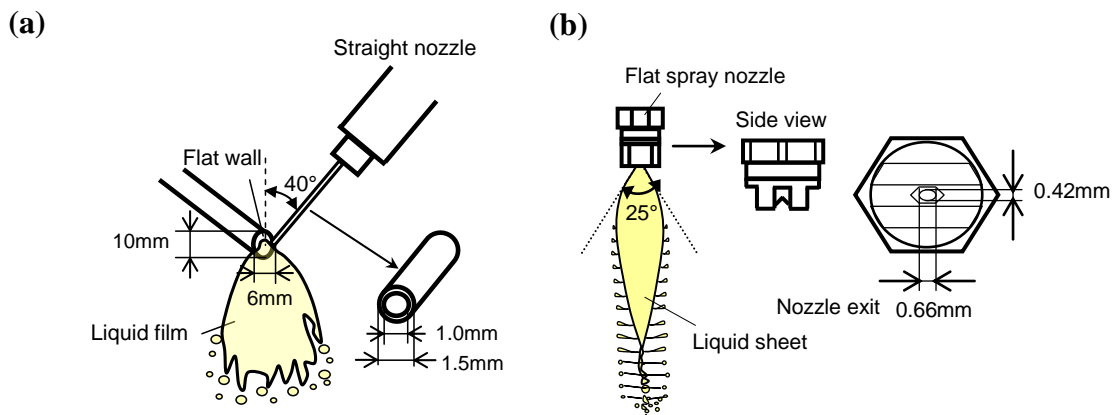**Fig. 4-1**   Schematic view of experimental setup for liquid sheet spray experiment

(a)

(b)

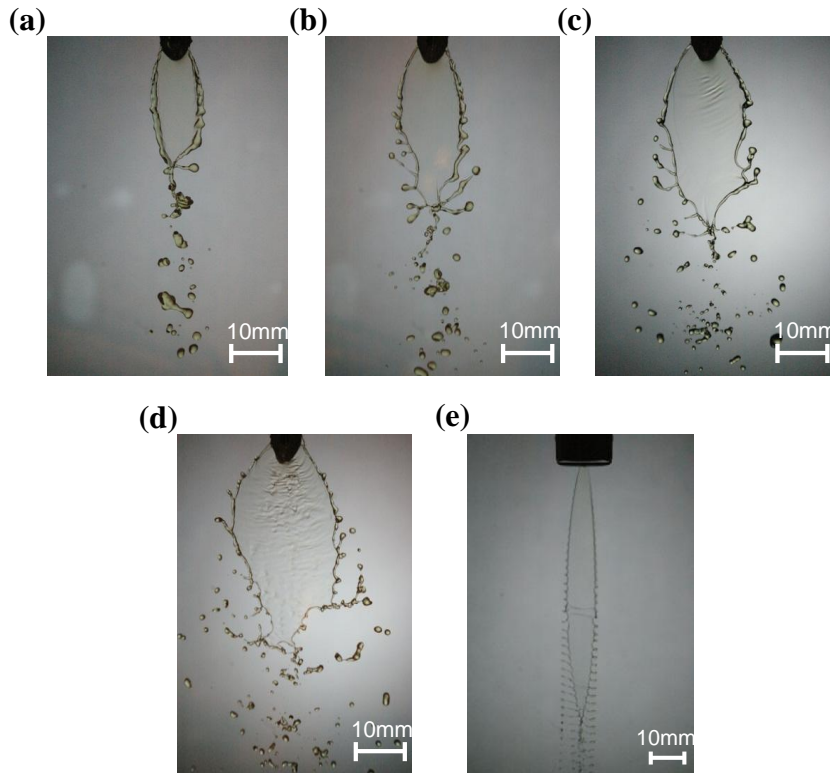**Fig. 4-2**   Schematic view of **(a)** impingement spray and **(b)** flat spray

Fig. 4-3 Sample images of impingement spray at different flow rates: **(a)** $Q=$ $1.98 \times 10^{-6} \, \text{m}^3/\text{s}$, **(b)** $Q= 2.54 \times 10^{-6} \, \text{m}^3/\text{s}$, **(c)** $Q= 3.14 \times 10^{-6} \, \text{m}^3/\text{s}$, **(d)** $Q= 3.66 \times 10^{-6} \, \text{m}^3/\text{s}$ and **(e)** flat spray at flow rate, $Q= 1.98 \times 10^{-6} \, \text{m}^3/\text{s}$

The impingement spray was formed by imposing impingement on the working fluid to a flat wall. The working fluid was injected from a straight nozzle (external diameter=1.5mm, internal diameter=1.0mm) that tilted 40° to the flat wall. On the other hand, the flat spray was formed through injection of the working fluid from a commercial flat spray nozzle (orifice diameter=0.66mm, spray angle=25° at 0.3MPa). The sample images of both sprays are shown in **Fig. 4-3**. The liquid sheet was then irradiated by pulses of UV laser (λ=355nm) from a Nd: YAG laser in order to form the photochromic dye traces. The laser pulse was 15ns in duration and 100mJ/pulse in energy.

The movement of the dye traces formed on the liquid sheet was then recorded by a high speed video camera (NAC's Memrecam fx 6000). The camera provides framing rates in excess of 200,000fps. For the impingement spray, the image was recorded with 5,000fps at 512×500 pixel resolution. Thus, spatial resolution of actual space and temporal resolution were respectively, 102μm and 0.2ms. For the flat spray, the image

was recorded with 10,000fps at 512×248 pixel resolution. And thus, the spatial resolution of actual space and temporal resolution were respectively, 123μm and 0.1ms.
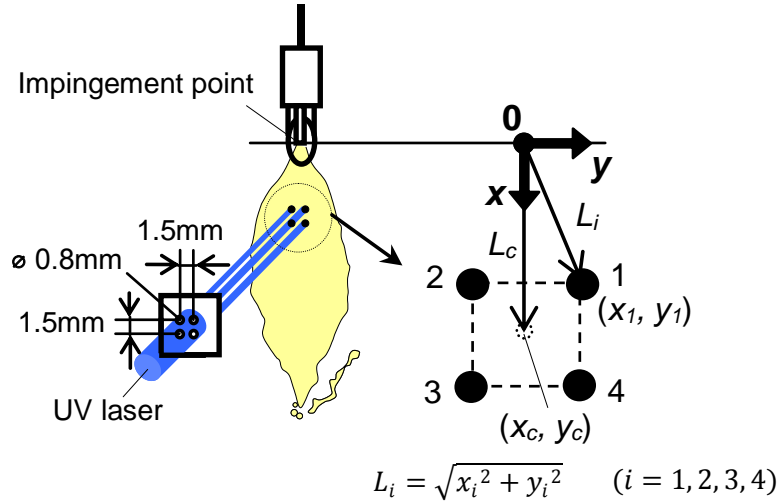

$$L_i = \sqrt{x_i{}^2 + y_i{}^2} \quad (i = 1, 2, 3, 4)$$

Fig. 4-4 Schematic view of measuring section upon UV light irradiation

Figure 4-4 shows the schematic view of the measuring section upon UV laser irradiation. As shown in the figure, a screen plate composed of 4 holes was placed on the UV laser passage in order to create a set of 4-points of dye traces on the liquid film with the same size of the holes (diameter=0.8mm, pitch=1.5mm). This is the smallest size of dye trace that we could effort for. The diameter of the dye traces could not be smaller than that as the high concentration of the dye traces color in the liquid sheet must be keep. Furthermore, although the pitch size must be smaller enough compared to the length scale of the flow phenomena, a relatively large pitch size between the dye traces is still needed in order to clearly track the movement of each dye trace for measuring the liquid deformation from the change of relative position of the dye traces. Therefore, this measurement length scale was the most appropriate size applicable this time.

As shown in **Fig. 4-4**, the origin was set as the impingement point and the nozzle exit, respectively for the impingement spray and flat spray. L_c represents the distance from the origin to the center position in between the 4-points of dye traces with the coordinate of the center position defined as (x_c, y_c). Moreover, L_i represents the distance from the origin to the center point of 4 dye traces with the coordinate of the center for each dye trace defined as (x_i, y_i) where, i=1, 2, 3 and 4. The coordinate (x_i, y_i) was digitized using the software provided with the camera.

The motion pictures captured by the camera were then transferred into a personal computer as a still image data. The sample image recorded by the camera is shown in **Fig. 4-5**. The dark points on the liquid sheet represent the dye traces point 1, 2, 3 and 4 tagged by the UV laser irradiation as shown in the figure. In order to clearly spot the dye traces appearance, the image sharpness was enhanced using image analysis method.
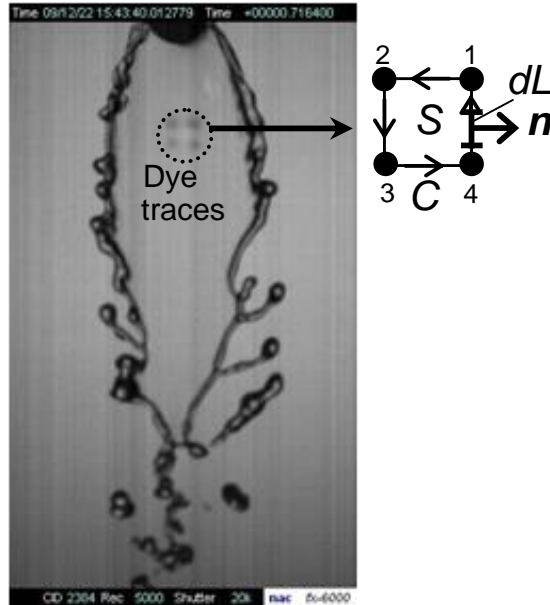

Fig. 4-5   Sample image of liquid sheet spray recorded by high speed video camera upon velocity measurement

4.3.2   Experimental condition

For the impingement spray, the velocity, strain and rotational motion measurement was taken at position L_c=10mm under different flow rate Q=1.98×10^{-6}m^3/s, 2.54×10^{-6}m^3/s, 3.14×10^{-6}m^3/s and 3.66×10^{-6}m^3/s. For the flat spray, the measurement was taken only at position L_c=13mm under flow rate Q=1.98×10^{-6}m^3/s. For each experimental condition, the velocity, strain, rotational motion and thickness measurement was repeated in the same way 4 to 9 times in order to achieve the most accurate result. The experiment was done at room temperature, T_e= 20~22 °C.

4.3.3 Measurement of liquid sheet velocity

The movement of liquid sheet was tracked by digitizing the center points of dye traces, i.e. coordinate (x_i, y_i) from its initial position as shown in **Table 4-1**.

Table 4-1   Initial position of center position (x_c, y_c) in between 4-points of dye traces and center point (x_i, y_i) of each dye trace

Position	Impingement spray	Flat spray
(x_c, y_c)	(10, 0)	(13, 0)
(x_1, y_1)	(9.25, 0.75)	(12.25, 0.75)
(x_2, y_2)	(9.25, -0.75)	(12.25, -0.75)
(x_3, y_3)	(10.75, -0.75)	(13.75, -0.75)
(x_4, y_4)	(10.75, 0.75)	(13.75, 0.75)

Unit: mm

Figure 4-6 shows the sample image of both sprays in which trajectory in the figure represents the movement of the dye traces. As can be seen, the dye traces in impingement spray can be tracked until the liquid sheet broken into ligament and droplets. However, the dye traces in flat spray can be tracked until the liquid sheet disintegrated into ligament. The local velocity, V_i of each dye trace along the trajectory was then calculated using the following equation:

$$V_i = \frac{\Delta L_i}{\Delta t} \qquad (i = 1, 2, 3, 4) \tag{4-1}$$

where, ΔL_i represents the displacement in two consecutive frames travelled by each dye trace 1, 2, 3 and 4. Δt represents the inter-frame spacing for the motion pictures of the camera, i.e. 0.2ms and 0.1ms, respectively for the impingement spray and flat spray. The direction of the velocity vector was derived from the movement direction of dye trace. The velocity components, u (x-direction) and v (y-direction) were also derived.
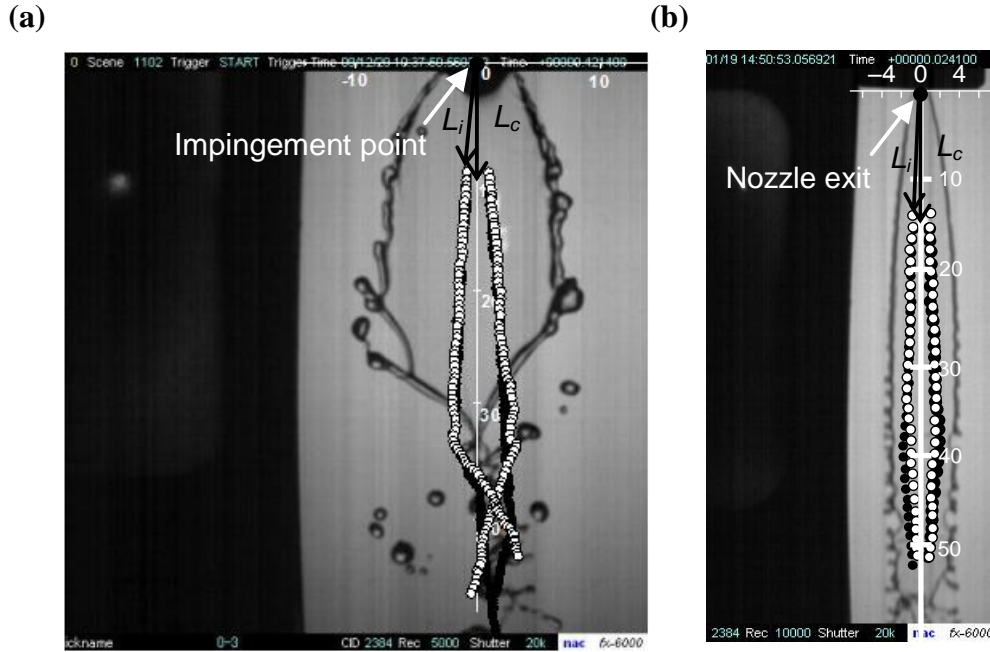
Fig. 4-6 Sample images of **(a)** impingement spray and **(b)** flat spray with trajectory of dye traces

4.3.4 Measurement of average thickness of liquid sheet

The time average liquid sheet thickness of impingement spray was also measured using a light absorption method. This method was conducted based on the light absorption of liquid containing a fluorescence dye such as coumarin153.

The coumarin153 was dissolved with 0.06wt% of concentration to the working fluid that was also dissolved with the photochromic dye beforehand. A diode laser (λ=408nm) was used as the light source. The light absorption method was referred from the well-known theory of Beer-Lambert law which described by the following equation:

$$B = \log T = \log(I_0 / I) = ec\delta \tag{4-2}$$

where, B is the measured absorbance, T is the transmittance, I_0 is the intensity of the incident light, I is the intensity of light passes through the liquid sheet, e is the molar extinction coefficient, c is the molar concentration, and δ is the path length, i.e. the thickness of the liquid sheet. In order to determine the relationship between the molar concentration of coumarin153 and the extinction coefficient, a calibration procedure is needed.
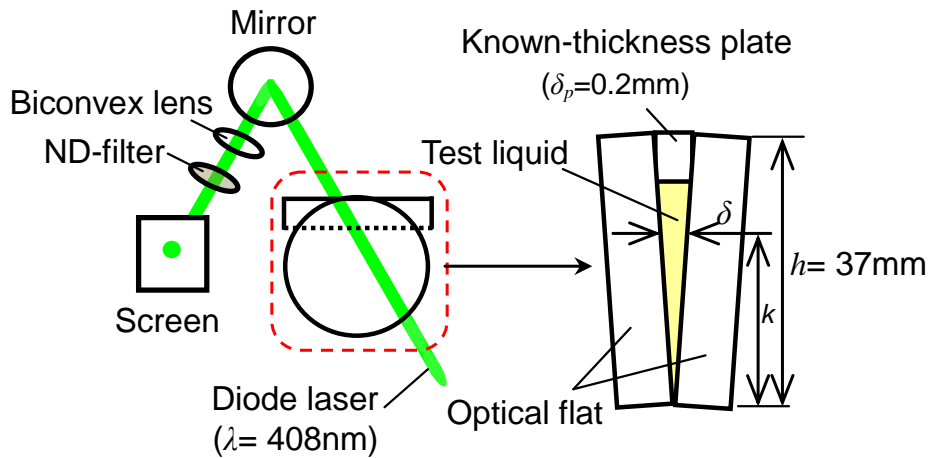
Fig. 4-7　Schematic view of calibration procedure of liquid sheet thickness measurement

Figure 4-7 illustrates the schematic view of the calibration procedure. The test equipment for the calibration procedure was made by sandwiching a known-thickness plate (δ_p=0.2mm) using two optical flat glasses. The plate was positioned on top of the two optical flat glasses while the remaining spaces were then filled up with the test liquid. The diode laser was irradiated to the test equipment in a range of distance from the bottom, k=3mm to k=30mm. The transmitted light was projected on a screen and the intensity was then quantified. The transmitted light intensity, I was estimated to decrease with increasing liquid sheet thickness, δ indicated by the distance from the bottom, k. The result of the calibration procedure is shown in **Fig. 4-8**. As can be seen, the liquid light intensity was found to linearly decrease with increasing liquid thickness. This calibration result was then used to determine the average thickness of liquid sheet.

Regarding the optical arrangement in the calibration procedure, a mirror was used to reflect the transmitted light to the screen while a biconvex lens and ND-filter were placed on the light path. The biconvex lens was used to focus the light. The ND-filter was used to filter the light intensity to ensure it does not exceed the measurable range of the camera. These devices were also employed in the actual experiment upon measuring the liquid sheet velocity as shown in **Fig. 4-9**.
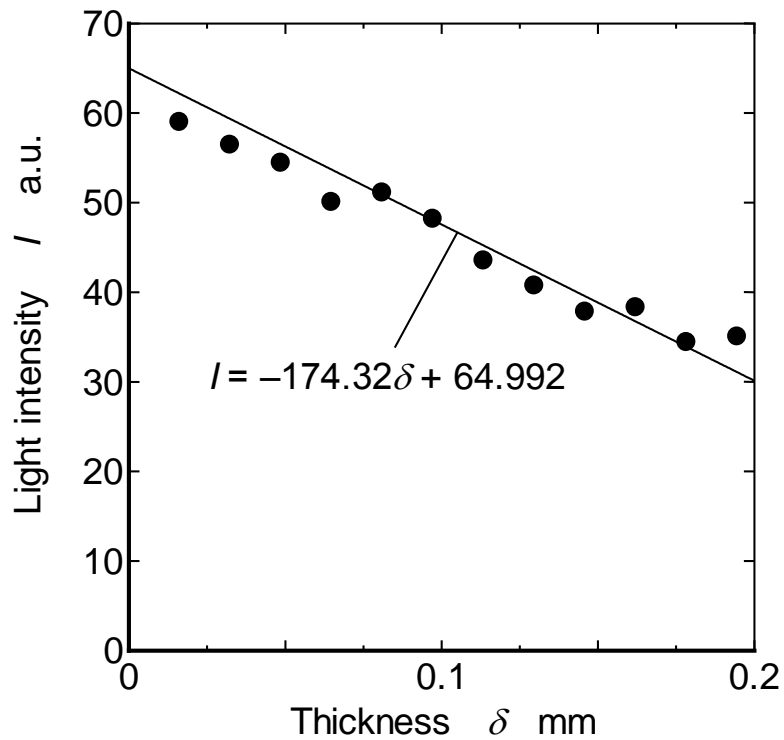
Fig. 4-8 Relationship between light intensity and liquid sheet thickness
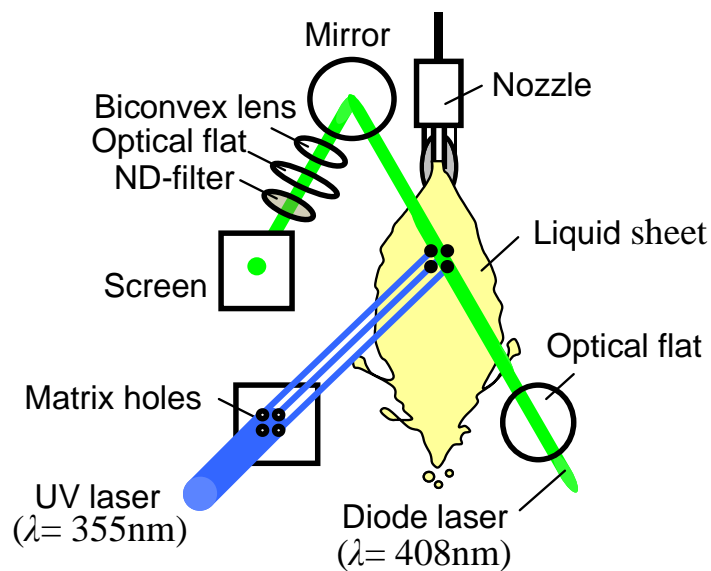

Fig. 4-9 Schematic view measuring section upon diode laser irradiation

The optical flat glasses used to make the test equipment in the calibration procedure were also used in the actual experiment in order to cancel the light reflection

effect of the glass surface. The diode laser was lead to the center position in between the 4-points of dye traces, i.e. coordinate (x_c, y_c) at the initial position of the dye traces as shown in **Table 4-1**. From the product of thickness at this initial position and the area obtained from the photochromic dye marking method, the initial volume of liquid sheet can be obtained. Then, the change of liquid sheet thickness can be calculated by dividing the initial volume by the change of area. Thus, the validity of photochromic dye marking method can be estimated. The image of the transmitted light projected on the screen was recorded in the same frame of the image of dye traces. **Fig. 4-10** shows the sample recorded image.
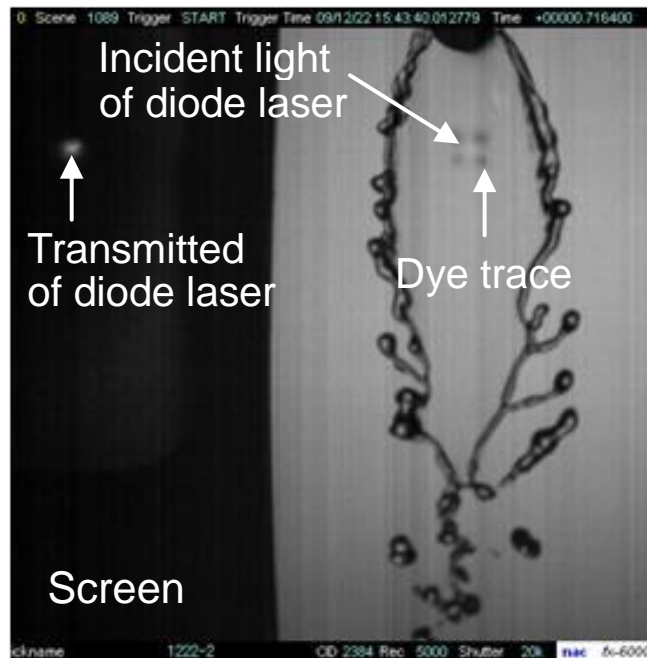

Fig. 4-10 Sample image liquid sheet spray recorded by high speed video camera upon thickness measurement

Taking into account the intensity distribution of the transmitted light and its fluctuated position due to the fluctuation of liquid sheet, only the transmitted light reflected on the screen that is most clearly visible and closed to the shape of the incident light was selected for its intensity quantifying. Therefore, only recorded image with such transmitted light was selected for the analysis procedure.

For the impingement spray, the thickness measurement was done at different position L_c=10mm, 15mm, 20mm, 25mm and 30mm under flow rate Q=2.54×10^{-6} m^3/s. For the flat spray, the measurement were done only at position L_c=13mm under flow

rate Q=1.98×10⁻⁶ m³/s. For each experimental condition, the measurement was repeated in the same way 4 to 9 times in order to obtain the most accurate result. From this multiply times of measurement results, the averaged value was determined as the average thickness of liquid sheet.

4.3.5   Estimation of measurement accuracy and resolution

The weakness in using the laser tagging method which could have affected the measurements accuracy probably comes from the size of tagged area, i.e. 4-points of dye traces originally projected from the screen holes (diameter=0.8mm, pitch=1.5mm). In order to maintain concentration of the dye traces color which easily fades by the liquid flow being measured, the size of tagged area in this experiment was the smallest size that can be operated.

From the diameter of each dye trace tagged in the liquid film, the center position which was coordinated manually by eye vision can be estimated to slip around ±0.02mm. Thus, the pitch size of the tagged area may also slip around 1.46 to 1.54mm. From here, the maximum measurement error of liquid surface area can be estimated as around 5%. For liquid velocity, the measurement error was estimated by the movement distance of dye trace within a time difference per frame. Taking example from the impingement spray, the movement distance of dye trace was about 0.5mm within $2.0×10^{-4}$s. Thus, the maximum measurement error for impingement spray was found approximately 20%.

In spite of those expected uncertainties, this experiment is still beneficial to pave the way in experimentally measuring the liquid sheet deformation. According to our survey, the measurement of flow deformation is still in critically needed. However, only a small number of experimental studies have been dedicated to provide such information. Therefore, more works must be done as recommendations to achieve a greater degree of accuracy and resolution in the future. The most critical part need to be done is enhancing the dye trace concentration and edge sharpness which were hardly achieved until now. The experimental design and tools in leading UV light to the liquid film for photochromic dye activation may be revised to meet such recommendation.

Thus, the center of dye trace can be accurately coordinated for more reliable data and the scale of tagged area also can be reduced for a greater resolution. Furthermore, the number of dye traces bounding the tagged area can be increased to highlight the edge of bounded area for upgrading the measurement accuracy.

4.4 Results and Discussion

4.4.1 Liquid sheet velocity

Figures 4-11 and **Fig. 4-12** show the result of local velocity change for one dye trace from its initial position respectively for impingement spray and flat spray as shown in **Table 4-1**. Both sprays were found to respectively illustrate two different trends of velocity change. In the impingement spray, the velocity seemed to keep a constant value in the film before suddenly increase around the broken point as shown in **Fig. 4-11(a)**.

The sudden increase indicates the moment of liquid sheet accumulated into the ligament. After broken into droplets, the velocity of the droplets was found to decrease with lower value than those in the liquid film. This can be attributed to the velocity component that arises in the opposite direction induced by the accumulation phenomenon caused by the effect of surface tension.
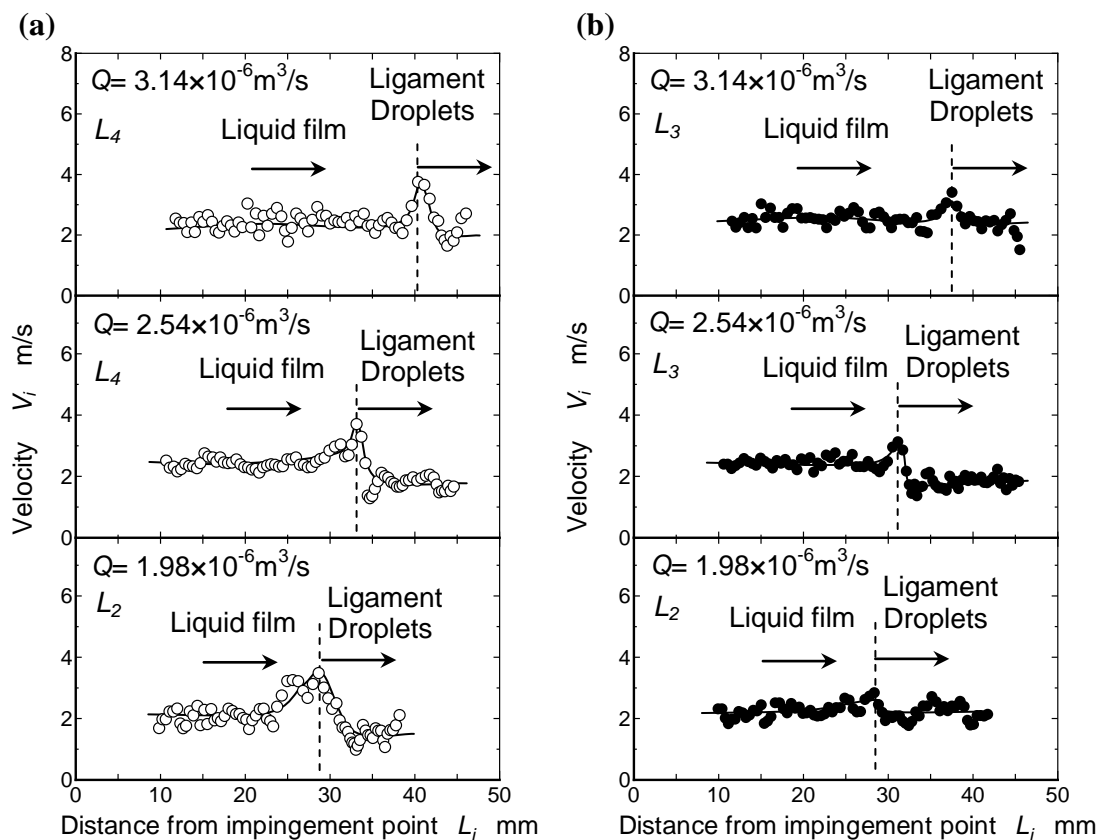

Fig. 4-11 Velocity change of impingement spray **(a)** with sudden increase and **(b)** without sudden increase
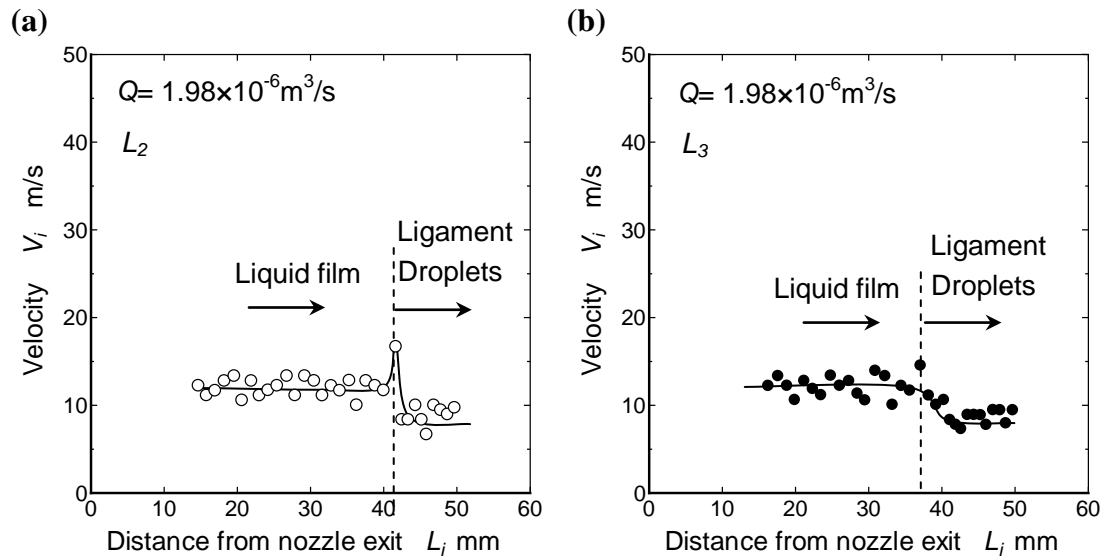
Fig. 4-12 Velocity change of flat spray **(a)** with sudden increase and **(b)** without sudden increase

However, the velocity difference did not always significantly occur. As can be seen in **Fig. 4-11(b)**, the sudden increase as well as the velocity reduction in the droplets was seen very weak.

On the other hand, the increment and decrement of velocity change in flat spray was seen even lower than those in impingement spray. As shown in **Fig. 4-12(a)**, the sudden increase of liquid velocity of flat spray upon transition to ligament and droplets was found but the peak of sudden increase was seen relatively lower than those in impingement spray. However, there was also case of the sudden increase did not occur upon the transition into ligament and droplets as can be seen in **Fig. 4-12(b)**.

Comparing the results between the impingement spray and flat spray, the velocity of flat spray was found 5 times larger than those in impingement spray. In the impingement spray, the liquid sheet velocity was independent of the increase in flow rate. This can be attributed to the greater rate of attenuation due to the strong impingement of liquid sheet onto the wall, which then leads to widen area of the film. Thus, the distance between the broken point and impingement point became larger with increasing flow rate. This behavior can be well confirmed by **Fig. 4-3**. In the flat spray, the position of liquid broken into ligaments at constant flow rate was seen around L_i=40mm.

Moreover, a general look to **Fig. 4-11** and **Fig. 4-12** suggested a quite variable result of velocity change. For example, the uncertainty in the velocity of L_2 at flow rate

Q=1.98×10^{-6}m^3/s in **Fig. 4-11(a)** was found to range around ±0.13m/s in the film and ±0.23m/s in the ligament and droplets. The uncertainty probably caused by the difficulty in coordinating accurately the center of the dye trace appeared along the trajectory due to its fading color further downstream.

4.4.2   Total normal strain of liquid sheet

Figure 4-13 shows the results of total normal strain distribution in x, y and z directions. The data was plotted as the total averaged value of the normal strain integrated by area starting from the initial position of the dye traces as shown in **Table 4-1**.
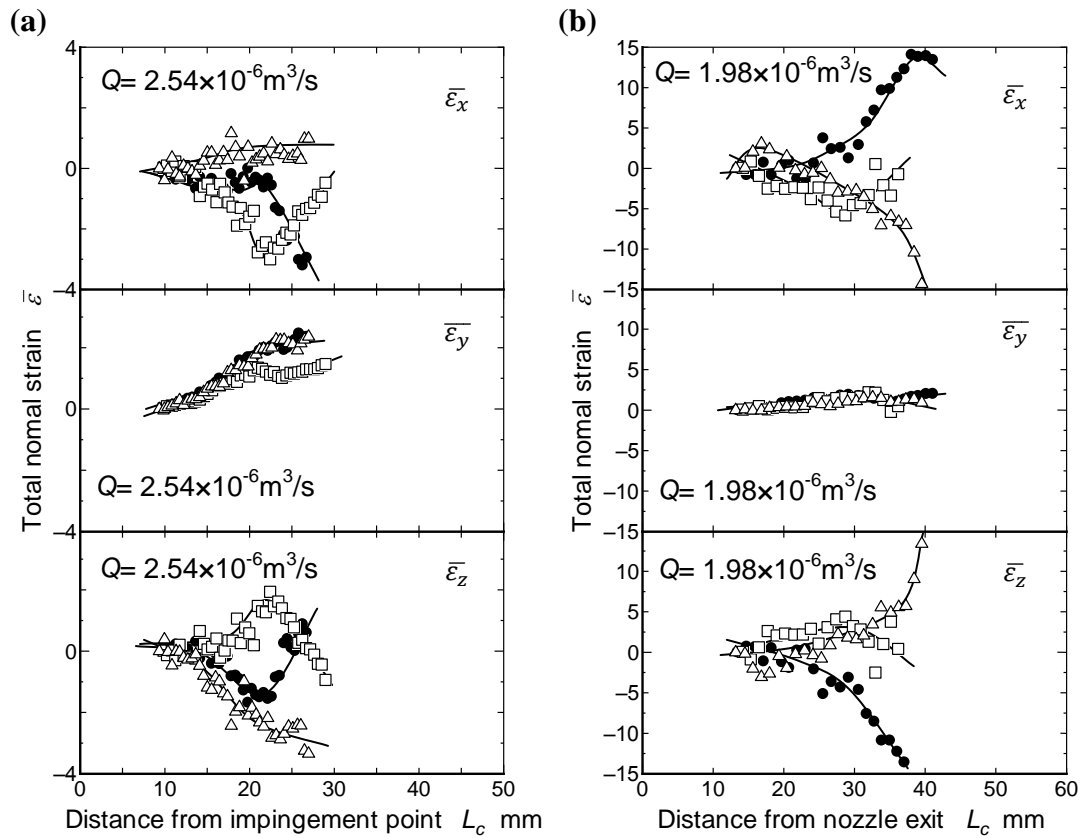

Fig. 4-13   Total normal strain distribution of **(a)** impingement spray and **(b)** flat spray

Further downstream, various trends of distribution was found under the same experimental condition. In the impingement spray, the normal strain in x direction shows various changes. The reason can be described by the dye traces behavior of impingement spray as shown in the images of liquid sheet in **Fig. 4-14**. The ligaments in the figure was found around L_c=20mm to 25mm in the liquid sheet. The decreasing

trend indicates the moment when the dye traces longitudinally shrank and drawn into the ligament, which then leads to the rises of liquid sheet thickness. On the contrary, the increasing trend indicates the moment when the dye traces were drawn into a thinner film in between ligament. This description can be confirmed from the results of liquid sheet thickness around L_c=25mm to 30mm in the next section. For the normal strain in y direction, all results were found to gradually increase. This can be attributed to the natural flow behavior of liquid sheet that extended transversely further downstream. Thus, the normal strain in z direction was found to mainly contrary with the results of x direction.

In the flat spray, the normal strain in x and z directions exhibited the same trends like the impingement spray. However, the normal strain in y direction showed very weak increase. This can be attributed to the natural flow behavior that mainly acted downstream, as can be confirmed by **Fig. 4-3**. Comparing the results between the impingement spray and flat spray, the results of flat spray showed a maximum difference of 5 times larger than the impingement spray. The uncertainties also occurred in the results of the total normal strain distribution. Taking example the data of x direction total normal strain in **Fig. 4-13(a)**, it was found to range around ±0.15.
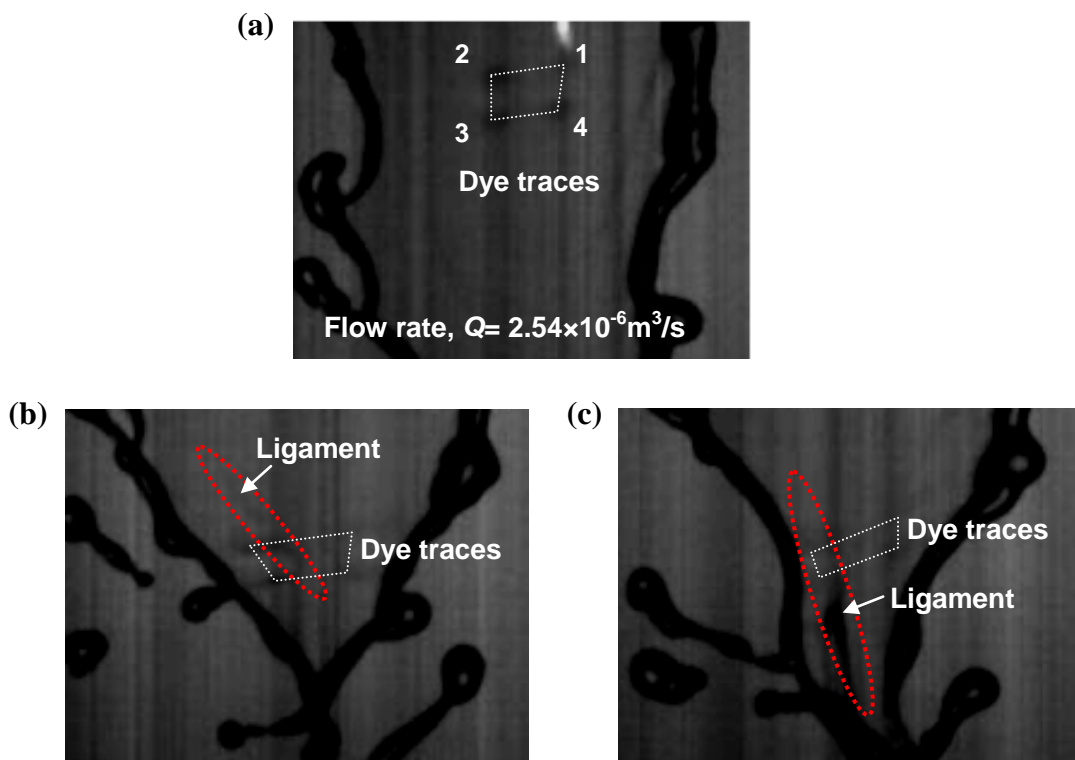

Fig. 4-14　Explanation of dye traces behavior from **(a)** initial position to **(b)** increasing trend and **(c)** decreasing trend of normal strain

4.4.3 Total shearing strain and rotational motion of liquid sheet

Figure 4-15 shows various trends of total shearing strain distribution appeared in the impingement spray. The data was also plotted as the total averaged value of the shearing strain integrated by area starting from the initial position of the dye traces as shown in **Table 1**.
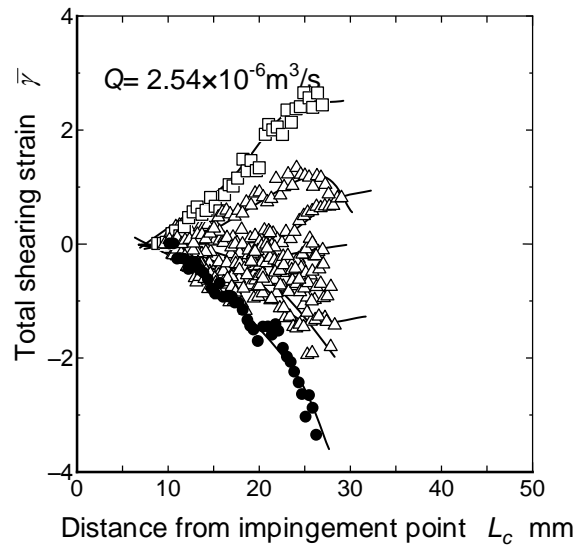

Fig. 4-15 Various trends of total shearing strain distribution appeared in impingement spray
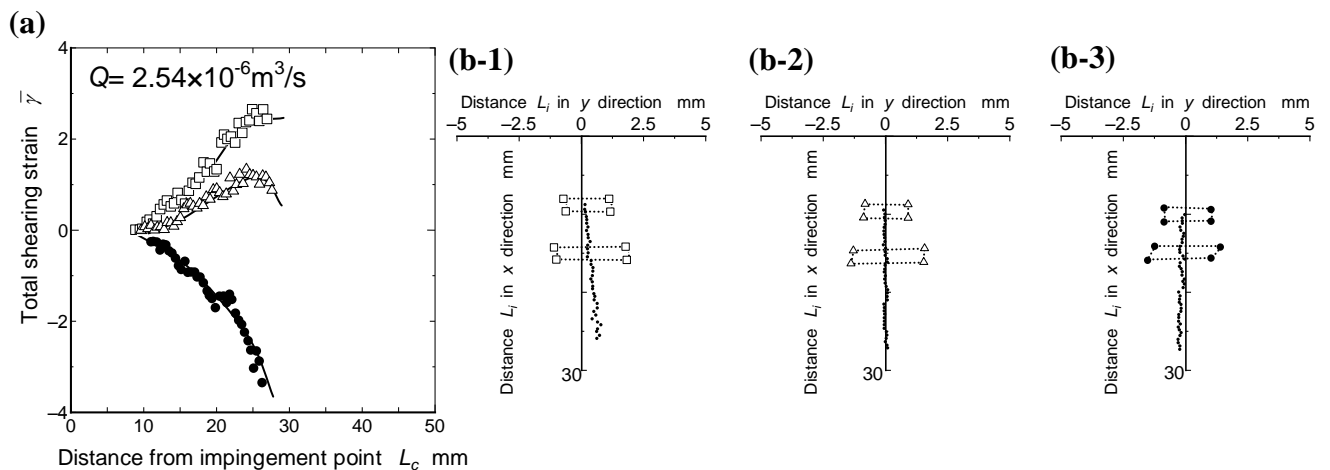

Fig. 4-16 Total shearing strain distribution of impingement spray in **(a)** typical representatives related with **(b)** position of dye traces against x and y direction

Total shearing strain means the total value of shearing strain experienced by the area bounded by the 4-points of dye traces from its initial appearance in the liquid film. It indicates how far the liquid body in the area bounded by the tags has been transformed from its original shape throughout its movement to downstream region. As can be seen, the shearing strain of impingement spray was found to increasingly, decreasingly and slightly change from its initial appearance. From these various trends of distribution, typical representatives is shown in **Fig. 4-16(a)**, where its relationship with the position of the dye traces against x and y directions is shown in **Fig. 4-16(b-1)** to **Fig. 4-16(b-3)**.

As can be seen, the total shearing strain of impingement spray in **Fig. 4-16(a)** increased when the dye traces were frequently shifted from the centerline in y direction as shown in **Fig. 16(b-1)**. Likewise, the total shearing strain decreased when the dye traces were frequently shifted from the centerline in $-y$ direction as shown in **Fig. 4-16(b-3)**. Moreover, the total shearing strain did not much change when the dye traces stably move downstream with very few deviations from the centerline as shown in **Fig. 4-16(b-2)**. Thus, the instantaneous deviation of dye traces shifted from the centerline either in positive of negative y direction was clarified. Taking example the data of **Fig. 4-16(a)**, the uncertainty was found to range around ± 0.08.

The deviation of dye traces can be attributed to the effect of liquid rim that pulled the liquid film in the mainstream. Without the liquid rim formation such as in an asymmetrical liquid sheet, the deviation may not occur.
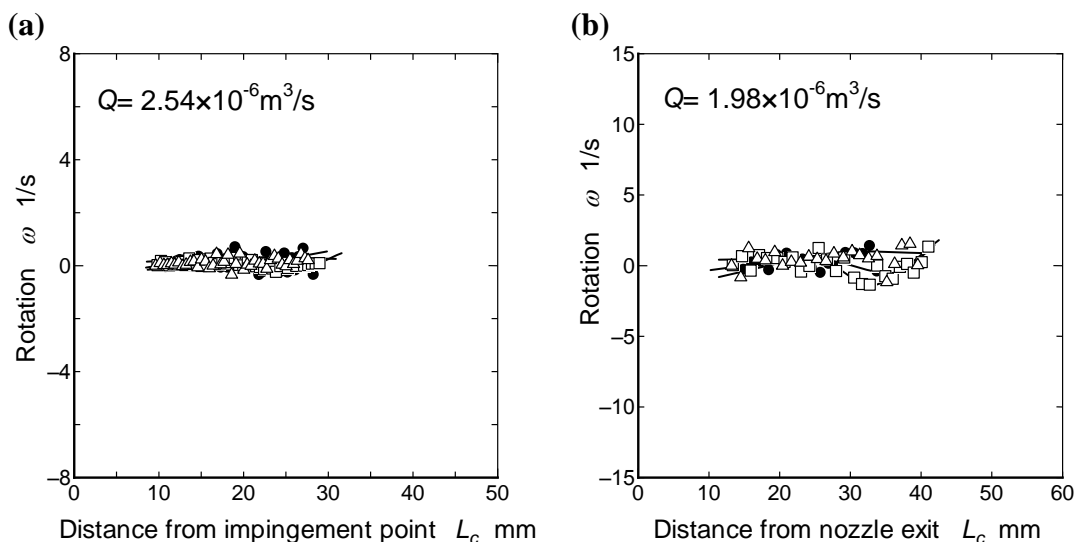

Fig. 4-17   Rotational motion of **(a)** impingement spray and **(b)** flat spray

Figure 4-17 shows the rotational motion, i.e. vorticity distribution obtained from the averaged value integrated by area. It was found that little to no rotational motion took place in the liquid sheet of both sprays. Taking example the data of **Fig. 4-17(a)**, the uncertainty was found to range around $\pm 0.07 \text{s}^{-1}$.

4.4.4　Average thickness of liquid sheet

（ⅰ）　**Thickness measurement of light absorption method**
Figure 4-18 shows the result of liquid sheet thickness of impingement spray with increasing flow rate. As can be seen, the average thickness was found to independent of the increase in flow rate, ranging around $154.3 \pm 3.2 \mu \text{m}$ from 4 times measurement. The results of liquid sheet thickness at different position L_c are discussed in the next section. For flat spray, the data was taken only at position L_c=13mm under flow rate Q=1.98$\times 10^{-6}$ m^3/s as mentioned before. The results are also discussed in the next section.
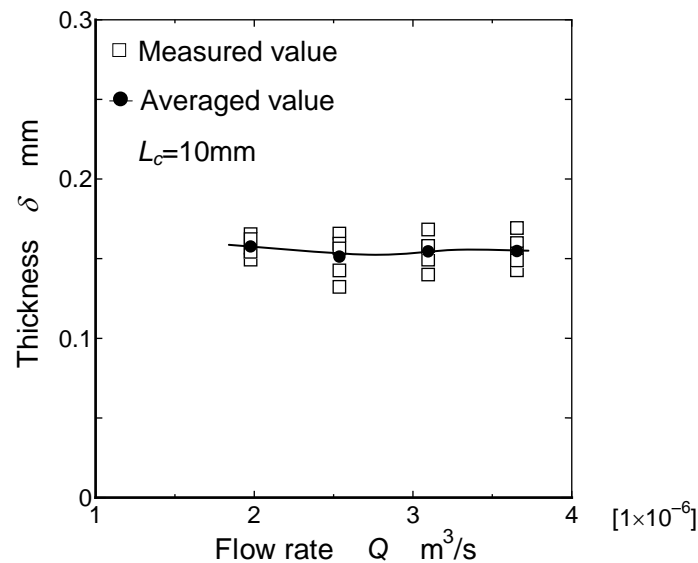

Fig. 4-18　Liquid sheet thickness of impingement spray with a increasing flow rate

（ⅱ）　**Observation of dye traces movement**

Figure 4-19 shows the change of area framed by the 4-points of dye traces. The results were found to gradually increase until approximately L_c=25mm and L_c=30mm respectively for impingement spray and flat spray. These results were then used to obtain the change of liquid sheet thickness.
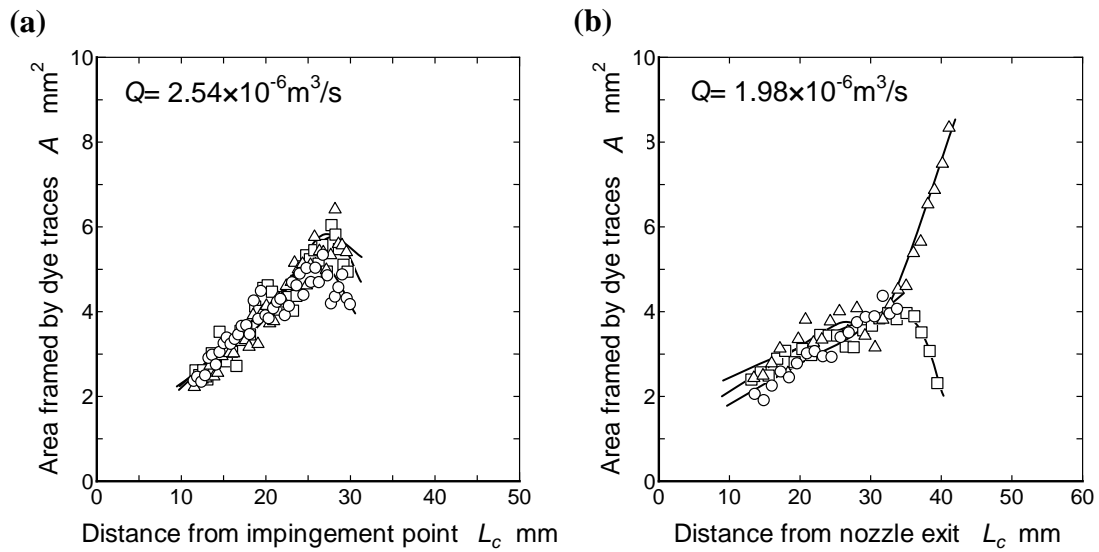
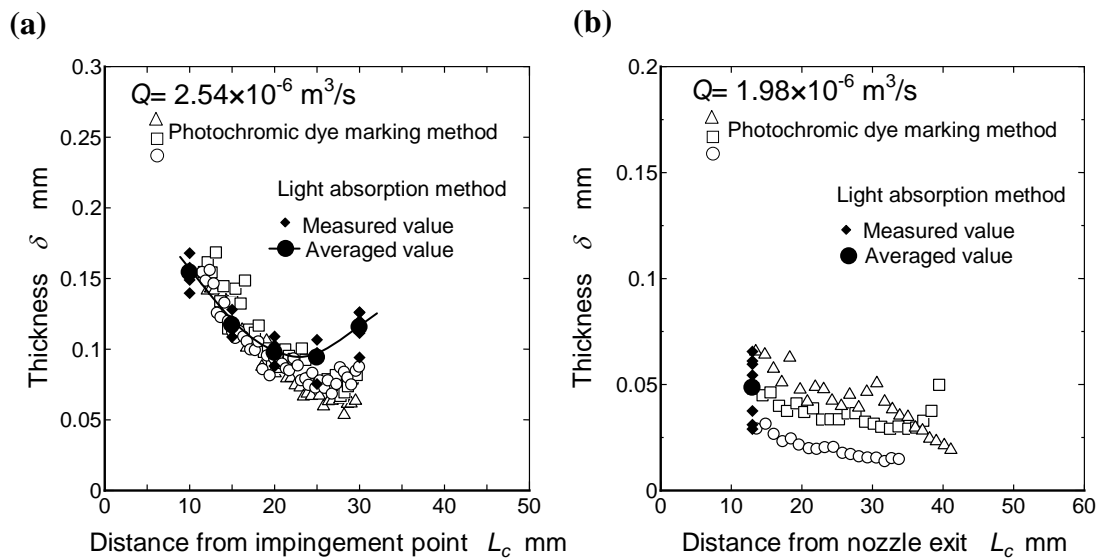**Fig. 4-19** Area framed by dye traces of **(a)** impingement spray and **(b)** flat spray

Fig. 4-20 Data comparison of liquid sheet thickness of **(a)** impingement spray and **(b)** flat spray

Figure 4-20 shows the comparison between the change of liquid sheet thickness obtained from the change of area as mentioned above and the liquid sheet thickness obtained from the light absorption method. For the impingement spray, the change of liquid sheet thickness was found to decrease until approximately L_c=25mm but then appeared to increase until the next 5mm. This tendency was seen to meet the results

obtained from the light absorption method. As can be seen, the average liquid sheet thickness further downstream obtained from the light absoprtion method was found to decrease into 94.1±14.0μm at L_c=25mm.

For the flat spray, the average liquid sheet thickness obtained from the light absoprtion method at L_c=13mm was around 36.6±12.2μm. As can be seen, the change of liquid sheet thickness obtained from photochromic dye marking method at the same region was also ranging around the results obtained from light absorption method. This similar tendency of liquid sheet thickness results between the two methods straighten the explanation of total normal strain distribution as mentioned before in **Fig. 4-14**. As can be seen, the liquid sheet thickness in **Fig. 4-20** was found to vary around L_c=25mm to 30mm.

This is the range of liquid sheet approaching the broken point in which the thickness in that region varied with the formation of ligament. Thus, a lower value of liquid sheet thickness at the region represents the moment when the liquid sheet drawn into a thinner film in between two ligaments as discussed in **Fig. 4-14**. Therefore, the validity of laser tagging method by photochromic dye was well confirmed.

Moreover, a closer look to the results of liquid sheet thickness of impingement spray obtained from the photochromic dye marking method suggests that further downstream the liquid sheet prior to the broken point became thinner up around 50μm to 80μm. For the flat spray, the liquid sheet prior to the broken point became thinner up around 13μm to 25μm.

4.5 Summaries

In this experiment, the laser tagging method using photochromic dye tracer was applied with aim to study the breakup process of liquid sheet as a fundamental study of atomization in detail, covering from the behavior in the film until disintegrated into ligament and droplets. The motions of the dye traces tagged by UV laser were analyzed as the liquid surface velocity. The conclusions of the present experiment can be drawn as below:

1. By forming a set of 4-points of dye traces on the liquid sheet, the change of relative position of the set of dye traces successfully allowed the measurement of deformation and rotational motion of the liquid sheet.
2. Liquid sheet was found to keep its velocity constantly in film before suddenly increase around broken point. However, it then decreased after broken into droplets.

3. The normal strain of the liquid sheet parallel to the flow direction was found to variously change depends on the liquid behavior against the ligament position. Whereby, the normal strain perpendicular to the flow direction was found to mainly increase further downstream due to natural behavior of the liquid sheet that extended transversely further downstream.
4. The shearing strain variously changed depends on the instantaneous deviation of liquid film in mainstream shifted from the centerline either in positive of negative y direction. Also, little to no rotational motion occurred in the liquid sheet.

Moreover, the measurement of average thickness of the liquid sheet was carried out using light absorption method. Several points can be highlighted as below:

5. The average thickness of the liquid sheet was independent of the increase in flow rate. Further downstream, the thickness decreased until nearly reaching the broken point and then increased thereafter due to the liquid accumulation occurs prior to the breakup process.
6. The similar tendency of liquid sheet thickness resulted from the laser absorption method and the change of area framed by the 4-points of dye traces confirmed the validity of using laser tagging method using photochromic dye tracer for the liquid free surface flow measurement.

Finally, despite the uncertainties occurred in the measurement results, this experiment has successfully paved the way to better understand the liquid sheet deformation experimentally. Further works as recommended are required to establish a greater degree of accuracy and resolution.

References

[1] Turner, M.R., Sazhin, S.S., Healey, J.J., Crua, C. and Martynov, S.B.: A Breakup Model for Transient Diesel Fuel Sprays, *Fuel*, **97** (2012), 288-305.
[2] Rashid, M.S.F.M, Hamid, A.H.A, Sheng, O.C. and Ghaffar, Z.A.: Effect of Inlet Slot Number on the Spray Cone Angle and Discharge Coefficient of Swirl Atomizer, *Procedia Engineering*, **41** (2012), 1781-1786.
[3] Shinjo, J., Xia, J. and Umemura, A.: Droplet/Ligament Modulation of Local Small-Scale Turbulence and Scalar Mixing in a Dense Fuel Spray, *Proceedings of the Combustion Institute*, In Press (2014).

[4] Vinci, V.J., Watten, B.J. and Timmons, M.B.: Gas-Phase Axial Dispersion in a Spray Tower, *Aquacultural Engineering*, **15**-1 (1996), 1-11.

[5] Watanawanyoo, P., Hirahara, H., Mochida, H., Furukawa, T., Nakamura, M. and Chaitep, S.: Experimental Investigations on Spray Characteristics in Twin-Fluid Atomizer, *Procedia Engineering*, **24** (2011), 816-822.

[6] Huo, M., Lin, S., Liu, H. and Lee, C.F.F.: Study on the Spray and Combustion Characteristics of Water–Emulsified Diesel, *Fuel*, **123** (2014), 218-229.

[7] Xiao, F., Dianat, M. and McGuirk, J.J.: LES of Turbulent Liquid Jet Primary Breakup in Turbulent Coaxial Air Flow, *International Journal of Multiphase Flow*, **60** (2014), 103-118.

[8] Tira, H.S., Herreros, J.M., Tsolakis, A. and Wyszynski, M.L.: Characteristics of LPG-Diesel Dual Fuelled Engine Operated With Rapeseed Methyl Ester and Gas-To-Liquid Diesel Fuels, *Energy*, **47** (2012), 620-629.

Chapter 5

Measurement of liquid film flow on inclined wall

5.1   Introductory remarks

The presence of falling liquid films are well known to extremely influence the transporting rates of heat and mass occurred in various industrial equipments. These transfer rates must be predicted accurately to support those equipments reliability. The study of falling liquid films has gained many attention over a century ago. Since then, even more studies have been carried out to better understand the behavior of falling liquid films.

For example, Yu et al. **[1]** have investigated the flow characteristics of water film falling on a vertical plate. Pavlenko et al. **[2]** studied the dynamics of laminar-wave flow of an intensively evaporating saturated liquid film on a vertical plate. Another laminar wavy motion of liquid film on a vertical wall has been discussed by Min and Park **[3]** from their numerical calculation method. On the other hand, phenomenology of falling liquid film flows achieved by research works in the past has been reported recently by Christian et al. **[4]**.

Moreover, our survey to previous literature suggested the wave structures occurred in the liquid film flows have grown as important discussion in the research studies. For examples, Chinnov and Kabov **[5]** clarified the thermocapillary effect on the rivulet structure of wave in liquid film falling down a heated inclined plate. Salque et al. **[6]** described the surface waves structure and its relation to the liquid film atomization in a venture. Kil et al. **[7]** in their integral approach clarified the wave characteristics of falling liquid film on a vertical circular tube.

Duprat et al. **[8]** discussed the phenomena of bound-state formation in a viscous film coating a vertical fiber. This matter then has been further discussed by Wehinger et al. **[9]** in their numerical simulations of liquid film also in a vertical fiber. Karimi and Kawaji **[10]** reported circulatory motions in their work to describe turbulence characteristics of wavy film falling down a vertical tube. Moran et al. **[11]** then extended the investigation to describe wavy film characteristics falling down an inclined plate. Their works proved that the circulatory motion occurred merely in the waves with very small thickness from substrate to peak.

As the falling liquid film flows mostly governed by the instable wavy flows structure, conducting experimental study of very thin liquid films has become considerably difficult. For this reason, the study on such flow structures is critically needed.

Here, the application of laser tagging method using photochromic dye tracer is further expanded to the liquid film flow on inclined wall to study the internal flow structure.

5.2   Objective of this experiment

In this experiment, the laser tagging method using photochromic dye tracer is applied with the aim to experimentally study the internal flow structure of liquid film flowing down an inclined wall. The motions of the dye traces tagged by UV laser are analyzed as the liquid surface velocity. The movement of the dye traces is then analyzed together with the movement of wave passing over the dye trace using image analysis method. Velocity difference between the liquid film and wave is then investigated.

Furthermore, a cross-correlation method is also used to measure the average wave velocity, based on irradiation of two parallel diode laser beams perpendicular to the liquid film flow. From one of the diode laser beams irradiation, liquid film thickness fluctuation is measured using a light absorption method.

Considering the change of dye trace shape is strongly influenced by the inner flow structure, the diameter change of dye trace marked on the film surface is also measured in order to discuss the internal flow structure of falling liquid film. Several interesting results are obtained and discussed in detail.

5.3   Methodology

5.3.1   Experimental apparatus and procedure

Figure 5-1 shows the schematic view of experimental setup for liquid film flow on inclined wall. The inclined wall was made of acrylic plate with reservoir area connected to the liquid delivery wall (length=300mm, width=120mm). A metallic mesh and semi-circular cylinder were set in the reservoir area to prevent overflow of the working fluid. The inclined wall was mounted on aluminum frames installed with free-angle brackets to allow alteration of the wall inclination angle, θ from horizontal to vertical direction. The working fluid passes through a pump, valve and flow meter before

entering the reservoir area. The liquid film then flow down the wall surface and come back to the liquid storage basin placed below the end of the wall surface.
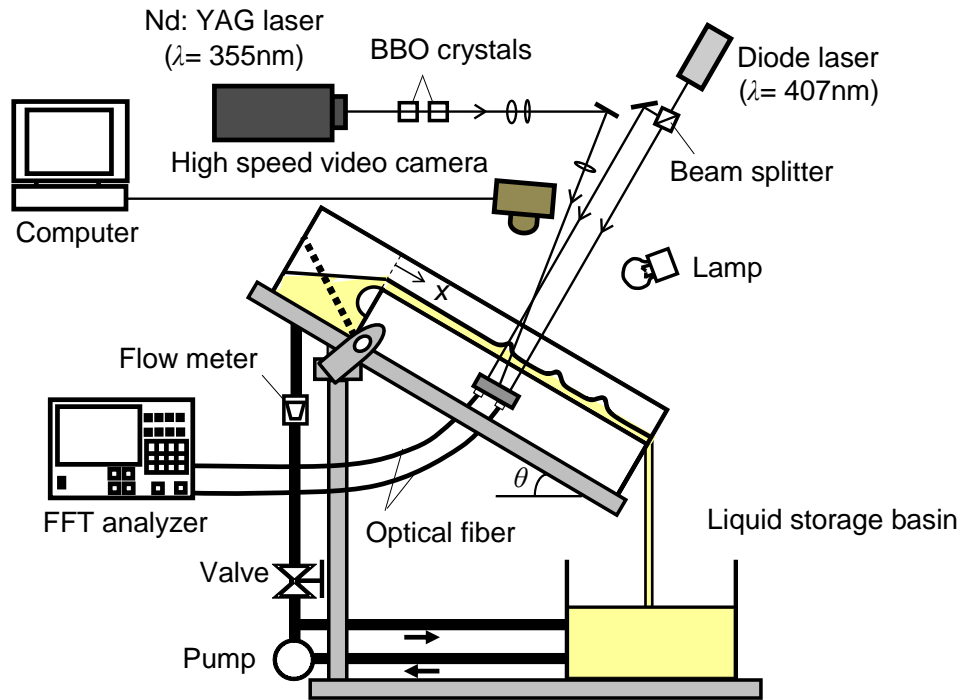

Fig. 5-1 Schematic view of experimental setup for liquid film flow on inclined wall

Pulses of UV light (λ=355nm) sourced from a Nd: YAG laser was irradiated to the flowing working fluid in order to form the photochromic dye traces. Combination of lens and mirror were used to lead the UV light to the liquid film, including a convex lens which was placed on the light path to ensure concentrated dye traces formation for the best analysis results. Simultaneously, the flow patterns and the movements of wave and dye trace formed in the liquid film were recorded by a high speed camera (CASIO's EX-F1). In the experiment of θ=20°, the image was recorded with 300fps at 512×384 pixel resolution. Thus, spatial resolution of actual space and temporal resolution were respectively, 98μm and 3.3ms. In the experiment of θ=30°, 60° and 90°, the image was also recorded with 300fps at 512×384 pixel resolution. Thus, spatial resolution of actual space and temporal resolution were respectively, 195μm and 3.3ms. A halogen lamp was also used to assist the visualization.

In order to obtain the wave shape formed in the falling liquid film, a screen drawn with lines was attached behind the inclined wall. By the aid of light refraction, approximate shapes of wave from the slant lines can be derived. The wave shape was

then captured by a digital camera placed on the side of the inclined wall. The sample images of dye trace and wave shapes are shown in **Fig. 5-2**. The dark point represents the photochromic dye trace tagged by the UV light.
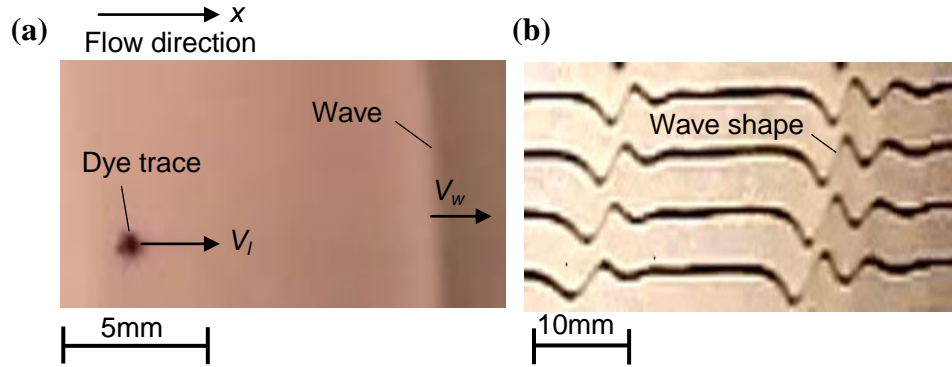

Fig. 5-2　Sample images of **(a)** dye trace and **(b)** wave shapes

The motion pictures recorded by the high speed camera were then transferred to a still image data. Images with wave passing over the dye trace were selected for analysis. The position of the dye trace and the wave were then determined by digitizing their coordinates.

5.3.2　Experimental condition

The Reynolds number, *Re* is defined by the following equation:

$$Re = \frac{\rho Q}{\eta b} \qquad\qquad (5\text{-}1)$$

where, ρ is the density, Q is the flow rate, η is the dynamic viscosity of the working fluid and b is the width of inclined wall. The experiment was done at room temperature, $T_e = 20\text{~}22\ °C$. Moreover, further experimental conditions are described as below:

（ⅰ）Liquid film and wave velocity with increasing wall inclination angle
The experiment was conducted at wall inclination angle, $\theta=30°$, $60°$ and $90°$ under constant Reynolds number, $Re=81.3$. The velocity difference between liquid film and wave were also investigated. Furthermore, the comparison of average wave velocity using the cross correlation method and the average velocity of wave passing the dye trace which obtained by the image analysis method were also investigated.

(ii)   Liquid film and wave velocity with increasing Reynolds number

Here, the experiment was conducted at Reynolds number, Re=91.5, 135.5 and 179.5 under constant wall inclination angle, θ=20°. Here, the velocity change of dye trace was related to the distance between the dye trace and the wave crest was also investigated. Furthermore, the diameter change of dye traces was measured to clarify the internal structure of the liquid film flow.

(iii)   Wave patterns and liquid thickness measurement

The wave patterns were recorded at various positions on inclined wall, i.e. distance from liquid inlet, L_m=60mm, 100mm, 140mm and 180mm upon Reynolds number, Re=50.8, 81.3, 108.4 and 138.9. Here, the liquid film thickness was also measured.

5.3.3   Measurement of liquid film surface and waves velocities

The liquid film surface velocity, V_l can be obtained from the displacement of the dye trace, ΔX_l over consecutive frames during a time interval, Δt as shown in the following equation:

$$V_l = \frac{\Delta X_l}{\Delta t} \tag{5-2}$$

The instantaneous velocity of wave, V_w can be obtained in the same way as shown in the following equation:

$$V_w = \frac{\Delta X_w}{\Delta t} \tag{5-3}$$

where, ΔX_w is the displacement of the wave.

5.3.4   Measurement of average wave and liquid film thickness

Figure 5-3 shows the schematic view of optical arrangement for the average wave velocity and liquid film thickness measurement. A pulse of diode laser light (λ=407nm) was directed to the liquid film in perpendicular to the inclined wall. For the average wave velocity measurement, a beam splitter was placed on the beam path in order to divide the original beam as shown in the figure. The two beams with a known-spacing (H=12mm) between them thus appeared on the liquid film flow with a parallel direction to the film flow.
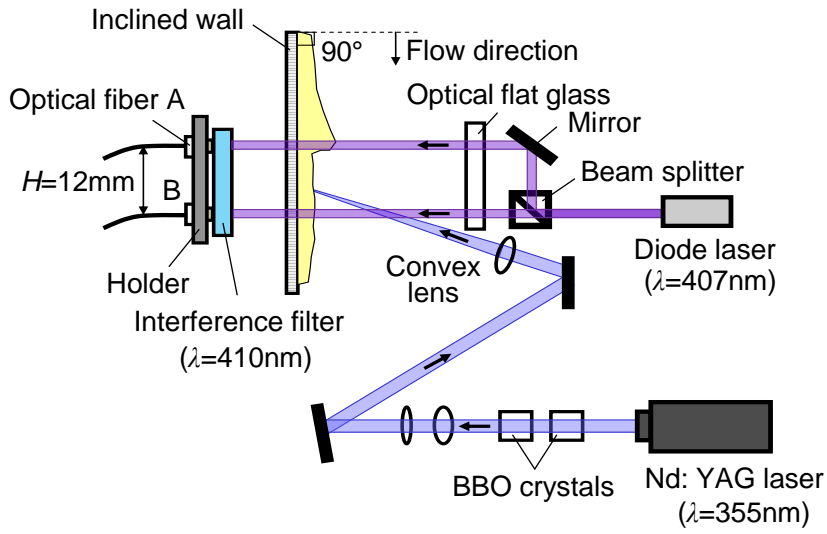
Fig. 5-3 Schematic view of optical arrangement for the average wave velocity and liquid film thickness measurement

A pair of optical fiber was attached behind the inclined wall with their surfaces covering the regions of the total incident light of the two beams. The core diameter of the optical fibers was relatively large, i.e. about 6.4mm compared to the diameter of diode laser light which was about 2mm. Therefore, the uncertainties that may come from the light refraction can be reduced. The light intensity was then converted into voltage signals by two photomultipliers connected to the other tip of the optical fibers. The two signals were then cross-correlated using a FFT analyzer, giving the time delay between the two signals. The cross-correlation was done in 16 events and thus the average wave velocity can be derived as the following equation:

$$\overline{U_w} = \frac{H}{\Delta \tau} \tag{5-4}$$

where, H is the known spacing between the two beams and $\Delta \tau$ is the time delay between the two signals from cross-correlation operated by the FFT analyzer. The results were than compared with the average velocity of wave passing the dye trace as mentioned above, $\overline{V_w}$.

Taking advantages from one of the laser beams irradiation, the working fluid thickness was measured based on the light absorption method which has been applied in the liquid sheet thickness measurement. Coumarin153 was dissolved with 0.06wt% of concentration to the working fluid. A blue interference filter (λ=410nm) was placed

between the inclined wall and the optical fibers in order to merely allow the transmission of light passed through the liquid film and reflect the fluorescence light occurred during the absorption.

In this study, the light absorption method was referred from the Beer-Lambert law which describes the relation between the molecular concentration of coumarin153 in the working fluid and the extinction coefficient. Therefore, a calibration procedure is needed to derive this relation. The calibration procedure was implemented by sandwiching a known thickness plate (δ_p=1.05mm) with an optical flat glass to the inclined wall, as shown in **Fig. 5-4**. The plate was positioned on top of the test piece while the remaining spaces were filled up with liquid film containing the coumarin153. The calibration procedure was done by moving the inclined wall from bottom to obtain the intensity of transmitted light conducted by optical A and B. The relationship between the transmitted light intensity and liquid film thickness was then obtained same as calibration procedure in liquid sheet spray experiment.

Moreover, the measured data of liquid film average thickness was also compared with the estimated data which was calculated by below equation:

$$\overline{\delta} = \sqrt{\frac{2\mu\overline{V_l}}{\rho g \sin\theta}}$$
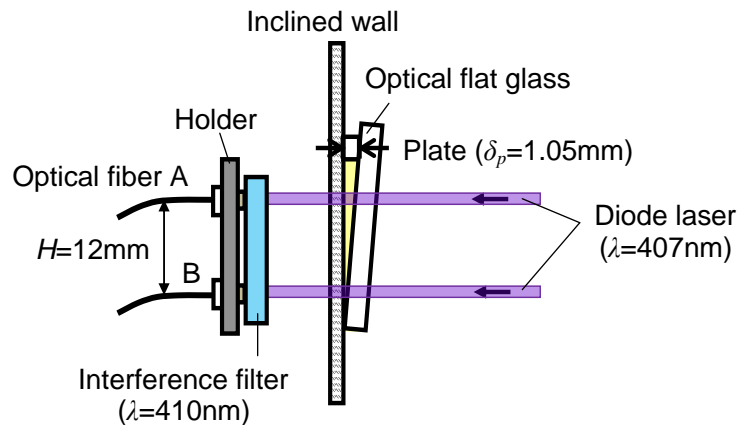
(5-5)

Fig. 5-4 Schematic view of calibration procedure of liquid film flow thickness measurement

66

5.3.5 Measurement of diameter of dye traces

In order to clarify in detail the flow structure during the presence of wave, the diameter change of the dye trace was obtained. When the UV light was irradiated to the liquid film, a round shape of dye trace on liquid film surface in the thickness direction under the surface was formed. As the liquid film flows down the wall, the dye trace moved along with the liquid film as shown in **Fig. 5-5(a)**. For this reason, a trace line was visible in the recorded image as shown in **Fig. 5-5(b)**. The diameters of dye trace parallel and perpendicular to the flow direction, d_1 and d_2 were respectively calculated as the following equations:

$$d_1 = x_1 - x_3 \tag{5-6}$$

$$d_2 = y_4 - y_2 \tag{5-7}$$

where, x and y are the coordinate point in x and y direction, respectively.
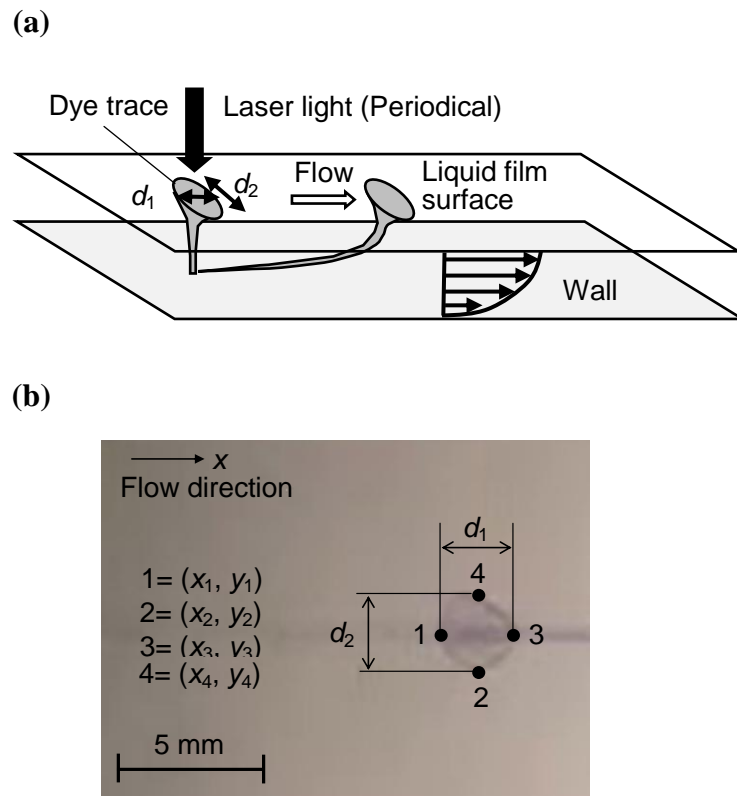
(a)

(b)

Fig. 5-5   Schematic view of dye traces diameter measurement with **(a)** illustration of dye traces appearance and **(b)** definition of diameters, d_1 and d_2

5.4 Results and discussion

5.4.1 Visualization of wave patterns

The images of wave patterns on liquid film upon wall inclination angle, θ=30°, 60° and 90° are shown in **Fig. 5-6** to and **Fig. 5-8**. A general view to all figures suggested interesting wave patterns that change with the angle variations. In the case of θ=30° (**Fig.5-6**), the waves formed as a group of parallel wave train further downstream. In the case of θ=60° (**Fig. 5-7**), the waves formed nearly linear in the beginning but then evolved into larger U and W-shapes. In the case of θ=90° (**Fig. 5-8**), irregular U and W-shape of waves were observed.
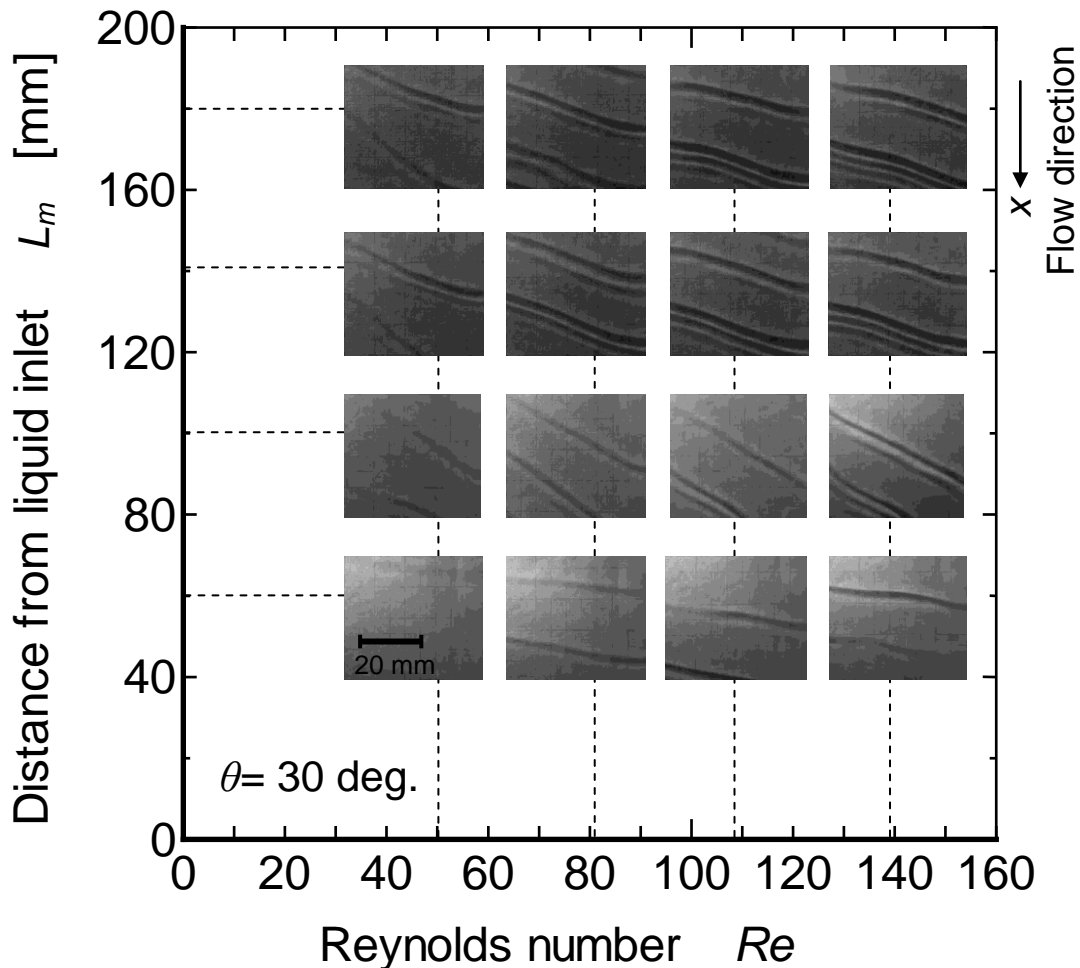

Fig. 5-6 Wave patterns of liquid film upon wall inclination angle, θ=30°

In **Fig. 5-6**, the waves crest was found to inclined further downstream. This can be attributed to the non-uniform distribution of film flow on the test wall surface due to the unbalanced inclination angle as stated by Zhou et al. **[12]**. In other words, the inclined wall might be inclined heavier on the right side which leads the liquid film to accumulate on the heavier side and forced to travel faster than other side. The waves were formed initially in solitary-type pattern which then accumulated into two to four layers of parallel wave train around the downstream region (L_m>100mm) in higher Reynolds number (Re>50.8). However, in this region the waves seemed to travel further downstream in a stationary manner regardless of Reynolds number increases or not. Brauner and Maron **[13]** stated that the onset of the film waves is easily developed at relatively lower Reynolds number.
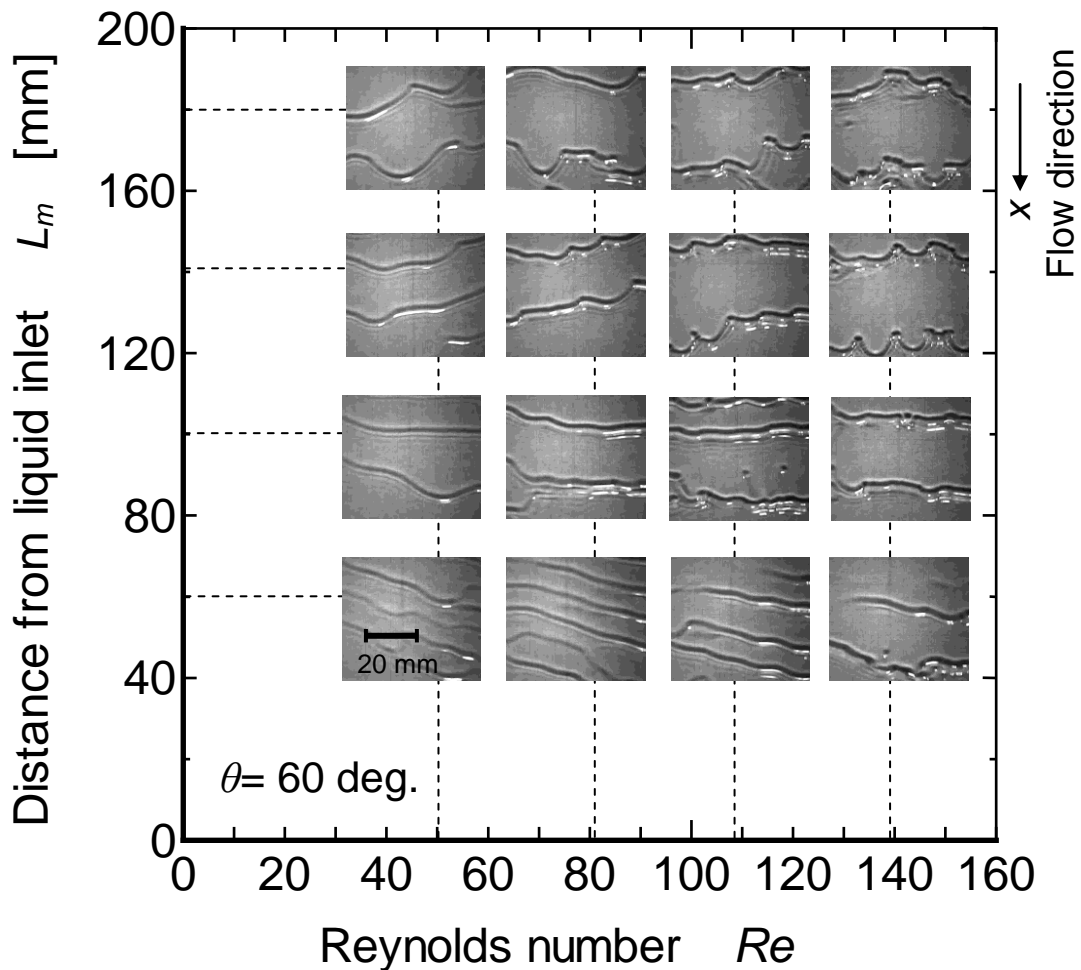

Fig. 5-7   Wave patterns of liquid film upon wall inclination angle, θ=60°

However, comparing the wave patterns of larger inclination angle in this study, images on the lower Reynolds number ($Re>108.4$) of upper stream region ($L_m<100$mm) reveal the imperfections of wave formation. This can be attributed to the reduction of gravitation influence at smaller inclination angle that caused the delay in wave inception, as described by Zhou et al. [12].

In **Fig. 5-7**, waves were clearly observed on all measurement positions. It travelled in larger wavelength with increasing of distance from liquid inlet and Reynolds number. In the beginning, the waves were found to smoothly flow as waves nearly solitary-type pattern, before slightly slant around the upper stream region ($L_m<100$mm). Further downstream, it then grew up into large tear-drop humps, forming U or W-shape of waves. Also, the wave shapes seemed to be intensified by increasing Reynolds number. A closer look to the wave patterns also reveals the presence of short forerunner wave right in front of the main waves.
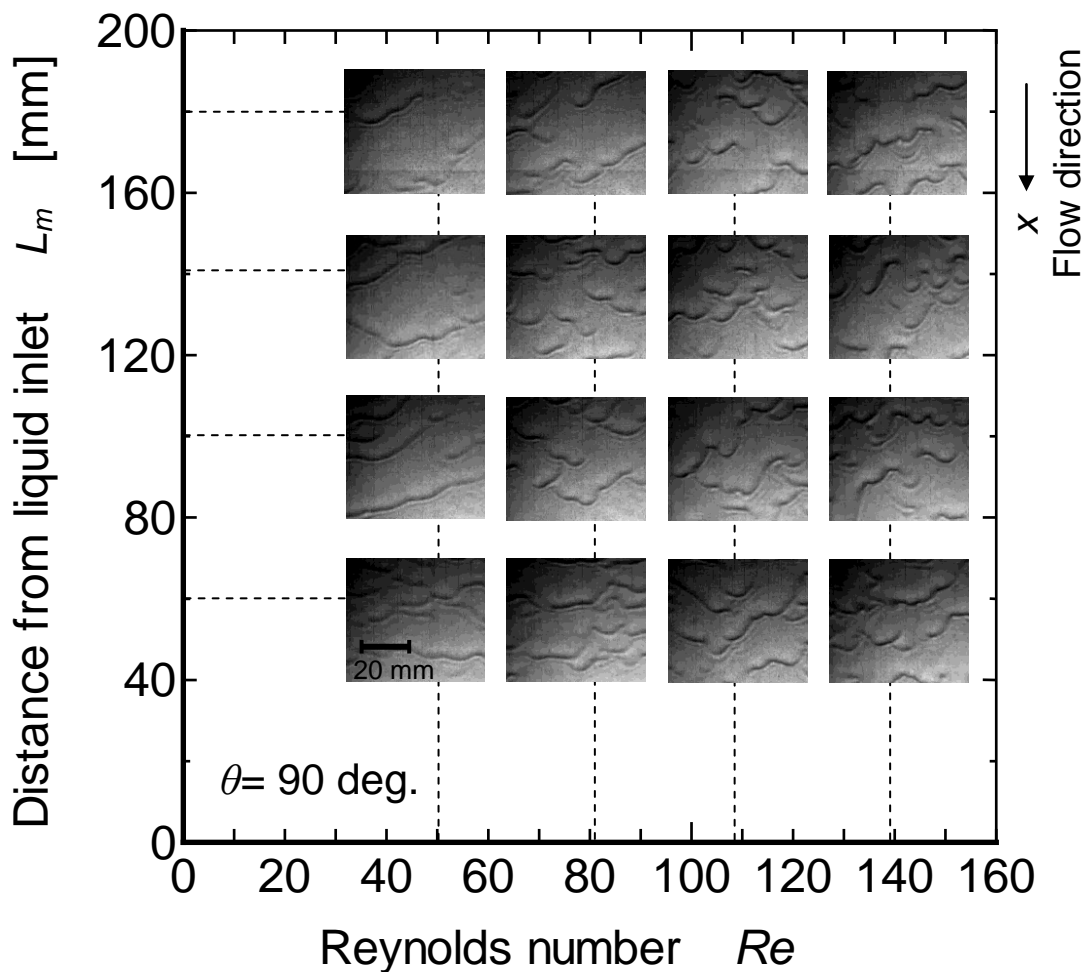

Fig. 5-8   Wave patterns of liquid film upon wall inclination angle, $\theta=90°$

In **Fig. 5-8**, the waves were found to travel in larger wavelength with the increasing of distance from liquid inlet but became smaller with the increasing Reynolds number. They were formed in irregular U and W-shape of waves. This can be described by the strong influence of gravitation which dominates the film dynamics, which thus amplifies the wave shape formation in larger inclination angle, as stated by Drosos et al. **[14]**.

5.4.2 Liquid film surface and wave velocities

（ⅰ） Effect of increasing wall inclination angle

The time series movement of liquid film and wave under same Reynolds number, Re=81.3 at wall inclination angle, θ=30°, 60° and 90° are shown in **Fig. 5-9** to **Fig. 5-11**. In each figure, **(a)** represents the positional relation between the liquid film and wave, while **(b)** represents the velocity profile. The crossing point between the plotted data points of **(a)** in each figure represents the intersection between wave and dye trace during the liquid film flows along the inclined wall.
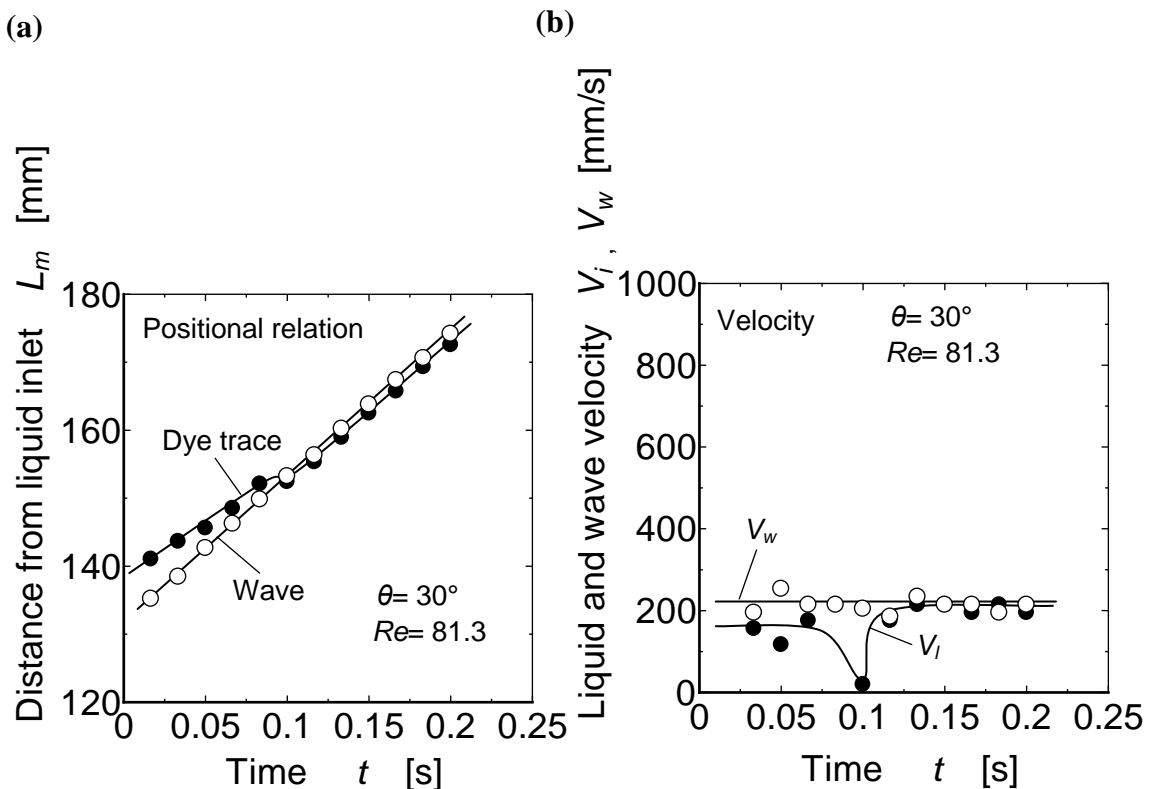
(a)   **(b)**

Fig. 5-9 Time series movement in **(a)** positional relation and **(b)** velocity of liquid film and wave upon Re=81.3, θ=30°

As can be seen, the wave was found to gradually move downstream. However, the liquid film which represented by the dye trace movement seemed to slightly shrink its gradual movement when approached by the wave, and then gradually move again after the intersection. This movement trend was confirmed by the velocity profile as shown in **(b)** in each figure. As it can be observed, the wave apparently remained unaffected and moved in almost constant velocity even after passing over the liquid film.

On the other hand, the liquid film was found to move in almost constant velocity, but then slightly decrease around the same timing of the intersection. Thereafter, the liquid film velocity showed a rapid increase till reaching a remained constant. As time passed by, the liquid film velocity then returned to its normal gradual velocity in lower value.
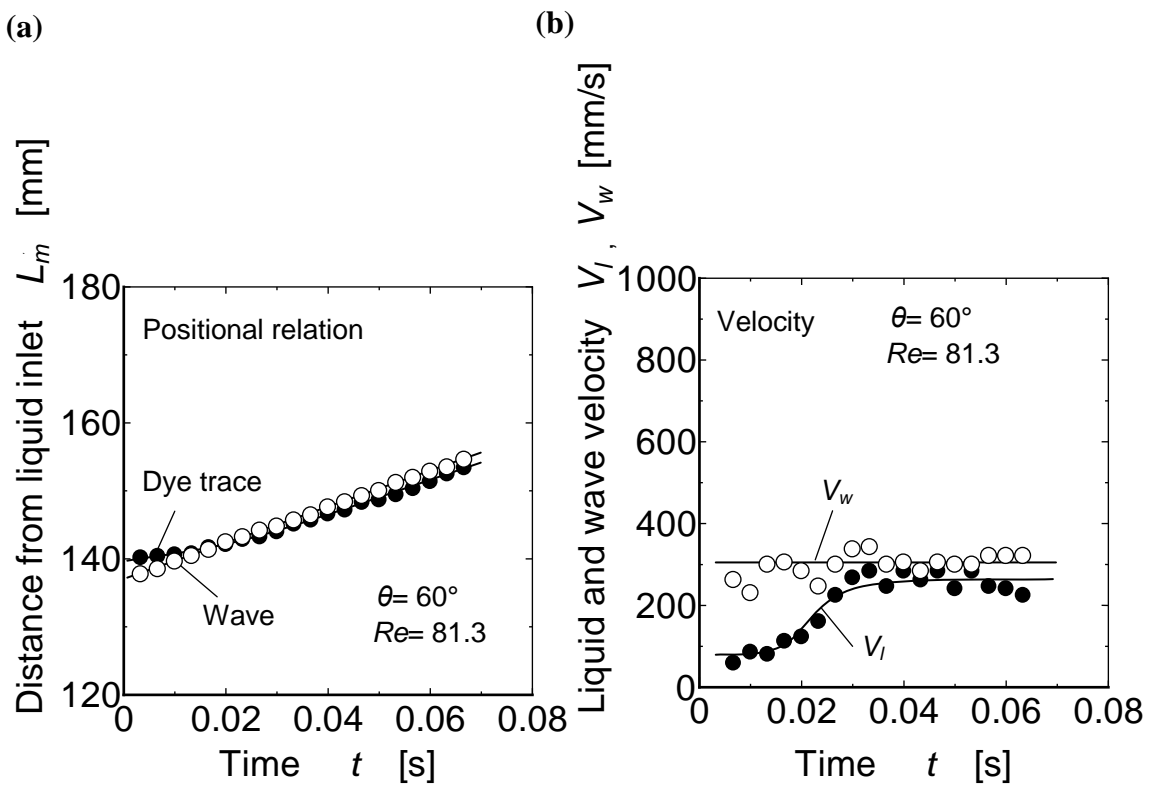
(a)   **(b)**

Fig. 5-10   Time series movement in **(a)** positional relation and **(b)** velocity of liquid film and wave upon Re=81.3, θ=60°
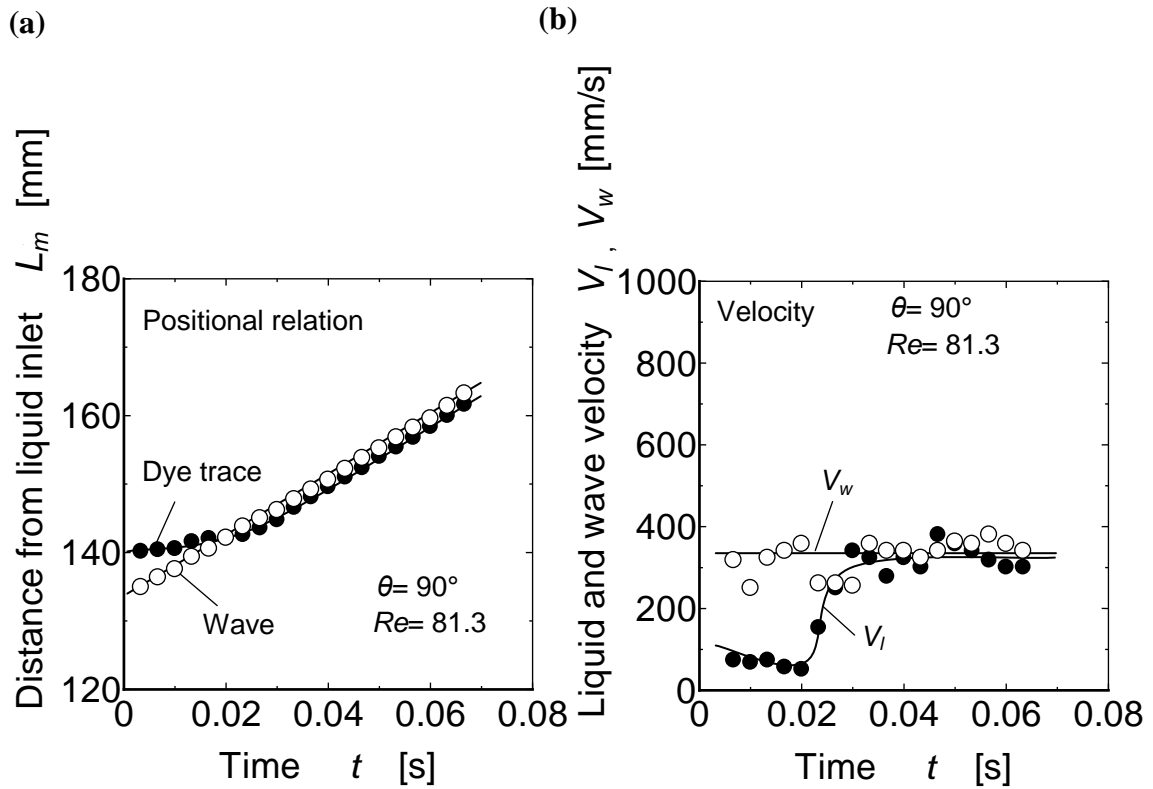
Fig. 5-11 Time series movement in **(a)** positional relation and **(b)** velocity of liquid film and wave upon Re=81.3, θ=90°
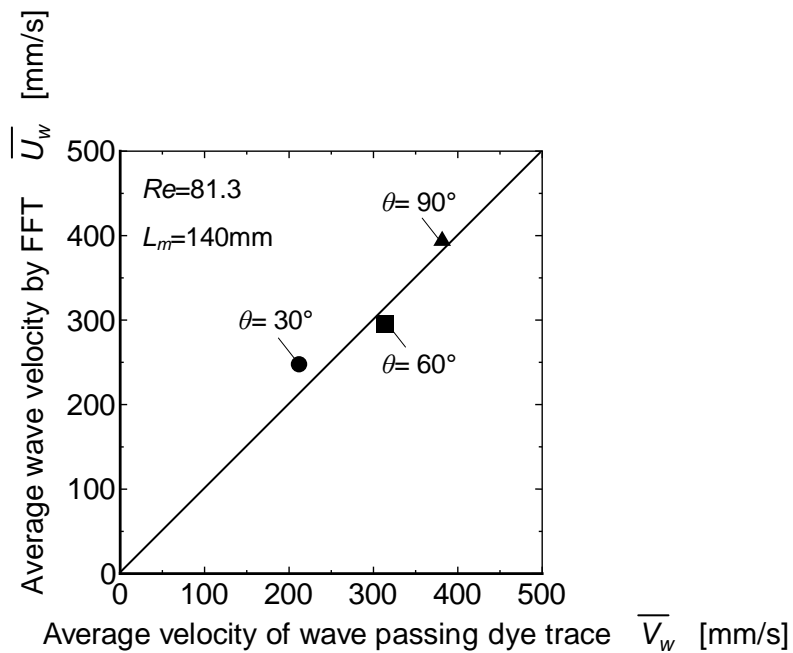

Fig. 5-12 Comparison of average wave velocity between cross correlation and image analysis methods

Figure 5-12 shows the comparison of average wave velocity using the cross correlation method and the average velocity of wave passing the dye trace which obtained by the image analysis method. As can be seen, the results between both methods were nearly agreed.

Figure 5-13 shows the velocity difference between liquid film and wave with increasing wall inclination angle at Reynolds number, Re=81.3. As can be seen, wave and liquid film velocities after the wave passing over were found to increase with increasing wall inclination angle. On the other hand, liquid film velocity before the wave passing over was found to decrease. Thus, velocity difference between wave and liquid film before the wave passing over was found to increase with increasing wall inclination angle. This can be attributed to the strength of gravitation influence presence in different inclination angle. The larger inclination angle, the stronger gravitation influences the kinetic energy of the wave which then leads to the wave velocity increase. Thus, the more energy of wave accelerates the movement of liquid film after the wave passing over it.
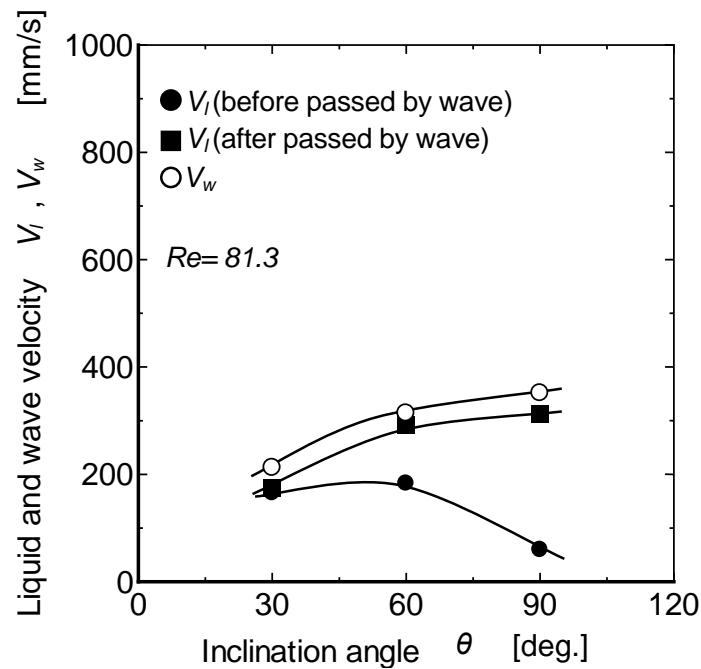

Fig. 5-13   Velocity difference between liquid film and wave with increasing wall inclination angle at Reynolds number, Re=81.3

(ii) Effect of increasing Reynolds number

The time series movement of liquid film and wave upon wall inclination angle, θ=20° and Reynolds numbers, Re= 91.5, 135.5 and 179.5 are shown in **Fig. 5-14** to **Fig. 5-16**. In all figures, **(a)** represents the positional relation between dye trace and wave while **(b)** represents its velocity change. The crossing point between the plotted data points of **(a)** indicates the intersection between the liquid film and wave. When wave increasingly approached the dye trace, the dye trace seemed to slightly shrink its movement. It then continued moving again after the wave passed over. On the other hand, the wave appeared to remain unaffected and gradually moved further downstream.
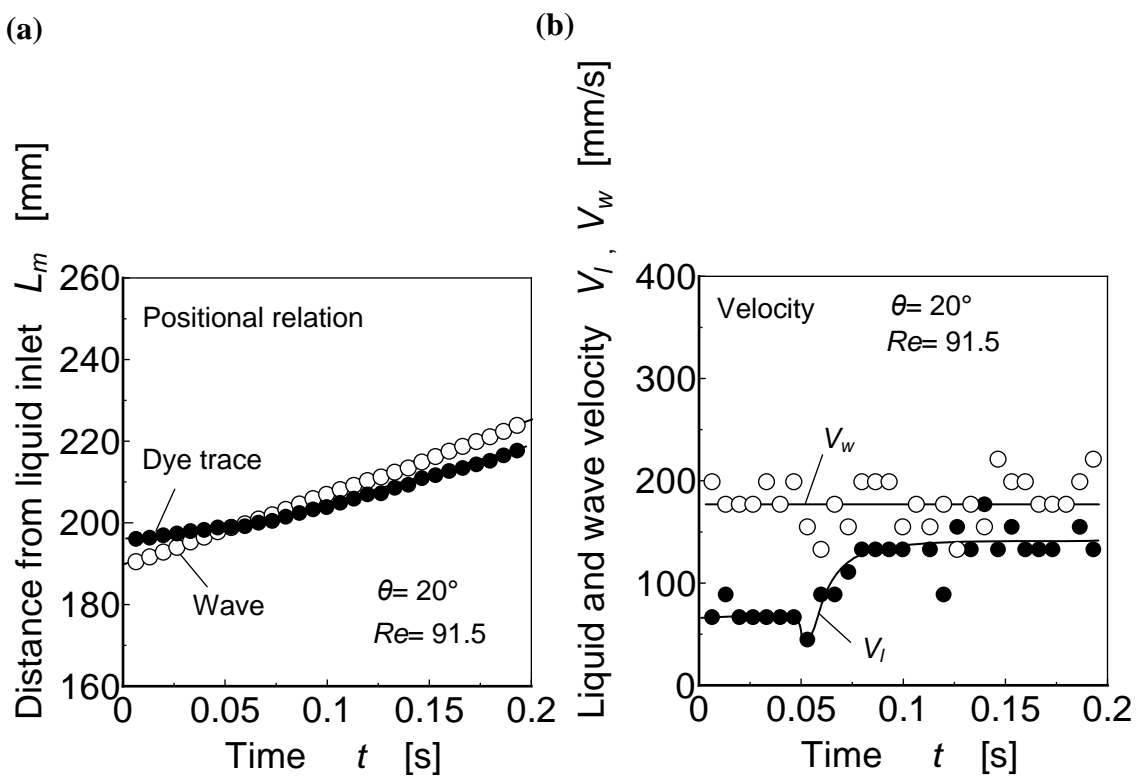
(a)

(b)

Fig. 5-14   Time series movement in **(a)** positional relation and **(b)** velocity of liquid film and wave upon θ=20°, Re=91.5

This kind of movement trend was confirmed by the velocity profiles as shown in **(b)**. In which, the liquid film velocity evidently decreased around the same timing of intersection. It then rapidly increased till reaching a maximum value of velocity higher than its initial appearance and remained constant. This movement trend is also consistent with the results as shown in increasing Reynolds number.
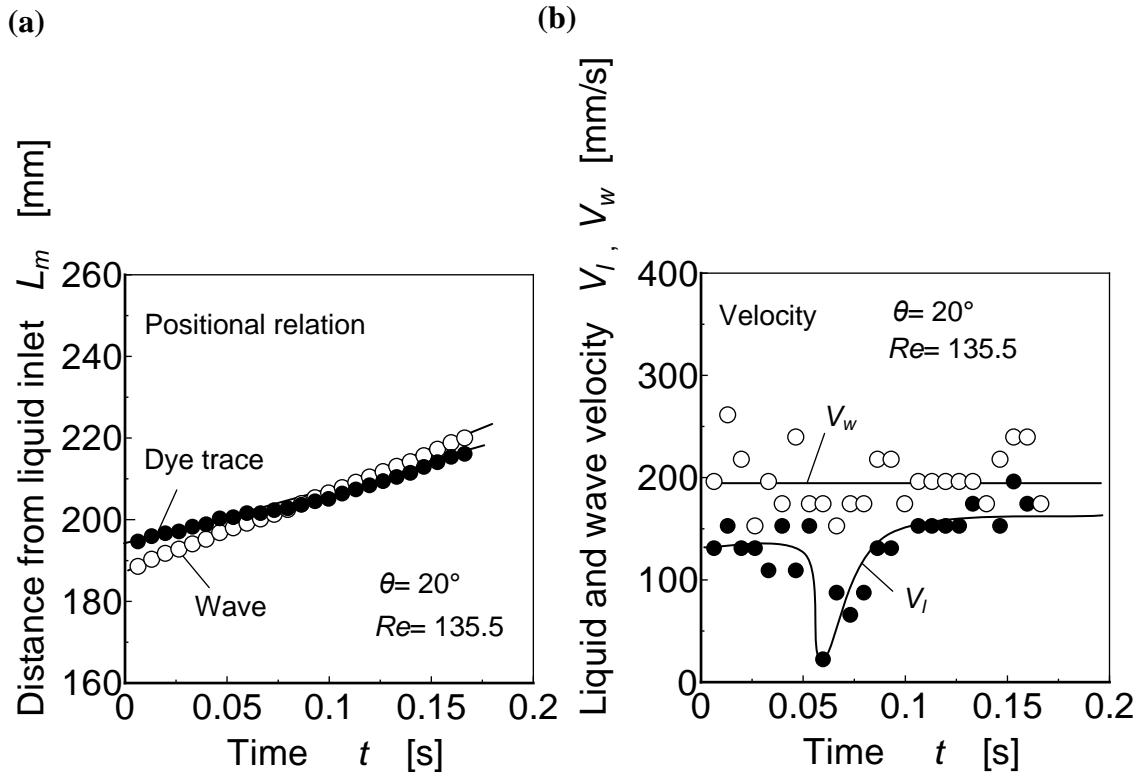
Fig. 5-15 Time series movement in **(a)** positional relation and **(b)** velocity of liquid film and wave upon $\theta=20°$, $Re=135.5$

The decreasing velocity of liquid film when the dye trace approached by wave represents the moment when the liquid elements were attracted by the wave, which had been also discussed by Wehinger et al. **[9]**. On the other hand, the rapid increase of velocity of liquid film can be attributed to the influence made by the wave after the overlapping. This reason accords with the statement made by Moran et al. **[11]**, who suggested that liquid film in the wave back may be accelerated by the wave and hence seemingly follows the wave movement.

In order to better explain the decreasing and increasing trends of liquid film velocity around the wave presence, the velocity change of dye trace was plotted against the distance between the dye trace and the wave crest as depicted in **Fig. 5-17**. From the figure, it is evident that the gradual velocity of dye trace decreased until around the wave crest, i.e. when the peak of wave coming from the dye trace rear increasingly approached the dye trace. It then suddenly increased after the overlapping, i.e. the wave peak increasingly precedes the dye trace and moves with higher gradual velocity.
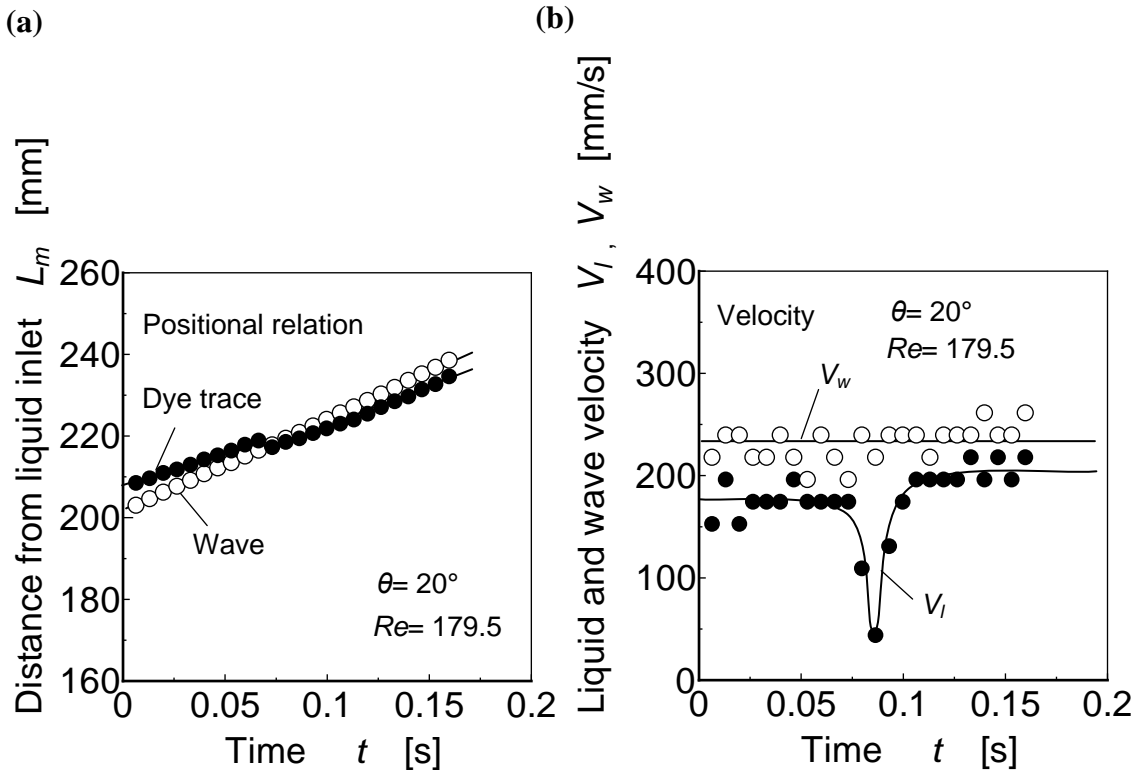
(a)

(b)

Fig. 5-16 Time series movement in **(a)** positional relation and **(b)** velocity of liquid film and wave upon $\theta=20°$, $Re=179.5$
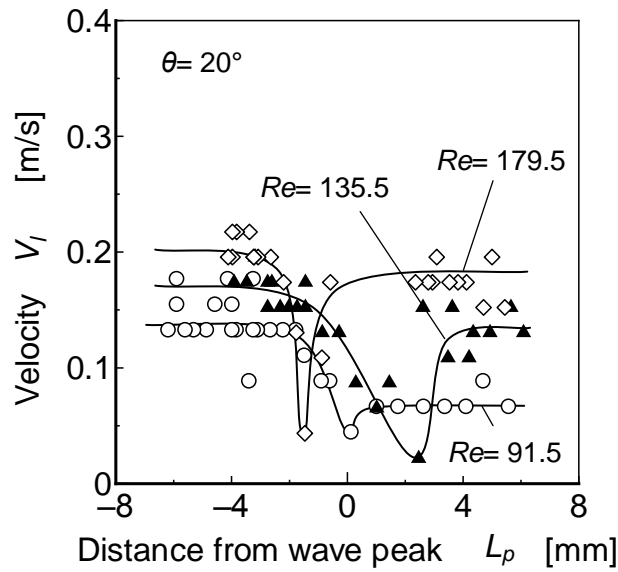

Fig. 5-17 Velocity change of dye trace against distance from wave peak

5.4.3   Diameter change of dye traces

Figure 5-18 shows the consecutive video images of dye trace and wave profiles in liquid film flows at Reynolds number, *Re*= 91.5 and inclination angle, θ=20°. Image **(a)** shows the appearance of dye trace when it was initially marked on the liquid film. It also shows a wave was approaching closer to the dye trace from the rear. As shown in image **(b)**, the wave then evidently passed over the dye trace, causing it to elongated parallel to the flow direction. Furthermore in image **(c)**, the wave continued to move and precede the dye trace, hence lead the length which was elongated before became shorter. As shown in image **(d)**, the dye trace was found to follow the wave with its length parallel to the flow direction became even shorter than its initial appearance.
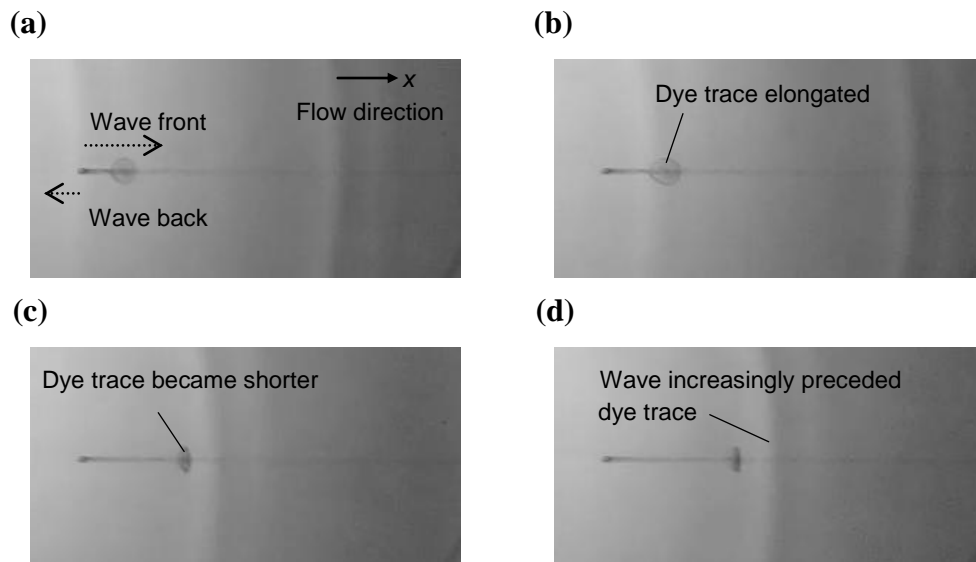

Fig. 5-18   Consecutive video images **(a)**, **(b)**, **(c)** and **(d)** of dye trace and wave profiles in liquid film flows (*Re*=91.5, θ=20°)

From the visualization of dye trace formation, the data of diameter change were plotted against the distance between the dye trace and the wave crest as shown in **Fig. 5-19**. This figure indicates that the diameter of the dye trace parallel to the flow direction gradually increased until the wave was overlapping it. This increasing trend of diameter represents the liquid attraction exerted by the higher velocity around the wave crest. Furthermore, the concentration of the dye trace in the wave back region became darker. This shows that the liquid film tend to accumulate after overlapped by wave, as shown in illustration of **Fig. 5-20**. Although Moran et al. **[11]** denied the existence of

vortex with relatively large velocity in very thin falling liquid films, it is believed that the accumulation represents the vortex was about to form in the liquid film at the wave back. However, attraction by the wave that governs the liquid film flow on that region prevented the vortex formation.

On the other hand, the diameter change of dye trace perpendicular to the flow direction was found very little. It is encouraging to compare with the appearance of dye trace images depicted in previous **Fig. 5-19**, which shows almost no difference of diameter change in perpendicular to the flow direction.
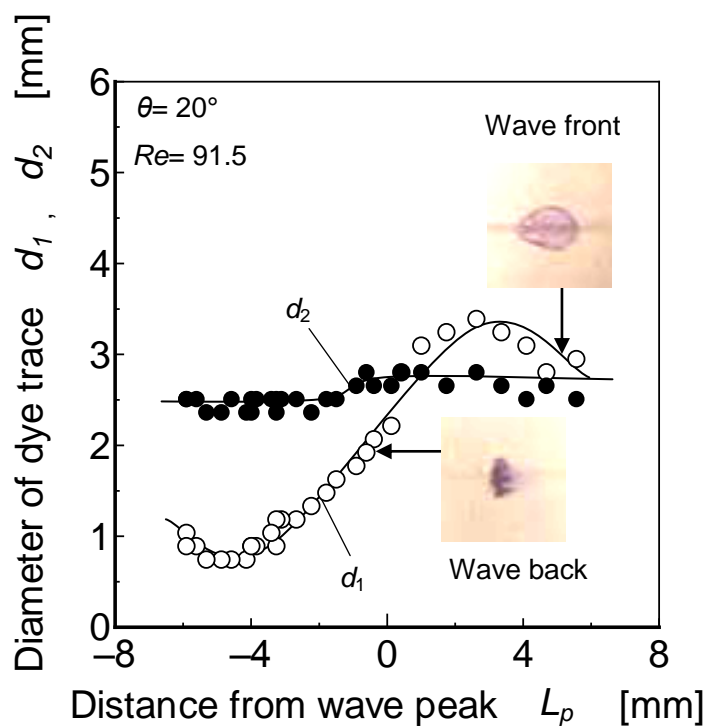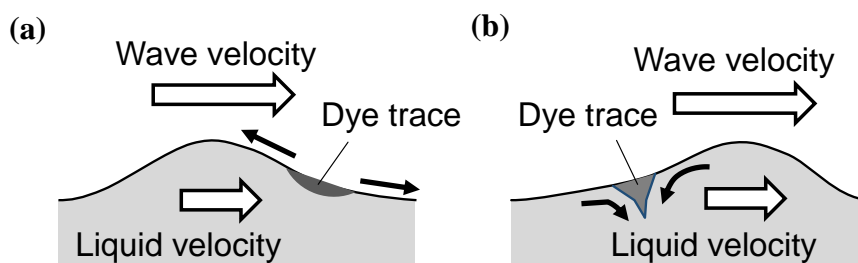

Fig. 5-19 Diameter change of dye trace

Fig. 5-20 Illustration of liquid film movement around **(a)** wave front and **(b)** wave back

5.4.4　Average liquid film thickness

From the data of light absorption method, the liquid film thickness was estimated. **Fig. 5-21** to **Fig. 5-23** show the liquid film thickness at various Reynolds number upon wall inclination angle, θ=30°, 60° and 90°. In each figure, **(a)** represents the time change of liquid film thickness, while **(b)** represents the wave shape from the measurement position, L_m=140mm. As can be seen, the presence of wave train patterns shown in **Fig. 5-6** was well confirmed by the wavy film layers appeared in **Fig. 5-21**.
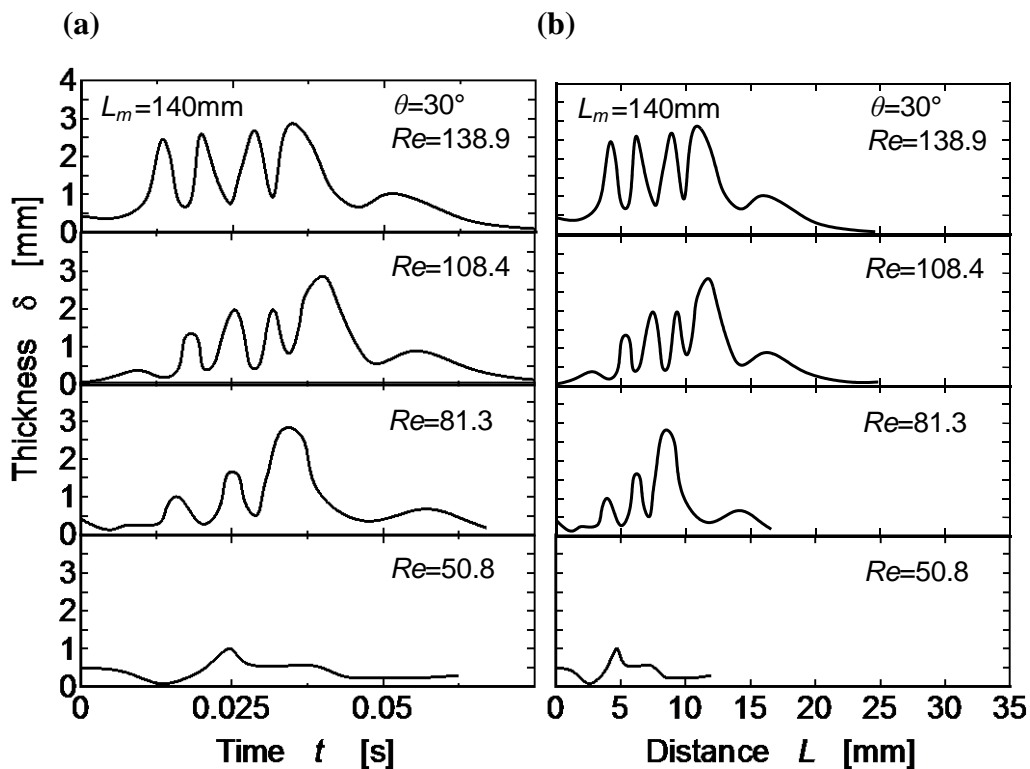

Fig. 5-21　Liquid film thickness represented as **(a)** time change of thickness and **(b)** wave shape in increasing Reynolds number at θ=30°
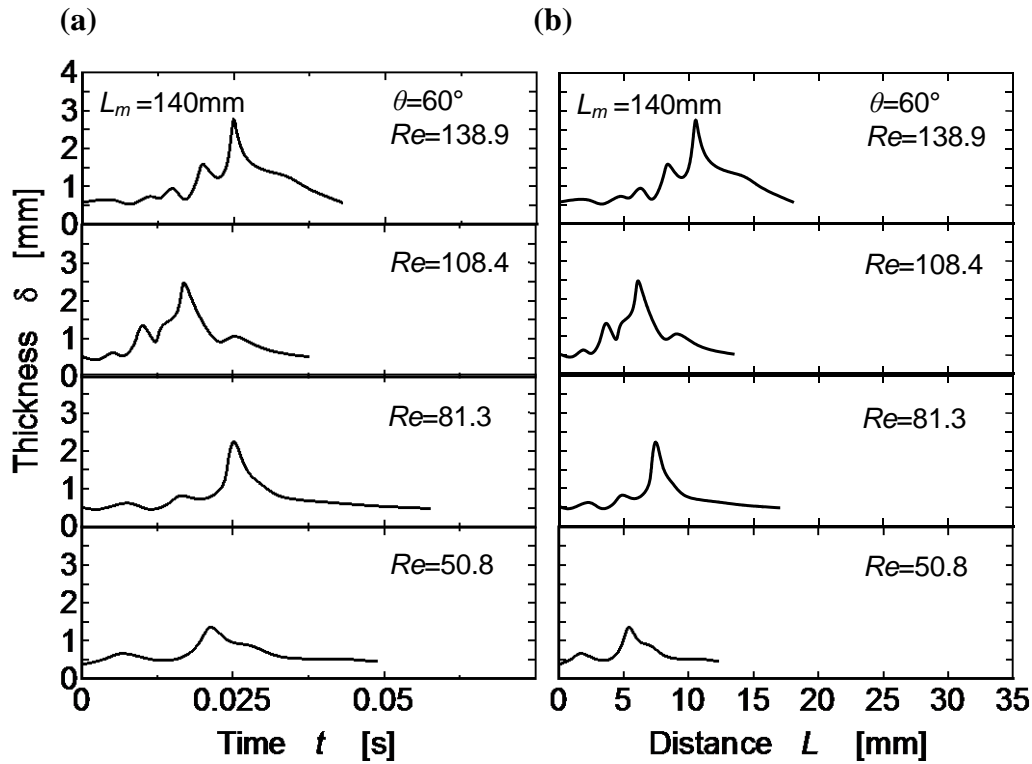
Fig. 5-22 Liquid film thickness represented as **(a)** time change of thickness and **(b)** wave shape in increasing Reynolds number at $\theta=60°$

The forerunner waves previously revealed in **Fig. 5-7** was also confirmed by the small wavy film formed in the beginning of the fluctuation depicted in **Fig. 5-22**. In **Fig. 5-23**, the waves with single wave peak in relatively smaller amplitude were observed. These waves represent the irregular U and W-shape of waves shown in **Fig. 5-8**.

Figure 5-24 shows the liquid film average thickness with increasing Reynolds number upon wall inclination angle, $\theta=30°$, $60°$ and $90°$. From this figure, the average thickness at $\theta=30°$ and $60°$ was found to increase with increasing Reynolds number. On the contrary, the average thickness was found to decrease with increasing Reynolds number at $\theta=90°$. The measured data of liquid film average thickness were also compared with the calculated data as shown in **Table 5-1**. The mismatch between the data can be attributed to the liquid film behavior in this study that formed quite a lot of waves on the liquid film surface compared to the laminar flow owned by the theoretical liquid film of **Eq. (5-5)**.

Fig. 5-23 Liquid film thickness represented as **(a)** time change of thickness and **(b)** wave shape in increasing Reynolds number at θ=90°

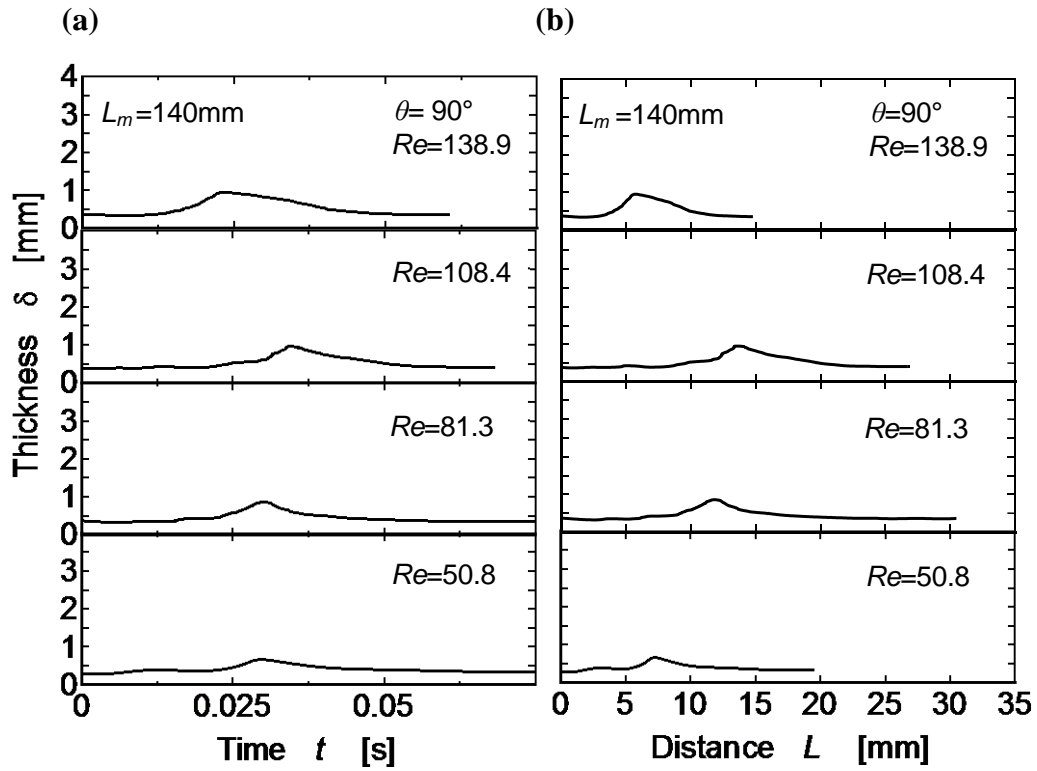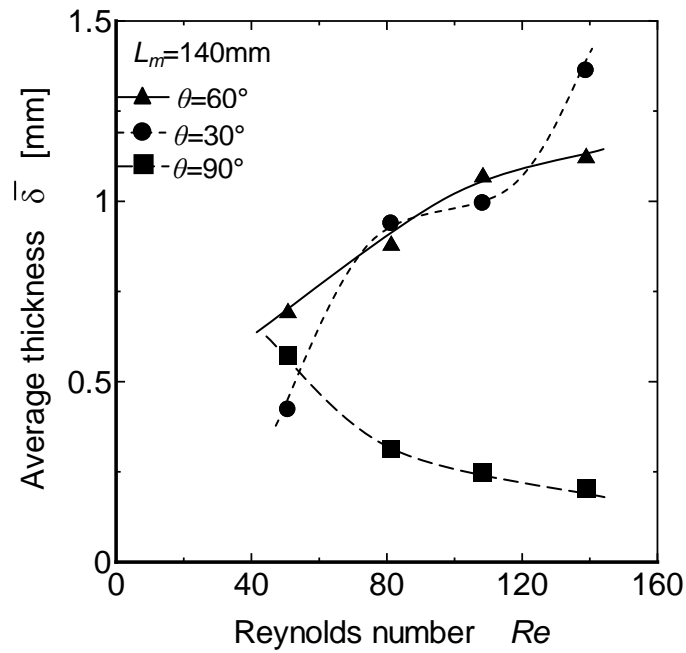**Fig. 5-24** Liquid film average thickness with increasing Reynolds number

Table 5-1 Data comparison of liquid film average thickness between calculated and measured value **(a)** before and **(b)** after wave passing dye traces (*Re*=81.3)

(a)

Inclination angle	Liquid film average velocity	Liquid film average thickness	
		Calculated value	Measured value
θ [deg.]	$\overline{V}_l$ [mm/s]	$\overline{\delta}$ [mm]	$\overline{\delta}$ [mm]
30	165.65	0.38	0.94
60	183.35	0.30	0.88
90	59.66	0.16	0.31

(b)

Inclination angle	Liquid film average velocity	Liquid film average thickness	
		Calculated value	Measured value
θ [deg.]	$\overline{V}_l$ [mm/s]	$\overline{\delta}$ [mm]	$\overline{\delta}$ [mm]
30	175.40	0.38	0.94
60	291.69	0.38	0.88
90	312.14	0.36	0.31

5.5 Summaries

In this experiment, the laser tagging method using photochromic dye tracer was applied with the aim to experimentally study the flow structure of liquid film flowing down an inclined wall. The motions of the dye traces tagged by UV laser were analyzed as the liquid surface velocity. The movement of the dye traces was analyzed together with the movement of wave passing over the dye trace using image analysis method. Velocity difference between the liquid film and wave was then investigated.

Furthermore, a cross-correlation method was also used to measure the average wave velocity, based on irradiation of two parallel diode laser beams perpendicular to the liquid film flow. From one of the diode laser beams irradiation, liquid film thickness fluctuation was measured using a light absorption method.

Considering the change of dye trace shape was strongly influenced by the inner flow structure, the diameter change of dye trace marked on the film surface was also measured in order to confirm the inner flow structures of falling liquid film. The conclusions of the present experiment can be highlighted as below:

1. Different wave patterns are confirmed to occur with different wall inclination angle.

2. Wave and liquid film velocities before and after the wave passing over displayed a gradual increase with increasing Reynolds number.

3. Further downstream, liquid film initially moved in almost constant velocity, but slightly decreases when approached by wave. When the wave was passing over the liquid film, the liquid film velocity rapidly increased as represented by the acceleration dragged by the wave which was moving in higher velocity.

4. From the measurement of diameter change of the dye traces, the inner flow structure when the liquid film passed by wave was clarified.

5. Velocity difference between wave and liquid film before the wave passing over increased with increasing wall inclination angle.

References

[1] Yu, Y.Q., Wei, S.J., Yang, Y.H. and Cheng, X.: Experimental Study of Water Film Falling and Spreading on a Large Vertical Plate, *Progress in Nuclear Energy*, **54** (2012), 22-28.

[2] Pavlenko, A.N., Lel, V.V., Serov, A.F. and Nazarov, A.D.: Flow Dynamics of Intensively Evaporating Wave Film of a Liquid, *Journal of Applied Mechanics and Technical Physics*, **42**-3 (2001), 475-481.

[3] Min, J.K. and Park. S.I.: Numerical Study for Laminar Wavy Motions of Liquid Film Flow on Vertical Wall, *International Journal of Heat and Mass Transfer*, **54** (2001), 3256-3266.

[4] Christian, R.Q., Kofman, N., Chasseur, D. and Mergui, S.: Dynamics of Falling Liquid Films, *The European Physical Journal E*, **37**-30 (2014).

[5] Chinnov, E.A. and Kabov, O.A.: Marangoni Effect on Wave Structure in Liquid Films, *Microgravity Science and Technology*, XIX-3/4 (2007), 18-22.

[6] Salque, G., Gajan, P., Strzelecki, A., Couput, J.P. and El-Hima, L.: Atomisation Rate and Gas/Liquid Interactions in a Pipe and a Venturi: Influence of the Physical Properties of the Liquid Film, *International Journal of Multiphase Flow*, **51** (2013), 87-100.

[7] Kil, S.H., Kim, S.S. and Lee, S.K.: Wave Characteristics of Falling Liquid Film on a Vertical Circular Tube, *International Journal of Refrigeration*, **24** (2001), 500-509.

[8] Duprat, C., Tseluiko, D., Saprykin, S., Kalliadasis, S. and Giorgiutti-Dauphine, F.: Wave Interactions on a Viscous Film Coating a Vertical Fibre: Formation of Bound States, *Chemical Engineering and Processing*, **50** (2011), 519-524.

[9] Wehinger, G.D., Peeters, J., Muzaferija, S., Eppinger, T. and Kraume, M.: Numerical Simulation of Vertical Liquid-film Wave Dynamics, *Chemical Engineering Science*, **22**-6 (2013), 934-944.

[10] Karimi, G. and Kawaji, M.: Flow Characteristics and Circulatory Motion in Wavy Falling Films with and without Counter-Current Gas Flow, *International Journal of Multiphase Flow*, **22** (1999), 1305-1319.

[11] Moran, K., Inumaru, K. and Kawaji, M.: Instantaneous Hydrodynamics of a Laminar wavy Liquid Film, *International Journal of Multiphase Flow*, **28** (2002), 731-755.

[12] Zhou, D.W., Gambaryan-Roisman, T. and Stephan, P.: Measurement of Water Falling Film Thickness to Flat Plate using Confocal Chromatic Sensoring Technique, *Experiment Thermal and Fluid Science*, **33**-2 (2009), 273-283.

[13] Brauner, N. and Maron, D.M.: Characteristics of Inclined Thin Films, Waviness and the Associated Mass Transfer, *International Journal of Heat Mass Transfer*, **25**-1 (1982), 99-110.

[14] Drosos, E.I.P., Paras, S.V. and Karabelas, A.J., Characteristics of Developing Free Falling Films at Intermediate Reynolds Number and High Kapitza Numbers, *International Journal of Multiphase Flow*, **30** (2004), 853-876.

Chapter 6

Conclusions

This research was developed to investigate the free surface flow behavior using the laser tagging method by photochromic dye tracer. The applicability of this technique for the measurement of liquid flow field was successfully confirmed by the experiment of creeping flow of moving cylinder. The applicability of this technique was then extended to the free surface flow measurement. It was successfully confirmed by the experiments of liquid sheet spray and liquid film flow on inclined wall. Furthermore, the laser tagging method was also applicable to clarify the inner flow structure. It was successfully confirmed by the measurement of diameter change of the dye trace when the dye trace passed by wave on the liquid film surface.

The main originality of this research lies in the set of 4-points of dye traces tagged by the UV light irradiation. Through the change of relative position of the set, not only the measurement of velocity but also the measurement of deformation and rotational motion of the free surface flow were successfully derived. Based on the temporary color change of liquid containing the photochromic dye when irradiated by UV light, the visualization of flow structure was enabled directly without using the seeding particles. Thus, we confirmed that the laser tagging method by photochromic dye tracer is a reliable technique to investigate the free surface flow behavior.

One source of weakness in this research which could have affected the measurement accuracy was the size of tagged area, i.e. 4-points of dye traces originally projected from the screen holes. The size of tagged area composed in this study was the smallest size that can be operated in order to maintain concentration of the dye traces color which easily fades by the liquid flow being measured.

In spite of the uncertainties occurred in the results, this research is still beneficial to pave the way in measuring the free surface flow deformation. To our knowledge, such exploratory is still critically needed but only been carried out in a small number of studies so far. Therefore, considerably more works must be done as recommendations to help us establishing a greater degree of accuracy and resolution for future study. What is mostly needed is to enhance the dye trace concentration and edge sharpness which were hardly achieved. The experimental design and tools in leading UV light to the liquid film for photochromic dye activation may be revised to meet such recommendation.

Thus, the center of dye trace can be accurately coordinated for more reliable data and the scale of tagged area also can be reduced for a greater resolution. Furthermore, it would be more impressive if the number of dye traces bounding the tagged area can be increased to highlight the edge of bounded area for reliable liquid deformation measurement.

In the future, the laser tagging method by photochromic dye tracer can be applied to investigate the non-Newtonian fluid behavior such as the melt flow of polymer in plastics molding process. As we know, plastics are extensively used in the industrial fields as well as in our daily life. In response to the increasing demands of better design and quality of plastics products, the plastics processing method must be efficient. The efficiency may be enhanced by investigating the flow behavior of molten plastics using the laser tagging method by photochromic dye tracer.

Appendix

Calculation accuracy of integral method

A.1   Calculation method based on Rankine's compound vortex model

In this appendix section, the accuracy of integral method for the calculations of vorticity and divergence are discussed using the given flow field. We assumed that the velocity data was obtained at random point in the flow field. Normally, the vorticity and divergence can be derived by using differential method. In order to calculate the differential, velocity data is required at grid points. Therefore, interpolation into grid points is required for the calculation. This matter can be simply described by **Fig. A-1**.

      On the other hand, if we used the integral method based on the Gaussian's theorem, Stoke's theorem and Green's theorem, the vorticity and divergence can be easily estimated from the velocity data of random points as shown in chapter 2.
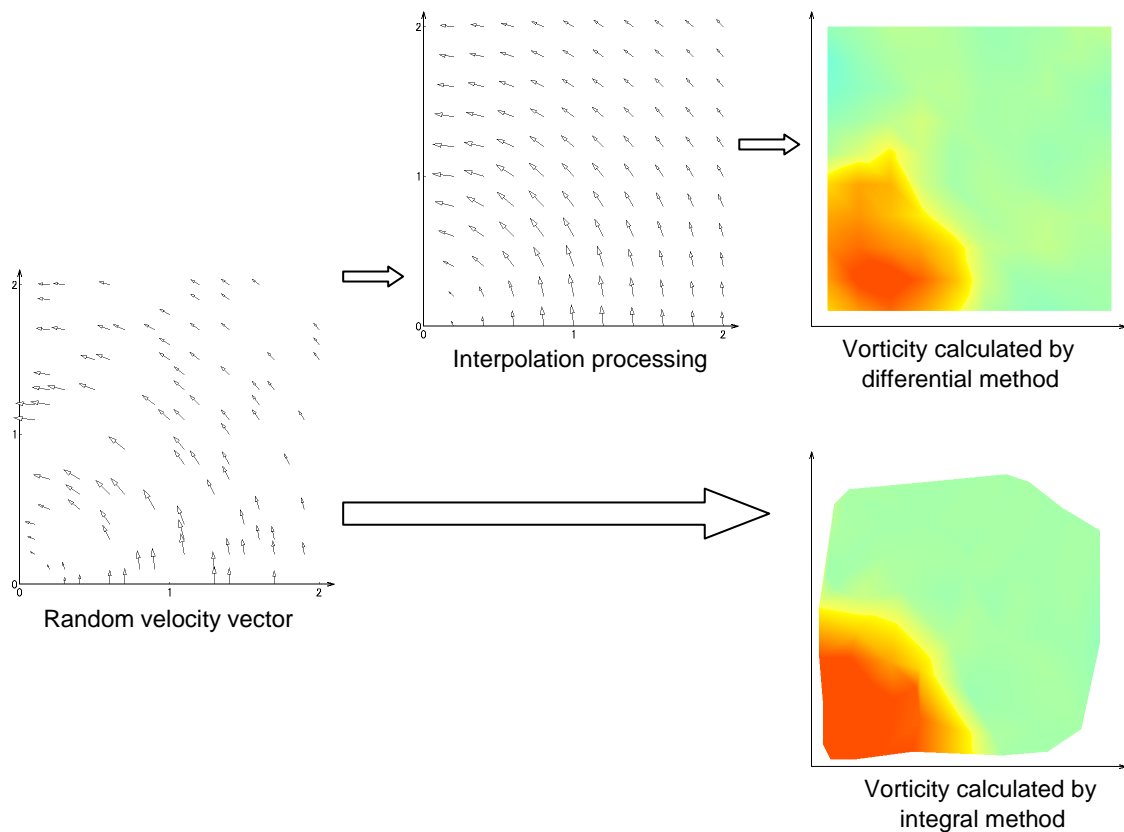

Interpolation processing

Vorticity calculated by differential method

Random velocity vector

Vorticity calculated by integral method

Fig. A-1   Simple description of vorticity calculation by using differential and integral method

In order to confirm the calculation accuracy of the integral method for the vorticity measurements in the research study, we compared the calculation between integral method and differential method. The comparison was made for vorticity and divergence measurements in Rankine's vortex model. As shown in **Fig. A-2**, Rankine's compound vortex refers to the principle in which, vortex in range of radius, $r<1$ is called as forced vortex while in range of radius, $r>1$ is called as free vortex.
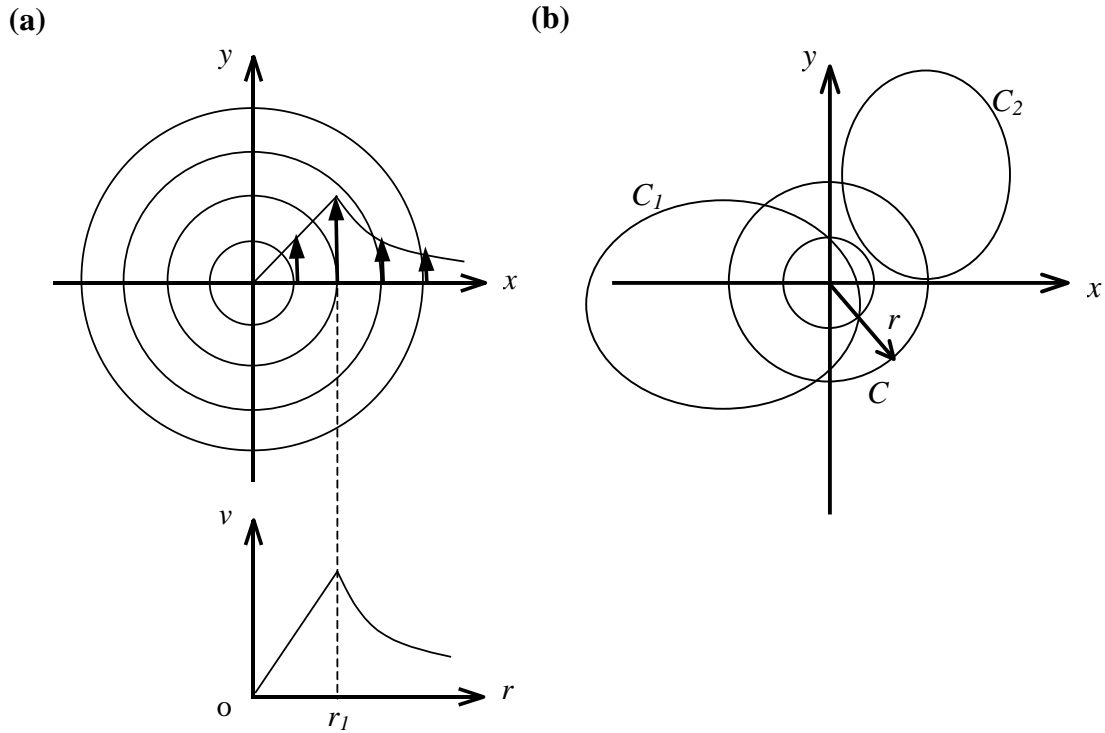

Fig. A-2   Illustration of **(a)** Rankine's compound vortex model with arbitrary radius, r and **(b)** path integration, C

As shown in **Fig. A-2(a)**, the circumference direction velocity at radius, r for the forced vortex region, v is given as below:

$$v = \Omega r \tag{A-1}$$

where, Ω is constant

$$\partial v / \partial r = \Omega \tag{A-2}$$

If we set the path of integration along the circumference of radius, r as C, the circulation, $\Gamma(C)$ can be obtained as below:

$$\Gamma(C) = \int_C v_s dr = \int_C \Omega r \cdot r d\theta = 2\pi r^2 \Omega \qquad \text{(A-3)}$$

As the area of circle is $S = \pi r^2$, vorticity, ω can be derived as below:

$$\omega = \frac{\Gamma(C)}{S} = 2\Omega \qquad \text{(A-4)}$$

In the theory of forced vortex, the vorticity at any position is constant at 2Ω. Moreover, the flow rate in the integration path is given as:

$$Q(C) = \int_C v_n dr = 0 \qquad \text{(A-5)}$$

Where, v_n is zero. Therefore, the divergence, Θ is also 0, as shown in below equation:

$$\Theta = \frac{Q(C)}{S} = 0 \qquad \text{(A-6)}$$

For the free vortex region, the velocity of circumference direction, v is given as below:

$$v = k/r \qquad \text{(A-7)}$$

Where, k is constant. If we set randomly closed line including origin point as C_1, the circulation, $\Gamma(C_1)$ can be obtained as below:

$$\Gamma(C_1) = \int_{C_1} v_s dr = \int_{C_1} \frac{k}{r} \cdot r d\theta = 2\pi k \qquad \text{(A-8)}$$

where, the circulation, $\Gamma(C_1)$ is constant regardless of integration path radius. The vorticity, ω is also a constant value as given below:

$$\omega = \frac{\Gamma(C_1)}{S} = \frac{2\pi k}{S} \qquad \text{(A-9)}$$

However, the circulation along the closed line C_2 excluding the origin point, $\Gamma(C_2)$ is given as:

$$\Gamma(C_2) = \int_{C_2} v_s dr = k \int_{C_2} d\theta = 0 \qquad \text{(A-10)}$$

The vorticity, ω is also 0, as shown below:

$$\omega = \frac{\Gamma(C_2)}{S} = 0 \qquad \text{(A-11)}$$

Moreover, the flow rate in the integration path, $Q(C)$ and divergence, Θ are also 0.

A.2   Comparison of results between differential method and integral method

The result of vorticity distributions of Rankine's compound vortex model calculated by using differential method after interpolation is shown in **Fig. A-3(a)**. The interpolation was done at grid point of 0.2×0.2. **Fig. A-3(b)** shows the relationship between the radius, r and vorticity, ω. As can be seen, there was quite variability of calculated result against the theory.

The result of vorticity distributions of Rankine's compound vortex model calculated by using integral method for random velocity data is shown in **Fig. A-4(a)**, while the relationship between the radius, r and vorticity, ω is shown in **Fig. A-4(b)**. Compared to the result calculated by differential method as shown in **Fig. A-3(b)**, the result of **Fig. A-4(b)** was found to match with the theory. Therefore, it was confirmed that variables were successfully reduced by using integral method.

The result of divergence distributions of Rankine's compound vortex model calculated by using differential method after interpolation is shown in **Fig. A-5(a)**. **Fig. A-5(b)** shows the relationship between the radius, r and divergence, Θ. Similar to the result of vorticity, the result of divergence were also found to quite mismatch with the theory.

On the other hand, the result of divergence distributions of Rankine's compound vortex model calculated by using integral method for random velocity data is shown in

Fig. A-6(a), while the relationship between the radius, *r* and divergence, $\varTheta$ is shown in **Fig. A-6(b)**. As can be seen, the result calculated by using the integral method was found to match greatly with the theory. Again, it was confirmed that variables were successfully reduced by using integral method and hence the result accuracy can be enhanced.
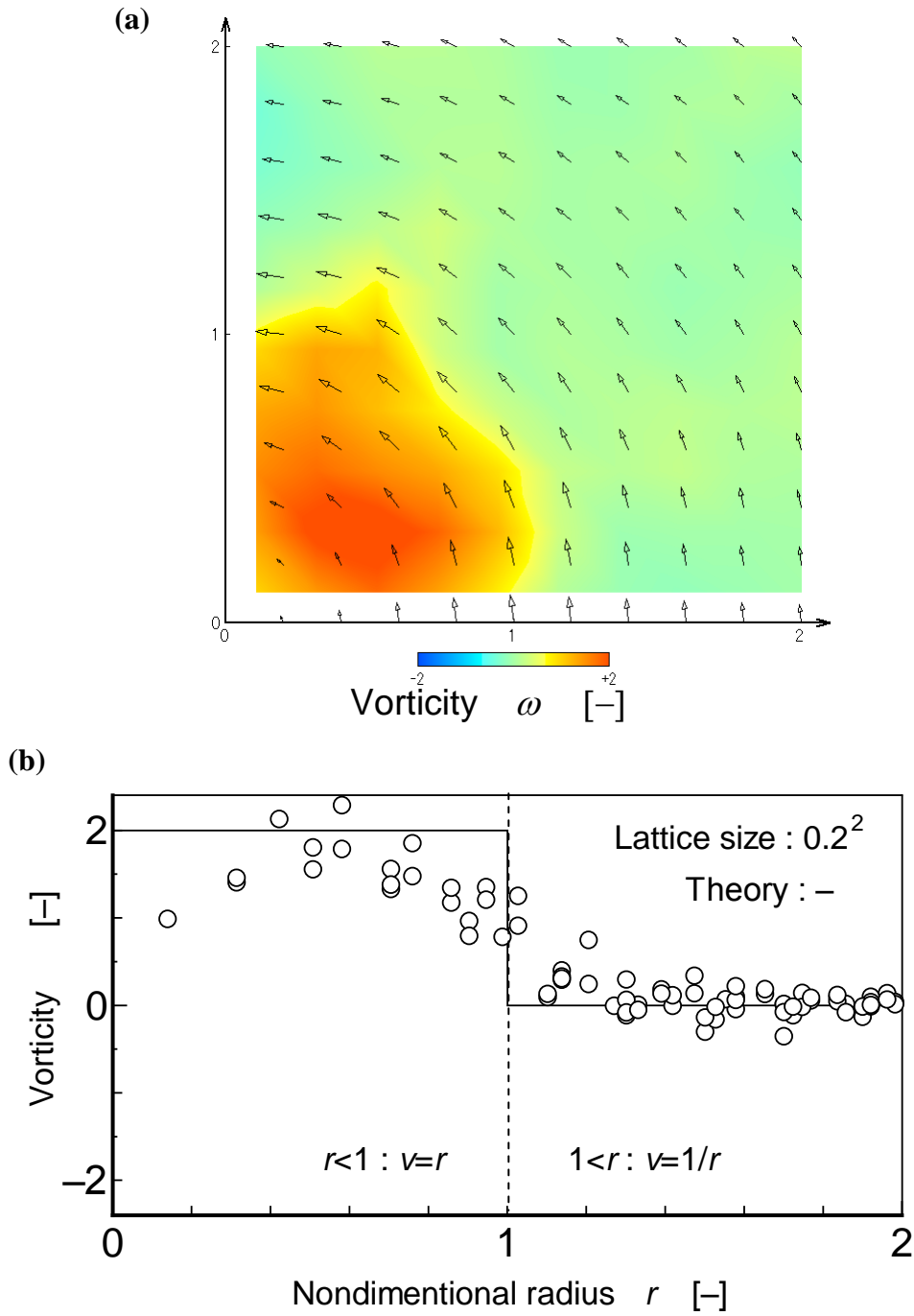

(a)

Vorticity ω [−]

(b)

Lattice size : 0.2^2

Theory : −

$r<1 : v=r$

$1<r : v=1/r$

Vorticity [−]

Nondimentional radius *r* [−]

Fig. A-3 Results of **(a)** vorticity distribution and **(b)** relationships between vorticity
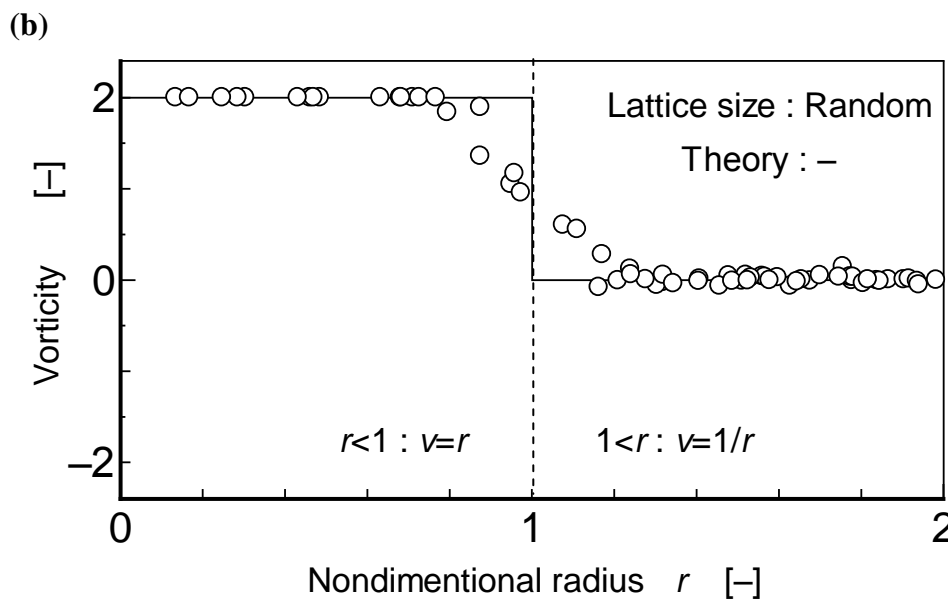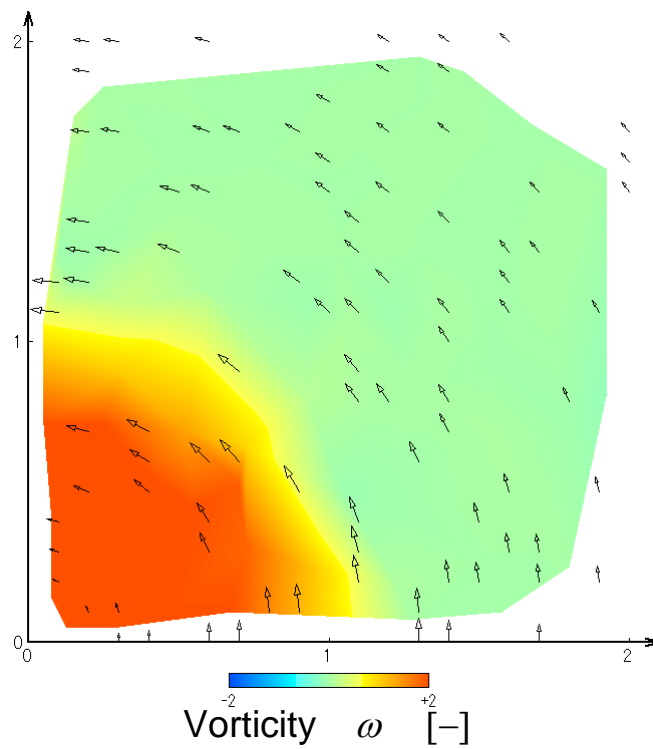(a) and radius calculated by using differential method

(b)

Fig. A-4 Results of **(a)** vorticity distribution and **(b)** relationships between vorticity and radius calculated by using integral method

(a)

Divergence Θ $[-]$

(b)

Lattice size : 0.2^2

Theory : $-$

$r<1 : v=r$ $1<r : v=1/r$

Divergence $[-]$

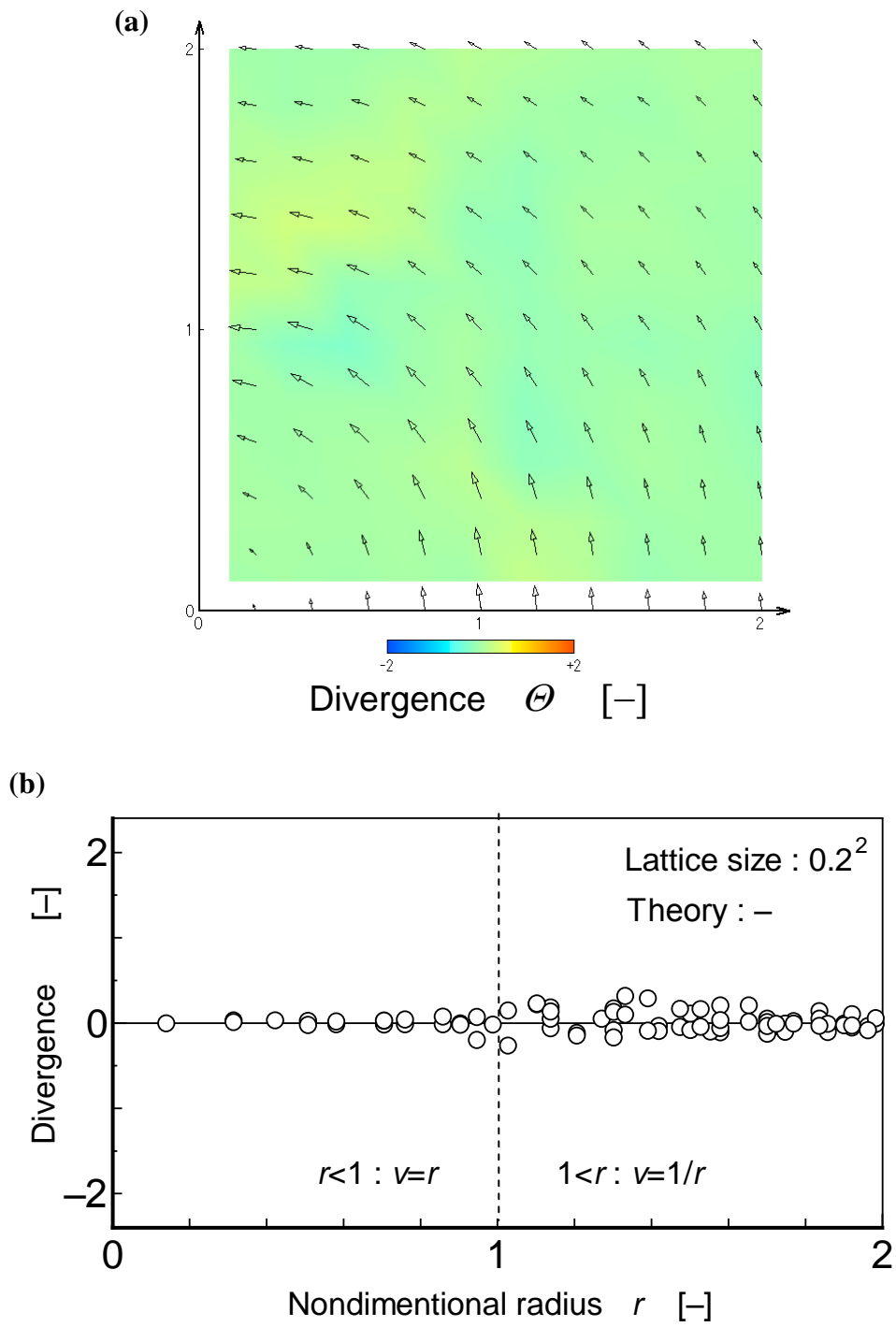Nondimentional radius r $[-]$

Fig. A-5 Results of **(a)** divergence distribution and **(b)** relationships between vorticity and radius calculated by using differential method

(a)

Divergence Θ [–]

(b)

Lattice size : Random

Theory : –

$r<1$: $v=r$

$1<r$: $v=1/r$

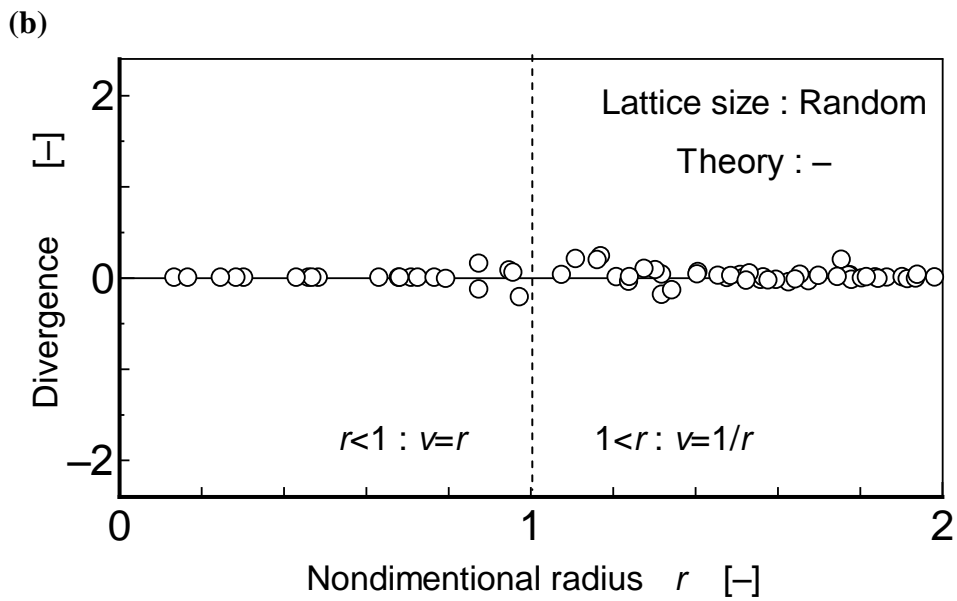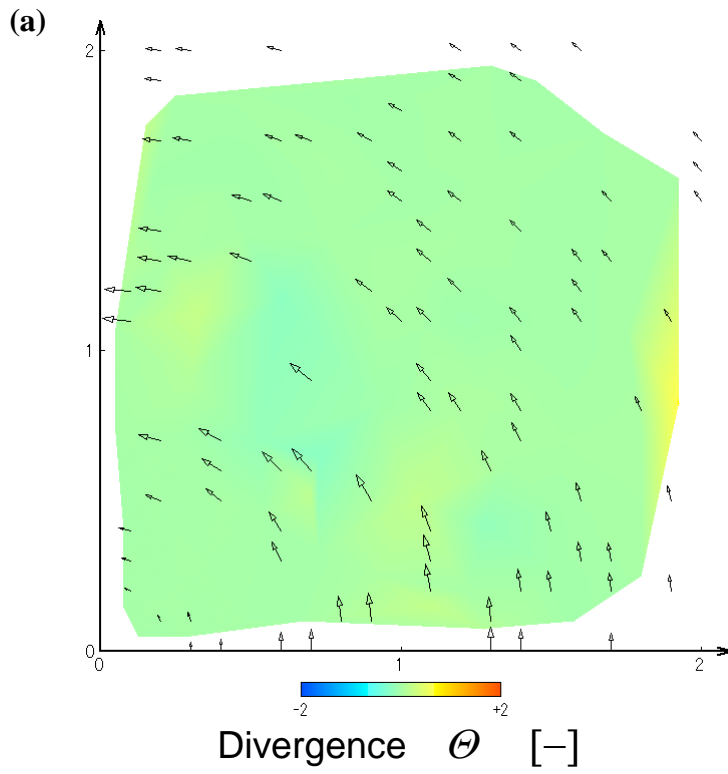Divergence [–]

Nondimentional radius r [–]

Fig. A-6 Results of **(a)** divergence distribution and **(b)** relationships between vorticity and radius calculated by using integral method

List of publications

Journal papers

1. Rosli, N., Toyooka, Y. and Amagai, K.: Velocity and Vorticity Measurement in Flow Field Using Laser Tagging Method by Photochromic Dye, *Journal of JSEM*, **11**-Special Issue (2011), 147-152.

2. Rosli, N. and Amagai, K.: Simultaneous Measurement of Liquid Surface and Wave Velocities for Falling Liquid Films, *Journal of JSEM*, **14**-Special Issue (2014), 19-24.

3. Rosli, N. and Amagai, K.: Measurement of Liquid Sheet Using Laser Tagging Method by Photochromic Dye, *Experiments in Fluids*, **55**-12 (2014), Paper no. 1843.

Conference papers

1. Rosli, N., Toyooka, Y. and Amagai, K.: Velocity and Vorticity Measurement in Flow Field Using Laser Tagging Method by Photochromic Dye, *Proceedings of 5th International Symposium on Advanced Science and Technology in Experimental Mechanics* (ISEM 2010) in Kyoto, Japan.

2. Rosli, N. and Amagai, K.: Simultaneous Measurement of Liquid Surface and Wave Velocities for Falling Liquid Films, *Proceedings of 8th International Symposium on Advanced Science and Technology in Experimental Mechanics* (ISEM 2013) in Sendai, Japan.

3. Rosli, N. and Amagai, K.: Study of Liquid Film Flow Structure on Inclined Wall using Photochromic Dye Marking Method, *Proceedings of 9th International Symposium on Advanced Science and Technology in Experimental Mechanics* (ISEM 2014) in New Delhi, India.

Acknowledgement

First and foremost, I would like to express my special gratitude to my supervisor, Professor Dr. Kenji Amagai for his continuous guidance and support throughout the journey of my study. Without his patience in training me for years in the research fields, I would not be here successfully completing my doctorate study.

Furthermore, I am thankful to Professor Dr. Masato Funatsu and Mrs. Kayo Shibusawa for their helps and advice during my study. I also truly appreciate Mr. Youichi Toyooka, Mr. Fuyuki Kokubu and Mr. Yuuta Koike for their help in setting up and collecting the data of this research study. My sincere gratitude also goes to my fellow lab mates of the 1st energy system laboratory through the joy and excitement we had together in working at the laboratory.

Moreover, I would like to extend my gratitude to Universiti Malaysia Pahang (UMP) and the Malaysia Government for giving permission and financial support to pursue my study in Gunma University.

Last but not least, I take this opportunity to express the profound gratitude to my beloved parents Rosli Bin Abdullah and Yatina Binti Abu Bakar, my husband Razuan Bin Md Radzi, my Malaysian family in Gunma University and my 'akhawat' sisters in Japan for their endless pray and support.